Density currents and salt intrusion

A.G. van Os and G. Abraham

January 1992

IHE DELFT

delft hydraulics

Kes

Density currents and salt intrusion

A.G. van Os and G. Abraham

DENSITY CURRENTS AND SALT INTRUSION

by A.G. van Os and G. Abraham, Delft Hydraulics

Chapter 1. Introduction

1. Density, density differences and density currents

2. Examples of density induced currents
    - 2.1 Flow through culvert
    - 2.2 Density induced exchange flows
    - 2.3 Gravitational circulation

3. Vertical displacements of fluids; homogeneous fluid versus stratified fluid
    - 3.1 Homogeneous fluid
    - 3.2 Effects of stratification
    - 3.3 Selective withdrawal; example of implications for flow
    - 3.4 Implications for vertical mixing

4. Effects of density differences on flow

5. Effects on transport processes

6. Classification of density currents
    - 6.1 Stratified flow (or two-layer flow)
    - 6.2 Partly mixed flow
    - 6.3 Completely mixed flow

7. Factors causing density differences; engineering significance
    - 7.1 Salt intrusion into fresh water reservoirs
    - 7.2 Salt intrusion into estuaries
    - 7.3 Density currents through reservoirs
    - 7.4 Case study: siltation of the Port of Cochin

8. References

Appendix: Density of sea water

Chapter 2, Two-layer flow

1. Notation

2. Equations of continuity

3. Equations of motion

4. Summary
    4.1 Homogeneous flow
    4.2 Two-layer flow

5. Backwater curve equation for two-layer flow

6. Long waves, concept of critical flow
    6.1 Homogeneous flow
    6.2 Two-layer flow
    6.3 Internal hydraulic jump

7. Application of critical flow concept
    7.1 Arrested salt wedge
    7.2 Density induced return current
    7.3 Selective withdrawal
    7.4 Summary

Appendix: Experimental data on interfacial shear

Chapter 3, Salt intrusion into estuaries; basic physical phenomena

1. Introductory remarks

2. Stratification of estuaries

3. Stratification parameters

4. Gravitational circulation

5. Field data on gravitational circulation

- 5.1 Chao Phya estuary, Thailand
- 5.2 Rotterdam Waterway estuary, The Netherlands
- 5.3 Mersey River estuary, United Kingdom

6. Rotation of earth

7. Large scale advective mixing

8. Independent variables

9. Time scales

10. Transient conditions versus equilibrium conditions

11. Saltintrusion formulae

Chapter 4, One-dimensional real-time salt intrusion models

1. Introduction

2. Notation, basic relationships

3. Governing equations
   - 3.1 Continuity equation for water
   - 3.2 Momentum equation
   - 3.3 Continuity equation for salt

4. Total transport of salt

5. Dispersive transport; dispersion coefficient

6. Field data on dispersive transport

7. Number of equations versus number of unknown

8. Boundary conditions

9. Dispersion coefficient

10 Implications for one-dimensional modelling

11. Examples

12. Concluding remarks

13. References

Chapter 5, One-dimensional long term salt intrusion models

1. Introduction

2. Tidal variations of salt concentration in conditions of equilibrium

3. One-dimensional long term continuity equation for salt
   3.1 Equilibrium condition
   3.2 Long term variation of salt concentration

4. Number of equations versus number of unknowns

5. Boundary conditions

6. Dispersion coefficients; applications
   6.1 Equilibrium condition
   6.2 Long term variation of salt concentration

7. Calculations over long periods

Chapter 6, Two- and threedimensional modelling, effect of stratification on turbulence

1. Introduction

2. Reynolds equations, turbulent shear stress and turbulent transport of mass

3. Limiting conditions at local level
    3.1 Limiting conditions based on gradient Richardson number
    3.2 Limiting conditions based on length scales of turbulence
    3.3 Connection between length scales and gradient Richardson number

4. Combined effect of geometry and stratification on turbulence
    4.1 Effect on length scales of turbulence
    4.2 Damping functions

5. Experimental data
    6.1 Steady flow
    6.2 Tidal flow

6. Final remarks

Chapter 7. Field surveys and physical scale modeling

1. Introduction

2. Field surveys
   2.1 First impression, salt intrusion formulae
   2.2 Models
      2.2.1 1D-models
      2.2.2 Two-layer models
      2.2.3 2DV-, 3D-models and hydraulic scale models

3. Physical scale modeling, problem areas
   3.1 Selection of model area and model scales
      3.1.1 Definition of model area
      3.1.2 Selection of model scales
   3.2 Model boundaries
   3.3 Roughness and mixing
   3.4 Model calibration and verification

4. Final remarks

Chapter 1, Introduction

1. Density, density differences and density currents

The density of a fluid (symbol ρ) is defined as

$$\rho = \frac{\text{mass}}{\text{volume}} \qquad \text{unit: } \frac{\text{kg (mass)}}{\text{m}^3}$$

The density difference between two fluids (symbol $\Delta\rho$) is defined as:

$$\Delta\rho = \rho_2 - \rho_1$$

where ρ_2 : density of heavier fluid

ρ_1 : density of lighter fluid

Due to its salt content sea water has a larger density than river water. In numbers (see appendix)

$$\begin{array}{lll} \text{sea water} & \rho_2 \approx & 1025\ \text{kg/m}^3 \\ \text{river water} & \rho_1 \approx & \underline{1000\ \text{kg/m}^3} \ - \\ & \Delta\rho \approx & 25\ \text{kg/m}^3 \end{array}$$

For this example both $\Delta\rho/\rho_1$ and $\Delta\rho/\rho_2$ are in the order of 2½ % (The symbol ε is often used for $\Delta\rho/\rho$).

Density differences of the above order have a definite effect on the flow of the fluids involved. Currents induced by or influenced by density differences are referred to as density currents.

2. Examples of density induced currents

2.1 Flow through culvert between reservoirs of different density

We consider a basin, which contains stagnant fresh water (density ρ). An other basin contains stagnant salt water (density $\rho + \Delta\rho$). The water surface in the fresh water basin is Δz higher than the water surface in the salt water basin. A short horizontal culvert connects both basins (see Fig. 1.1).

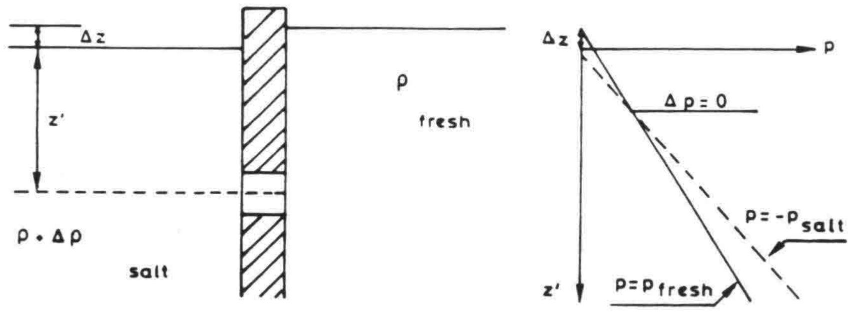

Fig. 1.1 Culvert between salt water and fresh water reservoirs

The direction of flow through the culvert depends on the distance z' between its axis and the water surface of the salt water reservoir. This is due to the effect of Δz on the hydrostatic pressure in the fresh water reservoir and that of $\Delta\rho$ on the hydrostatic pressure in the salt water reservoir. In formulae:

$$p_{fresh} = \rho g(z'+\Delta z) = \rho g z' + \rho g \Delta z$$

$$p_{salt} = (\rho+\Delta\rho)gz' = \rho g z' + \Delta\rho g z'$$

$$\Delta p = p_{fresh} - p_{salt} = \rho g \Delta z - \Delta\rho g z' \qquad (1.1)$$

where p_{fresh}: pressure in fresh water reservoir at level z'
p_{salt} : pressure in salt water reservoir at level z'
Δp : difference in pressure at level z'
g : acceleration due to gravity (10 m²/s)
(other symbols as explained in the text and Fig. 1.1)

If Δp is positive, the pressure in the fresh water reservoir at level z' is higher than the pressure in the salt water reservoir at this level. Then the flow through the culvert is from the fresh water reservoir to the salt water reservoir. The opposite applies when Δp is negative.

From Eq 1.1

$$\Delta p = 0 \qquad \text{for} \quad z' = \frac{\rho}{\Delta\rho}\Delta z \qquad (1.2)$$

For smaller values of z', than given by Eq 1.2, Δp is positive and the flow is from the fresh water reservoir to the salt water reservoir. For larger values of z', than given by Eq 1.2 Δp is negative and the flow is in the opposite direction.

For the value of z', given by Eq 1.2, in the upper part of the culvert there is a flow from the fresh water reservoir to the salt water reservoir, while in the bottom part of the culvert the flow is in the opposite direction (exchange flow).

As is illustrated graphically in Fig. 1.1, close to the water surface the direction of flow is determined by the difference in water level. At larger depth than given by Eq 1.2 the direction of flow is determined by the difference in density.

Some numerical values: for ρ = 1000 kg/m³, $\Delta\rho$ = 20 kg/m³ and Δz = 0.2 m, the flow through the culvert is from the fresh water reservoir to the salt water reservoir for z < 10 m and in the opposite direction for z' > 10 m. For z' = 20 m, u ≈ 2 m/s where u is the velocity of flow in the culvert.

2.2 Density induced exchange flows

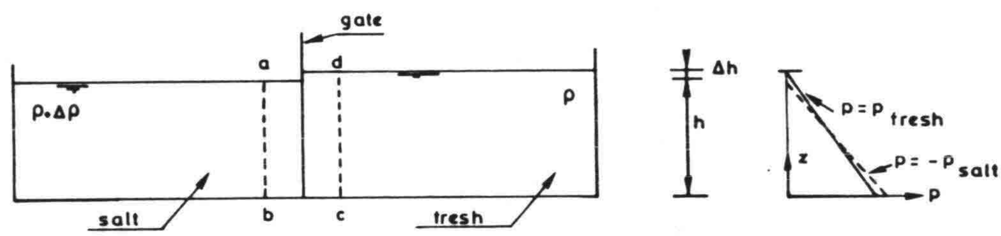

Fig. 1.2 Gate separating a fresh water reservoir from a salt water, density induced exchange flows occur when the gate is removed.

We consider a fresh water reservoir separated from a salt water reservoir by a gate. The water level of the fresh water reservoir is Δh higher than that of the salt water reservoir. This difference in water level has been selected so that the net force, due to the hydrostatic pressure on both its sides, acting on the gate is zero.

The force on the gate by the fresh water amounts to

$$F_{fr} = \tfrac{1}{2}\,\rho g(h+\Delta h)^2 \tag{1.3}$$

and that by the salt water

$$F_s = \tfrac{1}{2}(\rho+\Delta\rho)gh^2 \tag{1.4}$$

where F_{fr} : force on gate due to hydrostatic pressure acting on its fresh water side.

F_s : same acting on its salt water side

(other symbols as explained in the text and in Fig. 1.2)

F_{fr} being equal to F_s implies that when removing the gate, the net force acting on the element of fluid abcd (see Fig. 1.2) is zero. Hence, the depth averaged flow is zero when the gate is removed. However, as is illustrated graphically in Fig. 1.2, deriving Δp as explained in the preceding section, F_{fr} being equal to F_s implies that

$$\begin{array}{lll} \Delta p = p_{fresh} - p_{salt} > 0 & \text{if} & z > \tfrac{1}{2} h \\ \Delta p = 0 & \text{if} & z = \tfrac{1}{2} h \\ \Delta p < 0 & \text{if} & z < \tfrac{1}{2} h \end{array} \qquad (1.5)$$

where z: vertical coordinate (see Fig. 1.2)

Hence, removing the gate, an exchange flow is induced with a flow of fresh water into the salt water over the upper half of the depth and a flow of salt water into the fresh water over the lower part of the depth.

Fig. 1.3 gives a schematic picture of the density induced exchange flows produced when the gate is removed.

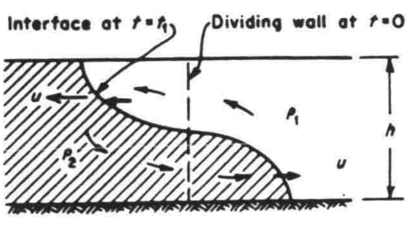

Fig. 1.3 Density induced exchange flow

Some numerical values: for ρ = 1000 kg/m^3 and $\Delta\rho$ = 25 kg/m^3 the velocity of propagation of the salt water front over the bottom and the fresh water front at the surface amounts 0.7 m/s for h = 10 m and 1.1 m/s for h = 20 m (Eq. 2.44).

2.3 Gravitational circulation

We consider a well mixed estuary with complete mixing over the depth. This assumption implies that the density does not vary over the depth. In a well mixed estuary the density varies with the distance from the mouth of the estuary, decreasing from the density of sea water to that of fresh water. Because of tidal action the density varies with time. In addition, because of tidal action the water depth varies both with the distance from the mouth of the estuary and with time. In formulae

$$\rho = f(x,t) \qquad\qquad h = f(x,t) \qquad (1.6)$$

where x : longitudinal coordinate (distance from mouth of estuary)
t : time

Density differences have a major effect on the estuarine flow because of their effect on the pressure. In an estuary the pressure is hydrostatic. For the considered well mixed estuary it is given by

$$p = \rho\, g\, (h + h_b - z) \qquad (1.7)$$

where z : vertical coordinate (see Fig. 1.4)
h_b: vertical coordinate of bottom (see Fig. 1.4)

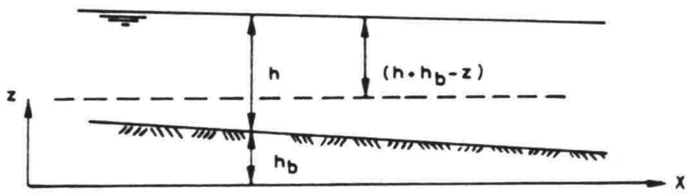

Fig. 1.4 Definition sketch for notation

If the pressure at level z on the seaward side of a given mass of water is larger than on the landward side, the difference in pressure will cause the mass of water to be subjected to a net landward force and therefore to a landward acceleration. In formula, the net landward force is given by

$$F_p = -\frac{1}{\rho}\frac{\partial p}{\partial x} \qquad (1.8)$$

where F_p: net landward force per unit mass of water caused by a variation of p with x.

If the pressure at the seaward side of a given mass of water is larger than that a the landward side and when x is positive in the landward direction, $\partial p/\partial x$ is negative. This explains the minus sign in Eq. 1.8 as both F_p and x are positive in the landward direction.

Differences between the pressure on either side of the considered mass of water may have two causes. Either there is a slope of the water surface or a difference in density. The essential difference between the two causes is that in the former case the difference in pressure is the same over the whole depth, whereas in the latter case the difference in pressure increases as the distance from the water surface, (h-z), increases. This difference is illustrated in Fig. 1.5 and it can be derived from Eq. 1.7 by differentiating the pressure p in the horizontal direction, keeping z constant.

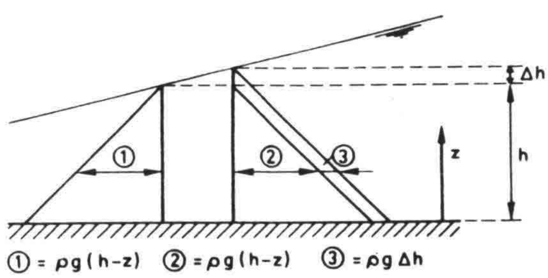

Fig. 1.5.a Pressure gradient caused by surface slope (constant density, horizontal bottom)

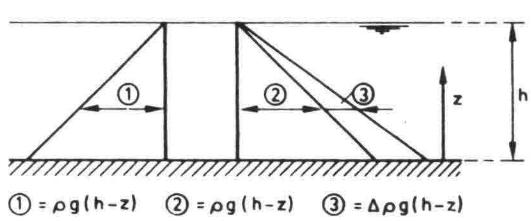

Fig. 1.5.b Pressure gradient caused by density gradient (well mixed estuary, horizontal bottom, horizontal water surface)

For a well mixed estuary satisfying Eq. 1.6 this procedure gives at any point in time

$$F_p = - g \frac{\partial(h+h_b)}{\partial x} - \frac{1}{\rho}(h+h_b-z)\, g \frac{\partial \rho}{\partial x} =$$

$$= \underset{(a)}{- g \frac{\partial(h+h_b)}{\partial x}} - \underset{(b)}{\frac{1}{\rho}\frac{1}{2}\, h\, g \frac{\partial \rho}{\partial x}} - \underset{(c)}{\frac{1}{\rho}(\frac{1}{2}\, h+h_b-z)\, g \frac{\partial \rho}{\partial x}} \qquad (1.9)$$

The instantaneous values of terms (b) and (c) of Eq. 1.9 are small compared with the instantaneous value of term (a). The ratio of term (b) over term (a) is of the order $\Delta\rho/\rho$. This also applies to the ratio of term (c) over term (a). Therefore the effect of term (a) on the instantaneous flow is dominant.

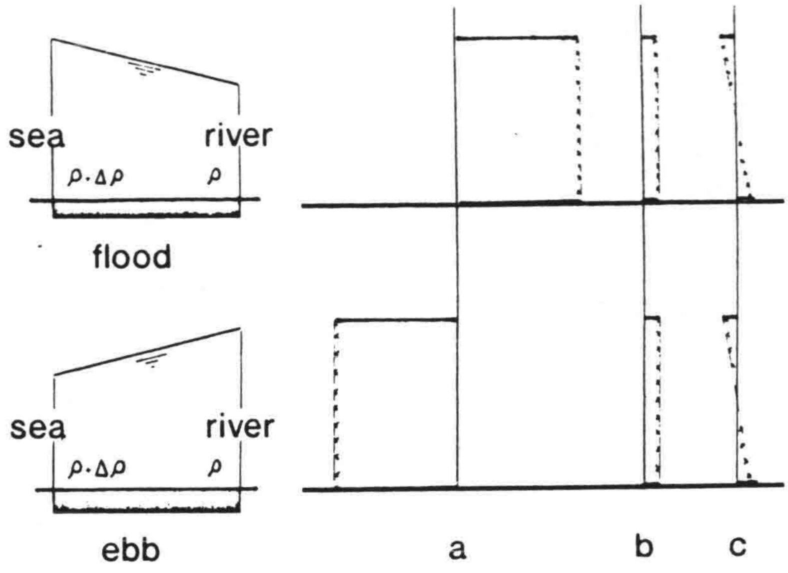

Fig. 1.6a Graphical representation of Eq. 1.9 causing gravitational circulation

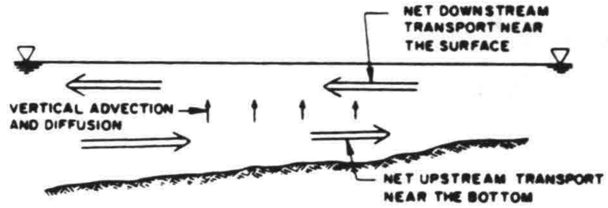

Fig. 1.6b Gravitational circulation in longitudinal direction (Fischer, 1976)

Fig. 1.6a gives the variation of h and ρ along the estuary and the variation of terms (a), (b) and (c) of Eq. 1.9 over the depth. Distinction is made between flood conditions and ebb conditions.

Term (a) represents the effect of the slope of the water surface on the net force acting on a unit mass of fluid. It does not vary over the depth. This explains why the tide, which causes the surface slope to change, accelerates the water equally over the depth. During flood $\partial h/\partial x$ is negative, therefore term (a) is positive (F_p in landward direction). During ebb $\partial h/\partial x$ is positive, and hence term (a) is negative (F_p in seaward direction).

Term (b) does not vary over the depth either. It represents the relatively small effect of density differences on the instantaneous depth-mean tidal flow. As the density decreases with increasing distance from the sea, $\partial \rho/\partial x$ is a negative quantity throughout the tidal cycle. Therefore, term (b) is positive throughout the tidal cycle (landward directed). Hence, its tidally-averaged effect may not be neglected compared with that of term (a), as the latter changes sign during the tidal cycle. Therefore, term (b) does have an effect on the tidally-averaged mean water depth.

Averaged over the depth, term (c) is equal to zero, meaning that it has no effect on the depth-mean tidal flow. However it varies linearly over the depth and therefore causes the velocity of flow to vary over the depth.
As $\partial \rho/\partial x$ is a negative quantity throughout the tidal cycle, term (c) does not change sign during the tidal cycle. Therefore, it has a dominant effect on the variation of the tidally-averaged flow over the depth. Throughout the tidal cycle, from the bottom to mid-depth ($0 < z < \frac{1}{2}h$) term (c) is positive, the water is subjected to a landward force and the tidally-averaged flow is in the landward direction. From mid-depth to the water surface ($\frac{1}{2}h < z < h$) throughout the tidal cycle term (c) is negative, the water is subjected to a seaward force and averaged over the tidal cycle the flow is in the seaward direction. This explains what is called the "gravitational circulation" as driving mechanism of the salt intrusion into rivers from the sea (Fig. 1.6b).

3. Vertical displacement of fluid; homogeneous fluid versus stratified fluid

3.1 Homogeneous fluid (Fig. 1.7)

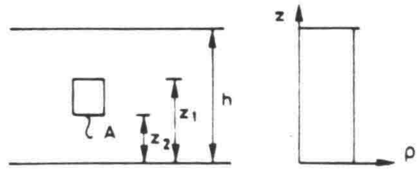

Fig 1.7 Hydrostatic pressure, homogeneous fluid

We consider an element of fluid with horizontal cross-section A, contained between the levels z_1, and z_2, in a homogeneous fluid of density ρ over the whole depth (see Fig. 1.7).

The pressure being hydrostatic, at levels z_1 and z_2 it is given by

$$p = \rho g\ (h-z_1) \qquad \text{at } z = z_1 \tag{1.10}$$
$$p = \rho g\ (h-z_2) \qquad \text{at } z = z_2$$

Hence, because of the hydrostatic pressure, acting on its upper and lower boundary, there is a net upward force, F_p, acting on the element given by

$$F_p = A\rho g(z_1 - z_2) \tag{1.11}$$

The volume of the element amounts to $A(z_1 - z_2)$. Hence, its weight, F_w, amounts to

$$F_w = A\rho g(z_1 - z_2) \tag{1.12}$$

Thus, when the fluid is homogeneous and the pressure is hydrostatic, the net upward force, F_p, acting on it is balanced by its weight. As this happens at all levels, under these conditions no energy is needed to lift or to lower the considered element of fluid.

3.2 Effects of stratification (Fig. 1.8)

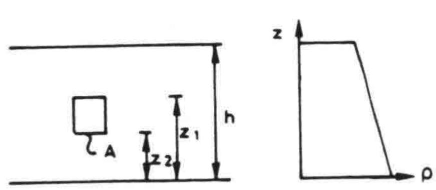

Fig. 1.8 Hydrostatic pressure, inhomogeneous fluid

When the element of fluid, considered in the previous section, is lifted or lowered in a stratified fluid it gets surrounded by fluid of a different density. Therefore, its weight is not balanced by the hydrostatic pressure acting on it and it is pushed back to its original position. This means that because of the stratification energy is needed to bring fluid from a given level with a given density to a different level with a different density.

3.3 Selective withdrawal, example of implications for flow

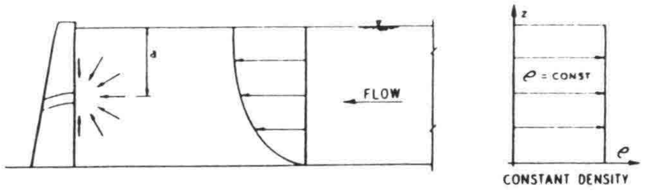

Fig. 1.9 a WITHDRAWAL FROM FULL DEPTH IN A HOMOGENEOUS FLUID

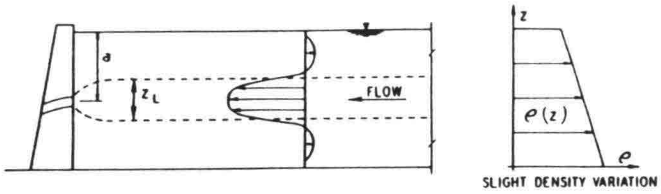

Fig. 1.9 b SELECTIVE WITHDRAWAL OF A FLUID WITH DENSITY VARIATION
EFFECT OF DENSITY VARIATION ON RESERVOIR VELOCITY DISTRIBUTION

Fig. 1.9 shows what happens when water is withdrawn from a reservoir, depending on whether the water in it is homogeneous or stratified.

When the density is constant (Fig. 1.9.a) at each level the weight of a given element of fluid is balanced by the net force by pressure acting on it. Hence, no energy is needed to lift a bottom element to the level of the outlet. Also no energy is needed to push a surface element down to the level of the outlet. Hence, when water is withdrawn from the reservoir by an outlet at mid depth, there is a flow towards the outlet over the full depth.

When the density varies over the depth (Fig. 1.9.b) the density of a bottom element of fluid is larger than the density of an element of fluid at the level of the outlet. Then energy is needed to lift a bottom element of fluid to the level of the outlet. The closer the bottom element gets to the level of the outlet the larger is the difference between its weigt and the net force by the pressure acting on it. For the same reason energy is needed to push a surface element of fluid down to the level of the outlet. Therefore, in this case the flow towards the outlet is concentrated in a zone of limited heigt (z_L in Fig.1.9.b). The larger the variation of density over the depth, the more energy is needed and the smaller is z_L. The smaller the discharge through the outlet, the smaller is the kinetic energy i.e. the energy which could cause mixing and the smaller is z_L.

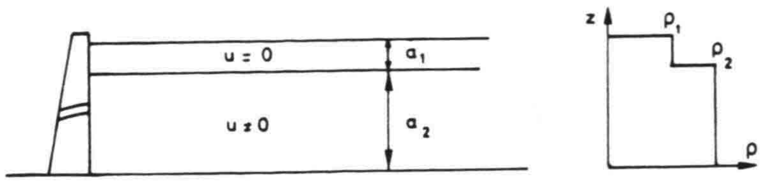

Fig. 1.9.c Selective withdrawal of lower layer fluid.

Fig. 1.9.c shows a system of a layer of heavy fluid (density ρ_2 and height a_2) underneath a layer of light fluid (density ρ_1 and height a_1). The interface is above the outlet. Then no energy is needed to bring lower layer fluid at the same level as the outlet, while energy has to be introduced to bring upper layer fluid down to the level of the outlet. Then, if the discharge through the outlet is sufficiently small, only water of the lower layer is withdrawn from the reservoir.

3.4 Implications for vertical mixing.

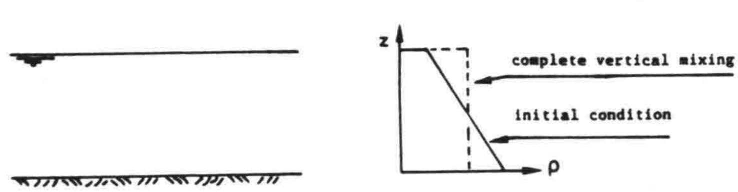

Fig. 1.10 Effect of vertical mixing

Fig. 1.10 shows the variation of density over the depth of a reservoir in its initial condition and after it has been mixed completely over the depth. In the initial condition there is heavy fluid near the bottom and light fluid near the surface and after the complete vertical mixing the fluid has the same weight over the whole depth. This means that after complete mixing the centre of mass of the fluid in the reservoir is at a higher level than in the initial condition. This means that potential energy must be supplied in order to eliminate or to reduce a stratification by vertical mixing.

Tidal currents may supply the energy required for vertical mixing in estuaries. The wind may do so for reservoirs.

4. Effects of density differences on flow

Density differences influence the hydrostatic pressure. Thereby they cause density induced exchange flows and tend to make the velocity distribution non-uniform over the depth. Both these effects have been shown by the examples given in Sections 2.2 and 2.3.

Density differences further cause stratification. Heavier fluid tends to spread under the lighter fluid (see example given in Section 2.2). Therefore, the density of a stratified body of water increases with depth (i.e with increasing distance from the surface).

When the density varies with depth, energy is needed to bring fluid from a given level with given density to a different level with a different density. As explained in Section 3, this may influence the flow and hampers vertical mixing.

5. Effects on transport processes

Flowing water may carry sediments, other natural substances or pollutants. These constituents move with the water and therefore are transported by the flow. While being transported, they may be mixed with surrounding water.

Density differences may have a considerable effect on these transport processes. Because of density induced currents the direction of flow, and therefore the direction of transport, may vary over the depth. There is less vertical mixing in density stratified water than there is under homogeneous conditions.

Because of the above reasons, density currents are a factor to be considered for instance when studying the sedimentation in estuaries or the transport of pollutants through estuaries (Fig. 1.6).

Within the above context distinction has to be made between active substances, which influence the density of the water and passive substances, which do not.

6. Classification of density currents

Density currents can be classified with respect to the degree of stratification (see Fig. 1.11).

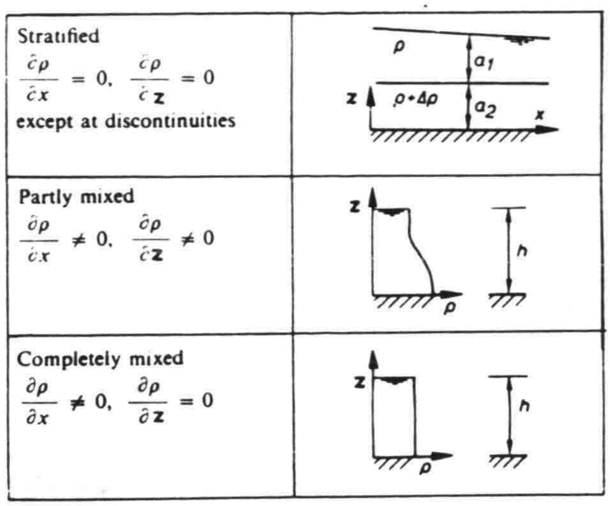

Fig. 1.11 Classification of density currents

6.1 Stratified flow (or two-layer flow)

Stratified flows (or two-layer flows) involve the flow of two super-imposed layers, each of constant density seperated by a distinct interface. They occur when there is little or no energy available to cause vertical mixing between both layers.

6.2 Partly mixed flow

Partly mixed flow systems are charaterized by gradually varying density, both in horizontal and vertical direction. They occur when there is enough energy to cause some vertical mixing but not enough for complete vertical mixing.

The effect of stratification on vertical mixing is an important factor, when studying partly mixed flows.

6.3 Completely mixed flow

Completely mixed flow systems are characterized by a constant density in vertical sense, while the density varies in the horizontal direction. They occur when there is enough energy to cause complete vertical mixing. The mixing being complete means that the effect of stratification on vertical mixing has been eliminated.

In completely mixed flows there is an effect of the horizontal density gradients on the hydrostatic pressure. In this respect they are different from homogeneous flow.

7. Factors causing density differences; engineering significance

Table 1.1 Factors causing differences in density

cause of differences in density	characterizing quality of fluids involved	examples of flows due to the differences in density considered	significance for engineering purposes
1. Difference in fluids a. non-miscible b. miscible	 no mixing at interface mixing at interface	 spreading of oil over water	 oil pollution, protection of intakes
2. Same fluids, difference in salt content $\frac{\Delta\rho}{\rho} < 3\%$	mixing at interface	flow phenomena in estuaries exchange flows in navigation locks along coast	salt water intrusion in rivers, siltation, navigability of harbour entrances, salt water intrusion through locks mooring forces due to exchange flows
3. Same fluids, difference in temperature $\frac{\Delta\rho}{\rho} < 5\,^{0}/_{00}$	heat transfer at watersurface and interface	spreading of heated cooling water over cold water, density flows through reservoirs	how to avoid short circuiting of cooling water
4. Same fluids, difference in concentration of solid matter	settling of particles	density flows through reservoirs, mud flocs	siltation

Table 1.1 shows factors which cause density differences and the engineering significance of the density currents which they induce. For some cases the engineering significance is elaborated upon in the following sub-sections.

7.1 Salt intrusion into fresh water reservoirs

We consider a navigation lock, which connects an inland fresh water reservoir and a body of salt water which is in open connection with the sea. We assume that initially the inner gate is opened and the outer gate is closed. In this situation the outer gate acts as a partition between fresh water in the lock and the salt water outside of it. When, in order to let navigation through, after closing the inner gate the outer gate is opened, the limited amount of fresh water in the lock chamber tends to spread over the salt water outside the lock. Initially this results in an exchange flow as shown in Fig. 1.3. When the outer gate is left open long enough, eventually a two-layer system is formed, the limited amount of fresh water forming a thin upper layer on top of the salt water (both in the lock chamber and outside of it), while the fresh water originally in the chamber has been almost completely replaced by salt water.

Then, when the outer gate is closed and the inner gate is opened, the limited amount of salt water in the lock chamber tends to spread over the bottom underneath the fresh water in the deeper parts of the fresh water reservoir. When the inner gate stays open long enough, the salt water originally in the lock chamber has been almost completely replaced by fresh water, except for a thin layer near the bottom. So, each time the lock is opened and shut, therefore, a quantity of salt water equal to the capacity of the lock-chamber (minus the volume of the ships) intrudes into the fresh water reservoir.
An equal quantity of fresh water is carried out to sea and lost for beneficial uses. In addition, wind induced or ship induced mixing between the fresh water and the underlying salt water may lead to salt pollution of the fresh water reservoir.

Leakage of salt water through gates, separating a fresh water reservoir from salt water may have a similar effect. The leakage may occur, even when the surface of the fresh water is at a higher level than that of the salt water. The leakage can be prevented by making this difference in level so large that Δp (Eq. 1.1) is positive over the whole height of the gate.

7.2 Salt intrusion into estuaries

Gravitational circulation is the driving mechanism for salt intrusion into estuaries, as is explained for well mixed estuaries in Section 2.3. Whether the mixing is complete or partial depends on the strength of the tide, which supplies the energy needed for mixing. If mixing is partial, there still will be density differences due to the differences between the salinity of the water near the surface and that on the river bed. If mixing is complete, the differences between the salinity at the surface and that at the bottom are negligible.

Salt intrusion may lead to salt pollution of fresh water intakes located along the estuary. The salt water can intrude further when the depth is made large or the river flow is made small. Therefore, this type of pollution may result from deepening the mouth of an estuary for navigation purposes or extracting river water upstream along the river for irrigation purpose.

In the area with salt intrusion, because of the gravitational circulation the time averaged flow over the bed is landwards. In the fresh water area further upstream the time averaged flow over the bed is seawards. Both areas are separated by a "null point" with a seaward time averaged flow over the whole depth, except near the bed where it is zero (Fig. 1.12).

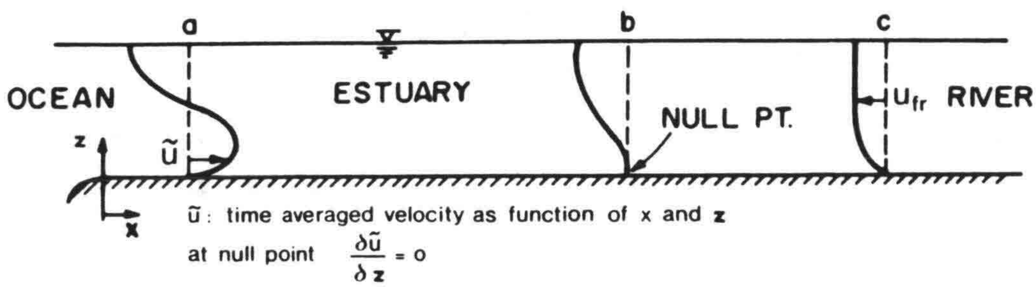

Fig. 1.12 Effect of salinity upon vertical distribution of velocity (Harleman and Ippen, 1969)

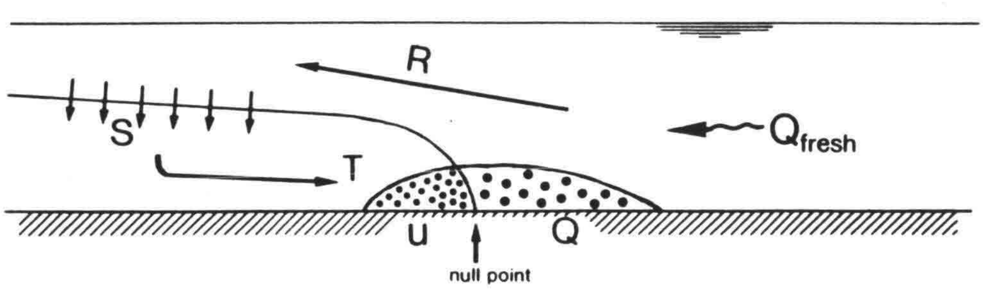

Fig. 1.13 Significance of null point in problems of shoaling (Harleman and Ippen, 1969)

Fig. 1.13 explains the significance of the null point in connection with sedimentation

- the river may bring coarse and fine material seaward,
- coarse material gets collected in zone Q,
- fine material may be transported as indicated by R,
- fine material may flocculate, flocs may fall through interface as indicated by S (see van Leussen (1988) for the effect of salinity on flocculation and settling velocity of flocs),
- fine material falling through the interface will be brought to zone U by predominantly landward flow as indicated by T,
- zone U is also the area where material brought from the sea tends to be collected.

Consequently, the maximum concentration of suspended sediment is found at the bottom near the null point, where siltation tends to occur (Ippen and Harleman (1969), Dyer (1988)).

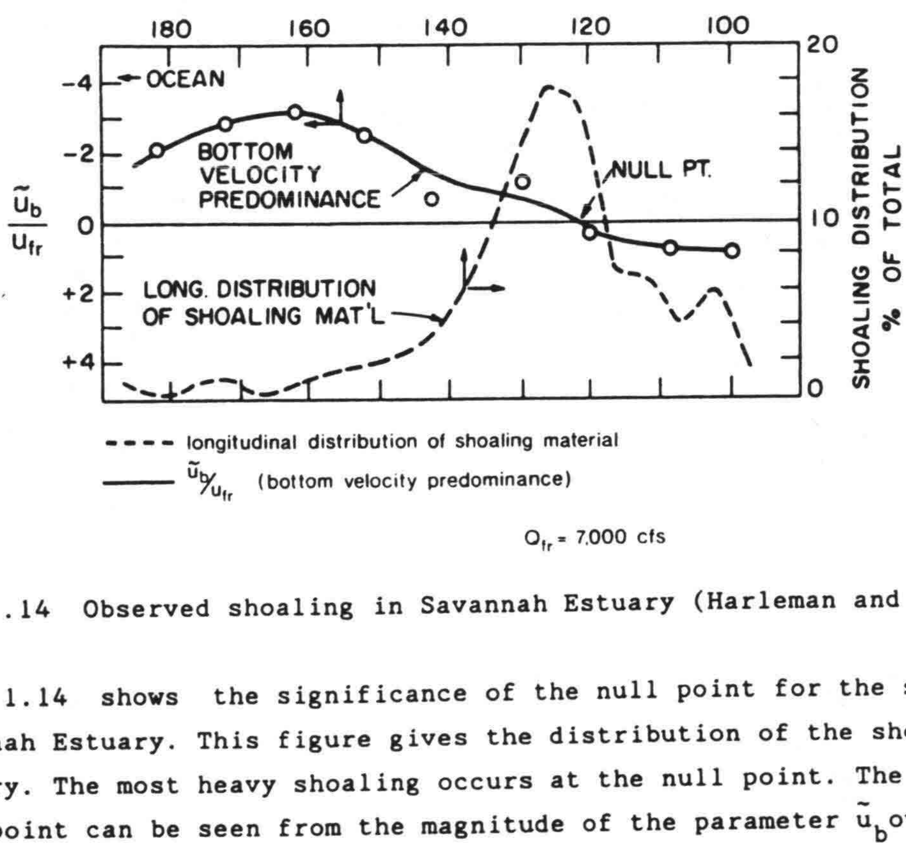

Fig. 1.14 Observed shoaling in Savannah Estuary (Harleman and Ippen, 1969)

Fig. 1.14 shows the significance of the null point for the siltation in the Savannah Estuary. This figure gives the distribution of the shoaling along the estuary. The most heavy shoaling occurs at the null point. The location of the null point can be seen from the magnitude of the parameter $\tilde{u}_b$ over u_{fr}, where $\tilde{u}_b$ is the time mean value of the velocity at the bottom and where u_{fr} is the river discharge over the cross-section.

The residual circulation, represented in Figs. 1.6 and 1.12 explains the association of the null point and the turbidity maximum with the salt intrusion and its movement in response to changes in river flow and tidal range.

7.3 Density currents through reservoirs

Figs. 1.15 and 1.16 show density currents through a reservoir. Density currents of the type of Fig. 1.15 influence the temperature regime of the reservoir, density currents of the type of Fig. 1.16 the siltation.

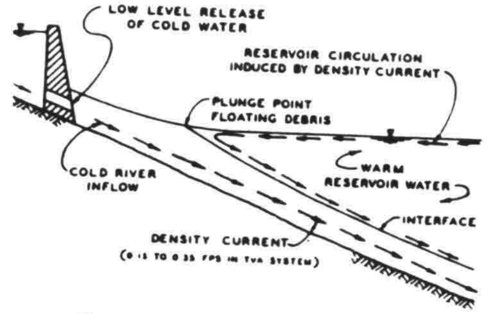

Fig. 1.15 **Upstream end of reservoir showing formation of density current due to low level release of cold water from upstream storage dam.**

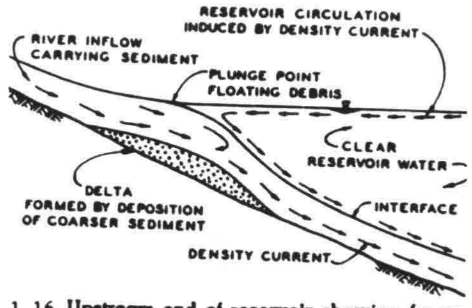

Fig. 1.16 **Upstream end of reservoir showing formation of density current due to sediment load.**

7.4 Case study: siltation of the Port of Cochin

Fig. 1.17 shows the Port of Cochin, located in the southern part of India. Sedimentation occurs both in the approach channel outside the Gut i.e. the entrance to Cochin Backwaters and the navigation channels inside the Gut near Willington Island.

The siltation in the navigation channels inside the Gut is primarily due to material derived from the sea, rather than from the rivers. Most of the siltation in the channels occurs during the wet monsoon, when the silt concentration at sea is high due to the prevailing winds.

Within the above schematization, the material settled inside must have been carried in by water flowing in from the sea through the Gut.

Available field data (Fig. 1.18) (Naik et al, 1983) show that during the wet monsoon the discharge of the rivers into the Cochin Backwaters is so large that a difference in density is maintained over the Gut with salt water at sea and depending on the stage of the tide almost fresh water inside the Gut. (Fig. 1.18, 2.00-12.00 hrs). Under these conditions fresh water flows out in the ebb direction over the whole tidal cycle, while the inflow of salt water from the sea is primarily due to density currents (Fig. 1.18). This means that a significant part of the siltation inside the Gut is due to density currents.

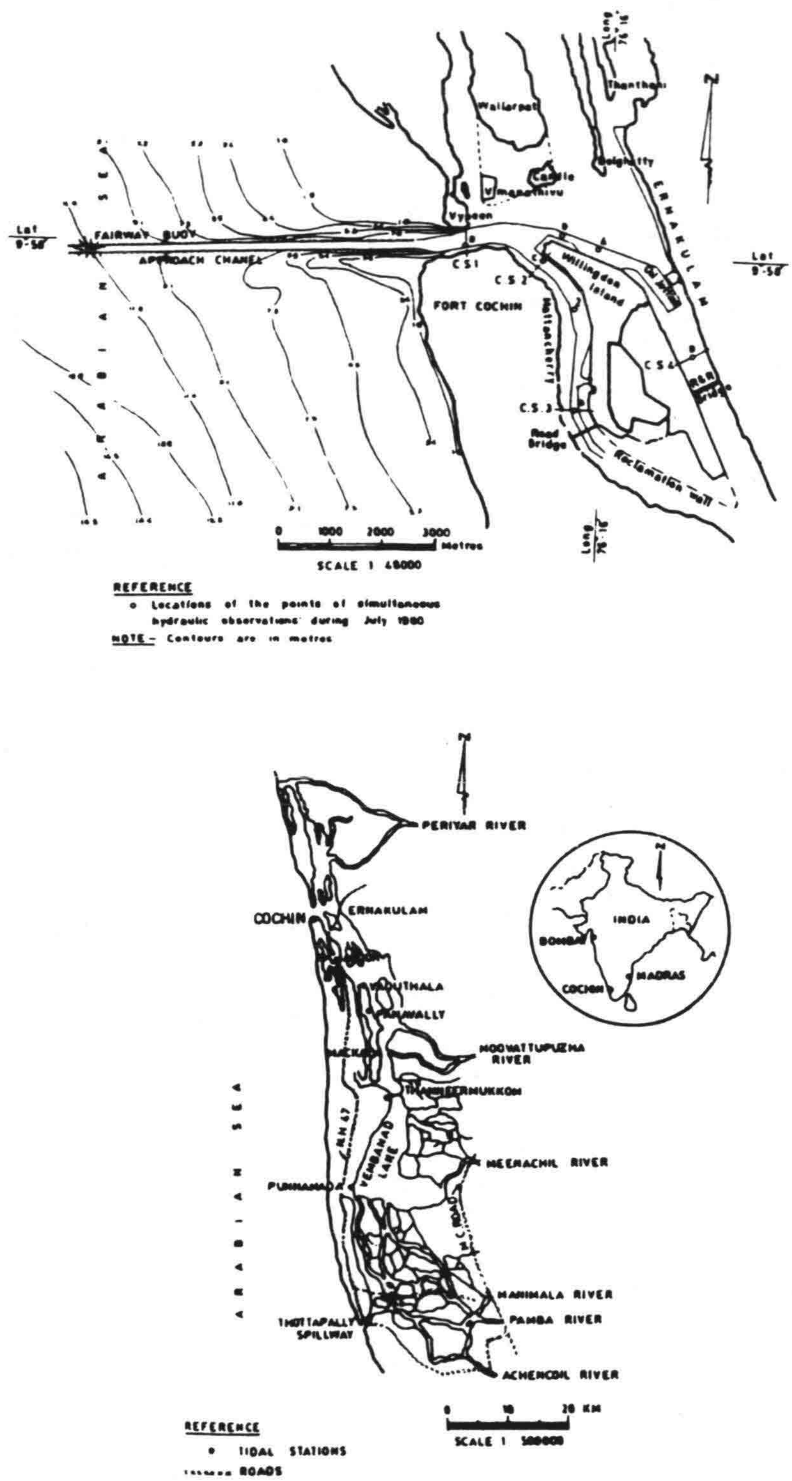

Fig. 1.17 General plan for Cochin Harbour and Cochin Backwaters (After Naik et al, 1983)

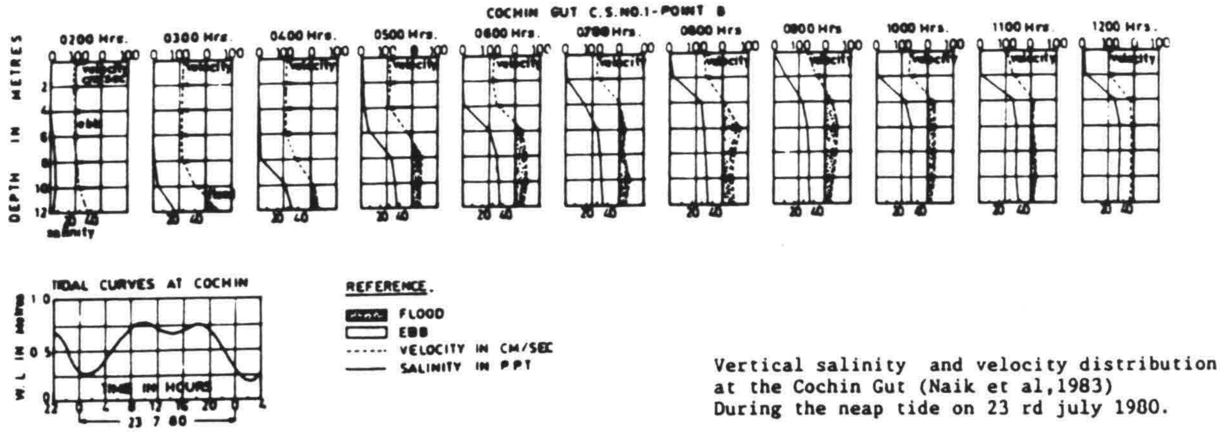

Fig. 1.18 Vertical salinity and velocity distribution at the Cochin Gut (Naik et al, 1983).

8. References

8.1 Density currents (general)

Harleman, D.R.F. Stratified Flow. Chapter 26, Handbook of Fluid Dynamics, Edited by V.L. Streeter, Mc Graw-Hill, New York (1961).

Proceedings of the international symposium on stratified flows (1973). Held at Novosibirsk, U.S.S.R. in 1972, published by ASCE, New York, N.Y.

Proceedings of the second international symposium on density stratified flows. (1980). Held at the Norwegian Institute of Technology, Trondheim, Norway, published by Tapir, Norway.

Third Internaional symposium on stratified flows. (1987). Held at California Institute of Technology at Pasadena, Calif. on Feb 3-5, 1987, published by Reidel Publishing Co., Dordrecht, The Netherlands (in press).

The proceedings of the third international symposium on stratified flows are summerized by:
Jirka, G,H, and List, E.J., Third international symposium on stratified flows. Journal of Hydraulic Engineering, American Society of Civil Engineers, Vol. 114, no. 2, February 1988, pp 125-13.

8.2 Density currents (fundamental aspects)

Turner, J.S. Buoyancy effects in fluids. Cambridge University Press. (1973).

Yih, C.S. Stratified flows. Academic Press, New York (1980).

8.3 Hydraulic transport processes (general)

Fischer, H.B., List E.J., Koh, R.C.Y., Imberger, J. and Brooks N.H. Mixing in inland and coastal waters. Academic Press, New York (1979).

8.4 Estuaries

Dyer, K.R. Estuaries, a physical introduction. J. Wiley, London (1973).

Mc Dowell, D.M., O´Connor, B.A. Hydraulic behaviour of estuaries, Mc Millan, London (1977).

Ippen, A.T. (editor). Estuary and Coastline Hydrodynamics. Mc Graw-Hill, New York (1966).

Fischer, H.B., Mixing and dispersion in estuaries, Annual Review of Fluid Mechanics, 8, 1976, pp 107-133

Chapter 7 of Fischer et al. (1979); see item 8.3.

Dronkers, J. and van Leussen, W. (editors), Physical processes in estuaries, Springer, Berlin (1988)

8.5 Shoaling of estuaries

Dyer, K.R., Fine sediment particle transport in estuaries, in Physical processes in estuaries, Dronkers, J. and van Leussen, W. (eds), Springer, Berlin (1988)

Fischer, H.B., Mixing and dispersion in estuaries, Annual Review of Fluid Mechanics, 8, 1976, pp 107-133

Harleman, D.R.F. and Ippen, A.T., Salinity intrusion effects in estuary shoaling, Proceedings American Society of Civil Engineering, Journal of Hydraulics Division, January, 1969, pp. 9-27

Leussen, W.van, Aggregation of particles, settling velocity of mud flocs: A review, in Physical processes in estuaries, Dronkers, J. and van Leussen, W. (eds), Springer, Berlin (1988)

8.6 Exchange flows

Rigter, B.P., Density induced return currents in outlet channel, Proceedings American Society of Civil Engineers, Journal of Hydraulic Division 96, No. HJ 2, 1970, pp. 529-546.

Simpson, J.E., Gravity currents; in the environment and the laboratory, Ellis Horwood Ltd, Chichester (1987)

8.7 Reservoirs

Chapter 6 of Fischer et al. (1979); see item 8.3.

8.8 Case study: siltation of the Port of Cochin

Naik A.S., Kankere V.H. and Vaidyaraman P.P. (1983), Effect of salinity and siltation in the Cochin Port, Proceedings of International Conference on Coastal and Port Engineering in Developing Countries, Colombo, March 20-26, pp. 1148-1159

Chandramohan P.V. (1989), Density currents and siltation with particular reference to Cochin, Master of science thesis, International Institute for Hydraulic and Environmental Engineering.

Appendix: Density of sea water

The density and the conductivity of sea water depend on the salt content and the temperature. The density and the salt content can be determined by simultaneous measurement of the conductivity and the temperature.

1. Density as a function of salt content and temperature

The salt content is either expressed in the salinity (symbol S) or the chlorinity (symbol Cl). The salinity is a measure for all dissolved salts, the chlorinity for the dissolved chloride ions only. The salinity and the chlorinity are defined as the mass of respectively all dissolved salts or the chloride fraction of it per unit mass of sea water. According to this definition the salinity and density are expressed as a mass ratio in the unit $^{\circ}/_{\circ\circ}$ (or ppt.). The density of undiluted sea water is about 1025 kg/m³. Hence a liter of sea water weights about 1.025 kilogramme. Therefore, in first approximation, instead of the unit $^{\circ}/_{\circ\circ}$ (or ppt.), the unit ~~milli~~grammes (weight) per liter may be used. ✱

The composition of the sea water differs little from the one location to another. Therefore the ratio between the salinity and chlorinity can be taken as being constant ($S \approx 1.807\ Cl$).

Fig. A1 gives the density difference with respect to fresh water with a temperature of 4°C as a function of salt content and temperature.

For $0 < S < 40$ ppt and $0 < T < 35°C$ the relationship between density, salt content and temperature may be expressed as (maximum error less than $5\ 10^{-2}\ kg/m^3$)

geldt voor NaCl ?
zeewater ← UNESCO-[illegible]

$$\rho = 999.846 + 6.124\ 10^{-2} T - 8.044\ 10^{-3} T^2 + 4.44\ 10^{-5} T^3 + 8.072\ 10^{-1} S - 3.073\ 10^{-3} S\ T + 3.34\ 10^{-5} S\ T^2 \quad \text{(A.1)}$$

For engineering purposes

$$(\Delta\rho)_T \approx 0.78\ S \approx 1.41\ Cl \quad \text{(A.2)}$$

where ρ : density in kg/m³
S : salinity in ppt
Cl : clorinity in ppt

T : temperature in °C

$(\Delta\rho)_T$: difference in density between water with dissolved salts with given temperature and water without dissolved salts and same temperature in kg/m³.

For $0 < S < 40$ ppt and $0 < T < 35$°C the $(\Delta\rho)_T$ values given by Eq A.2 vary between 1.05 and 0.95 times the values given by Eq A.1

2. Data of some seas

Red Sea	: mean salinity 40 °/₀₀
Mediterranean Sea	: mean salinity 38-39 °/₀₀
Atlantic and Pacific	: mean salinity 34-35 °/₀₀
North Sea	: mean salinity 31 °/₀₀
Black Sea	: mean salinity 22 °/₀₀

3. Density and salt content as a function of conductivity and temperature

The density and the salt content are often measured indirectly by simultaneous measurement of the conductivity and the temperature. Fig. A2. gives the relationship between the former parameters and the latter. Fig. A2 shows clearly that both the conductivity and the temperature must be measured in order to determine the density and salt content.

The dimension of the conductivity is resistance $^{-1}$ length^{-1}. It controls the resistance between two electrodes of equal size when an electric current passes through the water from the one electrode to the other. In formula

$$R = \frac{1}{\kappa_t}\frac{L}{A} \tag{A.3}$$

where R : resistance between electrodes (Ohm)

κ_t: conductivity (Ohm $^{-1}$ length^{-1})

L : distance between electrodes

A : surface area of electrodes

References

Dietrich, G. und K. Kalle, Allgemeine Meereskunde, 1957, Borntraeger, Berlin, p 45

Fischer, H.B., List, E.J., Koh, R.C.Y., Imberger, J. and Brooks N.H., Mixing in inland and coastal waters. Academic Press New York, 1979, Appendix A. An Estimator for the density of sea water.

Landolt-Börnstein, Zahlwerte und Functionen aus der Physik, Chemie u.s.w. 6 Aufl Band II/7, 1935, pp. 128-129.

Millero, F.J., Gonzalez, A. and Ward, G.K., The density of sea water solutions at one atmosphere as a function of temperature and salinity, Journal of Marine Research, 34, 1976, no 1, pp. 61-93.

Reebrugh, W.S. Measurements of the electrical conductivity of seawater, Journal of Marine Research 23, 1965, no. 3, pp 187-199.

Unesco, Technical papers in marine science, no.37 (1981).

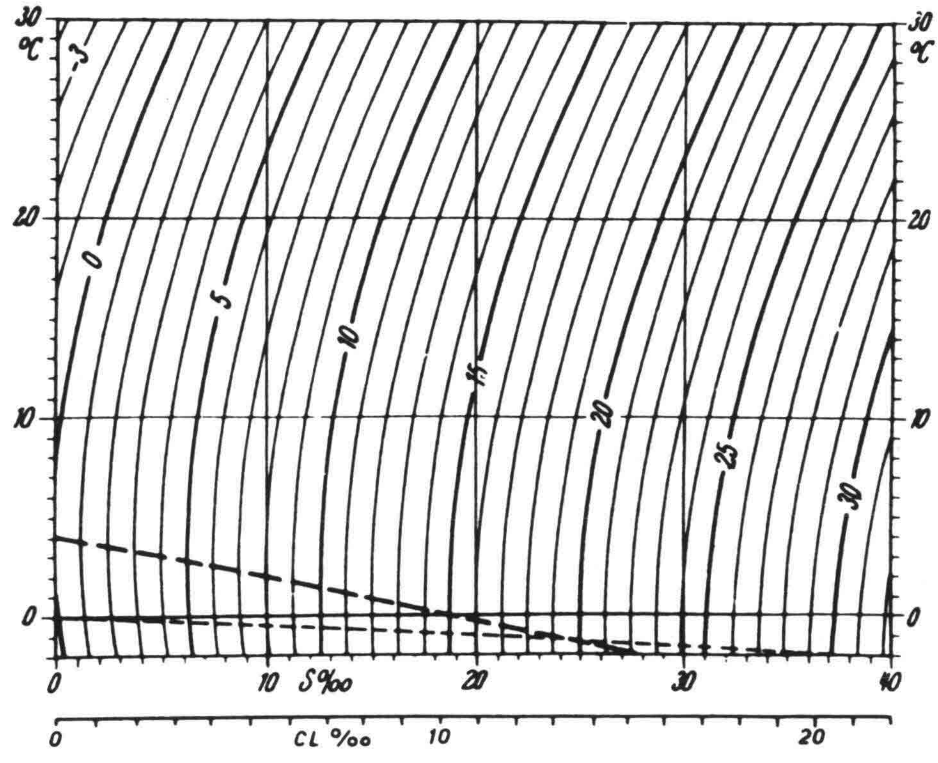

Fig. A.1 Density of sea water as function of temperature and salinity (numbers in curved lines refer to density minus density of pure water (S = 0) of 4°C, i.e. ρ −1000 in kg/m³. (after Dietrich and Kalle, 1957)

– – – – – – temperature where density has maximum value

----------- freezing point

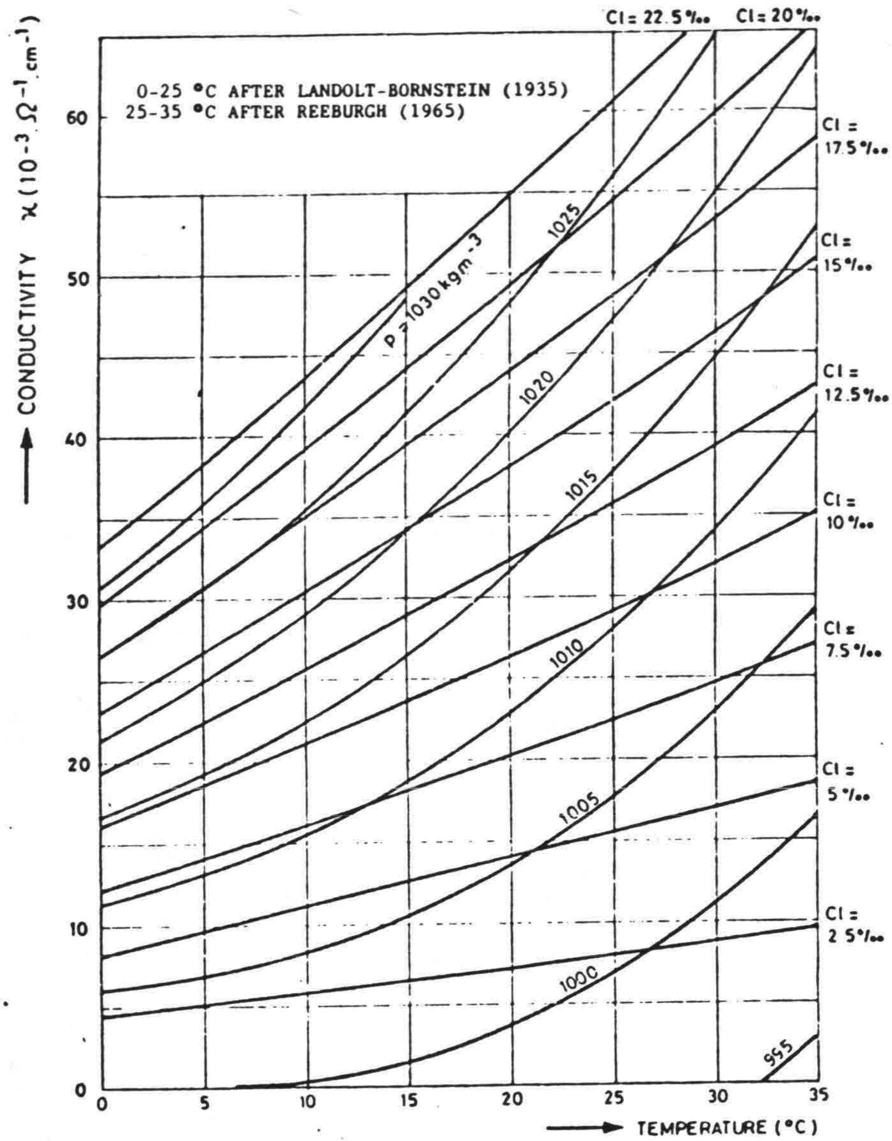

Fig. A.2 Conductivity and density as function of temperature and chlorinity.

Chapter 2, Two-layer flow

1.Notation

This chapter deals with the two-layer flow as defined in Section 6.1, Chapter 1, assuming that there is no mixing through the interface.

The notation and coordinate systems used are in accordance with Figs. 2.1 and 2.2.

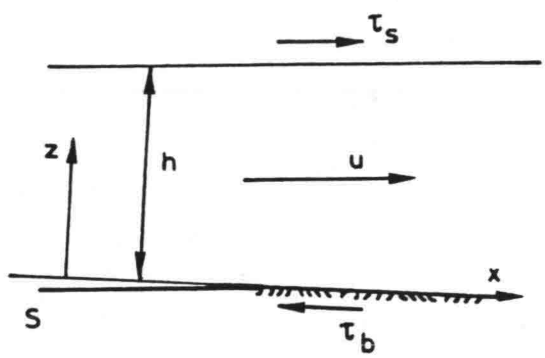

Fig. 2.1 Homogeneous flow

τ_s: by air(wind) on water
τ_b: by bottom on water

$\cos S \approx 1$
$\sin S \approx S$

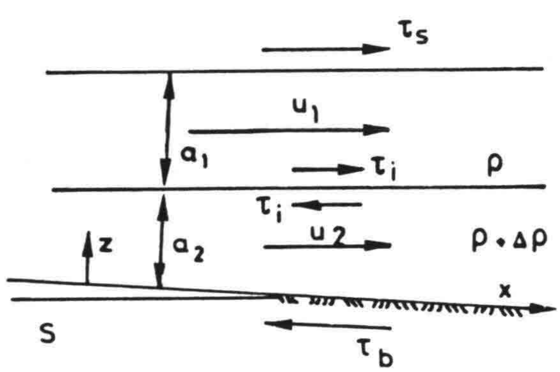

Fig. 2.2 Two-layer flow

τ_s: by air(wind) on upper layer
τ_i: by upper layer on lower layer (in + x-direction)
τ_i: by lower layer on upper layer (in - x direction)
τ_b: by bottom on lower layer

$\cos S \approx 1$ $\sin S \approx S$

2. Equations of continuity

For homogeneous flow the continuity equation reads

$$\frac{\partial h}{\partial t} + \frac{\partial uh}{\partial x} = 0 \tag{2.1}$$

where u: depth averaged horizontal velocity
h: water depth
x: horizontal coordinate
t: time

It states that there is no flow of fluid through the water surface and the bottom.

In a similar manner the continuity equation for the upper layer expresses that there is no flow of upper layer fluid through the water surface and the interface. Hence, the continuity equation for the <u>upper layer</u> can be obtained from that for homogeneous flow replacing h and u by a_1 and u_1, the thickness and velocity of the upper layer. In formula

$$\frac{\partial a_1}{\partial t} + \frac{\partial a_1 u_1}{\partial x} = 0 \qquad (2.2)$$

where a_1: thickness of upper layer
u_1: horizontal velocity averaged over thickness of upper layer.

Using the above procedure for the <u>lower layer</u>, one finds

$$\frac{\partial a_2}{\partial t} + \frac{\partial a_2 u_2}{\partial x} = 0 \qquad (2.3)$$

where a_2: thickness of lower layer
u_2: mean velocity of lower layer.

3. Equations of motions

For <u>homogeneous flow</u> the equation of motion reads

$$\frac{\partial u}{\partial t} + u\frac{\partial u}{\partial x} = -g\frac{\partial h}{\partial x} - \frac{(\tau_b - \tau_s)}{\rho h} + g\,S \qquad (2.4)$$

where τ_b: bottom shear stress (positive when directed as indicated in Fig. 2.1)
τ_s: surface shear stress (due to wind) (positive when directed as indicated in Fig. 2.1)

It states that the acceleration (at left hand side) is equal to the force per unit mass (at right hand side) . The force per unit mass is due to the surface slope (through the gradient of the hydrostatic pressure), the shear stresses and the bottom slope.

For homogeneous flow the hydrostatic pressure is given by

$$p = \rho g \ (h-z) \tag{2.5}$$

where z : vertical coordinate (see Figs. 2.1 and 2.2)

Hence

$$\frac{1}{\rho} \frac{\partial p}{\partial x} = g \frac{\partial h}{\partial x} \tag{2.6}$$

Eq. 2.6 explains how the surface slope, $\partial h/\partial x$, enters into Eq. 2.4

For the two-layer flow the hydrostatic pressure is graphically given in Fig. 2.3.

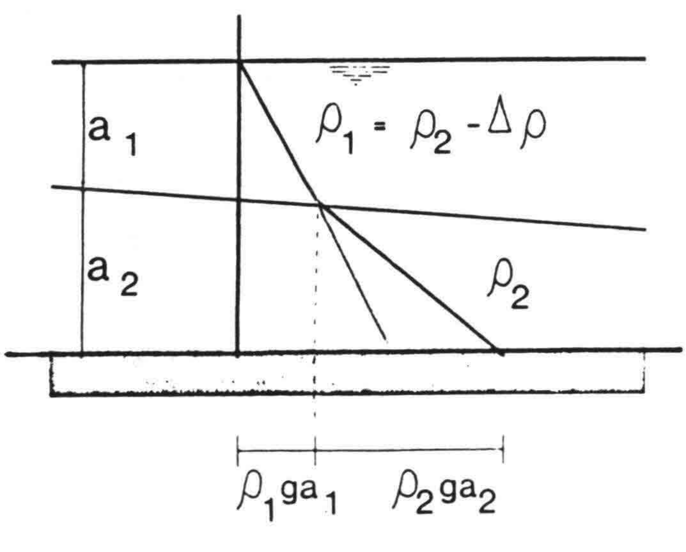

Fig. 2.3 Hydrostatic pressure distribution in two-layer flow

For the upper layer the hydrostatic pressure is given by

$$p = \rho_1 g \ (a_1 + a_2 - z) \qquad (z > a_2) \tag{2.7}$$

and

$$\frac{1}{\rho_1}\frac{\partial p}{\partial x} = g\,\frac{\partial(a_1+a_2)}{\partial x} \tag{2.8}$$

where ρ_1: density of upper layer

Hence, for the <u>upper layer</u>

$$\frac{\partial u_1}{\partial t} + u_1\frac{\partial u_1}{\partial x} = -\,g\,\frac{\partial(a_1+a_2)}{\partial x} - \frac{(\tau_i-\tau_s)}{\rho a_1} + g\,S \tag{2.9}$$

where τ_i: interfacial shear stress (positive when directed as indicated in Fig. 2.2)

τ_s: surface shear stress (positive when directed as indicated in Fig. 2.2)

For the upper layer the gradient of the hydrostatic pressure is due to the surface slope, $\partial(a_1+a_2)/\partial x$, only. This explains the similarity between Eqs. 2.4 and 2.9.

A different situation arises for the lower layer. For this layer the hydrostatic pressure satisfies

$$p = \rho_1 g\,a_1 + \rho_2\,g(a_2-z) = \rho_2 g(a_1+a_2-z) - \Delta\rho\,g(a_1+a_2) + \Delta\rho\,g\,a_2 (z < a_2) \tag{2.10}$$

where ρ_2: density of lower layer

$\Delta\rho = \rho_2 - \rho_1$

Accordingly

$$\frac{1}{\rho_2}\frac{\partial p}{\partial x} = (1 - \frac{\Delta\rho}{\rho_2})\,g\,\frac{\partial(a_1+a_2)}{\partial x} + \frac{\Delta\rho}{\rho_2}\,g\,\frac{\partial a_2}{\partial x} \tag{2.11}$$

For the lower layer the gradient of the hydrostatic pressure is due to both the surface slope, $\partial(a_1+a_2)/\partial x$, and the slope of the interface, $\partial a_2/\partial x$.

Hence for the <u>lower layer</u>

$$\frac{\partial u_2}{\partial t} + u_2\frac{\partial u_2}{\partial x} = -\,(1 - \frac{\Delta\rho}{\rho_2})\,g\,\frac{\partial(a_1+a_2)}{\partial x} - \frac{\Delta\rho}{\rho_2}\,g\,\frac{\partial a_2}{\partial x} - \frac{(\tau_b-\tau_i)}{\rho_2 a_2} + g\,S \tag{2.12}$$

4. Summary

4.1 Homogeneous flow

For homogeneous flow the following equations are well known

equations	unknowns
continuity equation (2.1) equation of motion (2.4)	h, u h, u, τ_b, τ_s
2 equations	4 unknowns

To make the number of equations equal to the number of unknowns τ_b must be expressed in h and u and τ_s in the wind velocity.

For homogeneous flow the bottom shear stress can be expressed in the Chézy coefficient.

$$\tau_b = \rho\ g\ \frac{u^2}{C^2} \tag{2.13}$$

where C : Chezy coefficient.

The magnitude of the Chezy coefficient can be found from textbooks as a function of the bottom roughness, the hydraulic radius and the Reynolds number of the flow.

Information on the relationship between the wind velocity and the wind shear stress acting at the water surface is given by Smith and Banks (1975).

4.2 Two-layer flow

equations	unknowns
continuity equation upper layer (2.2) continuity equation lower layer (2.3) equation of motion upper layer (2.9) equation of motion lower layer (2,12)	a_1, u_1 a_2, u_2 a_1, u_1, a_2, τ_i, τ_s a_1, a_2, u_2, τ_i, τ_b
4 equations	7 unknowns

To make the number of equations equal to the number of unknowns τ_i and τ_b must be expressed in a_1, a_2, u_1 and u_2 and τ_s in the wind velocity.

Dealing with two-layer flow, it is common to express τ_b and τ_i as

$$\tau_b = k_b \rho_2 \, u_2 \, |u_2| \tag{2.14}$$

and

$$\tau_i = k_i \rho \, (u_1 - u_2) \, |u_1 - u_2| \qquad \text{or} \tag{2.15^a}$$

$$\tau_i = k_{i,i} \rho \, (u_1 - u_2) \, |u_1 - u_2| + k_{i,b} \rho u_2 \, |u_2| . (\frac{a_1}{a_1 + a_2}) \tag{2.15^b}$$

where k_b : coefficient of bottom shear stress

k_i : coefficient of interfacial shear stress

$k_{i,i}$: coefficient of interfacial shear stress due to turbulence generated at the interface

$k_{i,b}$: coefficient of interfacial shear stress due to turbulence generated at the bottom

ρ : density (either of upper layer or lower layer, assuming $\Delta\rho/\rho_2 << 1$)

The coefficient of bottom shear stress is related to the Chezy coefficient

$$k_b = \frac{g}{C^2} \tag{2.16}$$

The coefficient k_b can be derived from the information on the Chezy coefficient for homogeneous flows, using the hydraulic radius and the Reynolds number of the lower layer instead of those of the homogeneous flow.

For field conditions ($Re > Re_{cr}$) the order of magnitude of C amounts to 60 $m^{1/2}s^{-1}$. Substituted into Eq. 2.16 this gives $k_b \approx 0.0028$ as the related order of magnitude of k_b.

Information available on the magnitude of k_i is summarized in the appendix.

5. Backwater curve equation for two-layer flow

This section gives the backwater curve equation for steady two-layer flow ($\partial/\partial t = 0$), neglecting the effect of wind ($\tau_s = 0$). For the considered flows $\Delta\rho/\rho_1 \ll 1$ and $\Delta\rho/\rho_2 \ll 1$.

Under the above conditions the equation of motion for the upper layer (Eq. 2.9) reduces to

$$u_1 \frac{du_1}{dx} = - g \frac{d(a_1 + a_2)}{dx} - \frac{\tau_i}{\rho_1 a_1} + g S \tag{2.17}$$

and that for the lower layer (Eq. 2.12) to

$$u_2 \frac{du_2}{dx} = - g \frac{d(a_1 + a_2)}{dx} + \frac{\Delta\rho}{\rho_2} g \frac{da_1}{dx} - \frac{(\tau_b - \tau_i)}{\rho_2 a_2} + g S \tag{2.18}$$

Subtracting Eq. 2.17 from Eq. 2.18 and substituting $\frac{da_1}{dx}$ from Eq. 2.17 gives

$$- u_1 \frac{du_1}{dx} + u_2 \frac{du_2}{dx} =$$

$$\underline{- \frac{\Delta\rho}{\rho_2} u_1 \frac{du_1}{dx} - \frac{\Delta\rho}{\rho_2} g \frac{da_2}{dx} - \frac{\Delta\rho}{\rho_2} \frac{\tau_i}{\rho_1 a_1} + \frac{\Delta\rho}{\rho_2} g S} + \frac{\tau_i}{\rho_1 a_1} - \frac{(\tau_b - \tau_i)}{\rho_2 a_2} \tag{2.19}$$

In Eq.(2.19) the sum of the underlined terms is equal to $(\Delta\rho/\rho_2)g(da_1/dx)$ as can be seen from Eq. 2.17.

At this stage of the derivation it is justified to consider the consequences of the condition $\Delta\rho/\rho_2 \ll 1$. Because of this condition Eq. 2.19 reduces to

$$- u_1 \frac{du_1}{dx} + u_2 \frac{du_2}{dx} + \frac{\Delta\rho}{\rho_2} g \frac{da_2}{dx} = \frac{\tau_i}{\rho_1 a_1} - \frac{(\tau_b - \tau_i)}{\rho_2 a_2} + \frac{\Delta\rho}{\rho_2} gS \tag{2.20}$$

From Eqs. 2.2 and 2.3 for steady conditions one can derive that

$$\frac{du_1}{dx} = - \frac{u_1}{a_1} \frac{da_1}{dx} \tag{2.21}$$

and

$$\frac{du_2}{dx} = -\frac{u_2}{a_2}\frac{da_2}{dx} \tag{2.22}$$

Eqs. 2.21 and 2.22 into Eq. 2.20 gives

$$\frac{u_1^2}{a_1}\frac{da_1}{dx} - \frac{u_2^2}{a_2}\frac{da_2}{dx} + \frac{\Delta\rho}{\rho_2} g \frac{da_2}{dx} = \frac{\tau_i}{\rho_1 a_1} - \frac{(\tau_b - \tau_i)}{\rho_2 a_2} + \frac{\Delta\rho}{\rho_2} gS \tag{2.23}$$

Velocity differences between the upper layer and the lower layer require differences in the forces per unit mass acting on both layers. Shear tends to reduce velocity differences between the layers. Hence velocity differences must be caused by differences in the hydrostatic pressure gradients for both layers. From Eqs. 2.8 and 2.11

$$\frac{\Delta(\frac{1}{\rho}\frac{\partial p}{\partial x})}{(\frac{1}{\rho}\frac{\partial p}{\partial x})_1} = -\frac{\Delta\rho}{\rho_2} + \frac{\frac{\Delta\rho}{\rho_2}\frac{\partial a_2}{\partial x}}{\frac{\partial(a_1+a_2)}{\partial x}} = \frac{\Delta\rho}{\rho_2}\left[\frac{\frac{\partial a_2}{\partial x}}{\frac{\partial(a_1+a_2)}{\partial x}} - 1\right] \tag{2.24}$$

where $\Delta(\frac{1}{\rho}\frac{\partial p}{\partial x})$: difference between $\frac{1}{\rho}\frac{\partial p}{\partial x}$ for lower layer and upper layer

$(\frac{1}{\rho}\frac{\partial p}{\partial x})_1$: $\frac{1}{\rho}\frac{\partial p}{\partial x}$ for upper layer

Eq. 2.24 gives the difference in the forces due to the hydrostatic pressure gradient for both layers as a fraction of the force due to the hydrostatic pressure gradient for the upper layer, each per unit mass of fluid. This fraction is of the order $\Delta\rho/\rho$, i.e. much smaller than one, unless the slope of the interface ($\partial a_2/\partial x$) is much larger than that of the water surface ($\partial(a_1+a_2)/\partial x$). Hence, velocity differences between both layers occur only when

$$\left|\frac{\partial a_2}{\partial x}\right| >> \left|\frac{\partial(a_1+a_2)}{\partial x}\right| \tag{2.25}$$

which implies

$$\frac{\partial a_1}{\partial x} \approx -\frac{\partial a_2}{\partial x} \tag{2.26}$$

Eqs. 2.25 and 2.26 represent the conditions to be satisfied in order to have a difference in velocity between the upper layer and the lower layer. Eq. 2.26 in Eq. 2.23 gives

$$\frac{da_2}{dx} = \frac{S + \dfrac{\tau_i}{\Delta\rho g a_1} - \dfrac{(\tau_b - \tau_i)}{\Delta\rho g a_2}}{1 - \dfrac{u_1^2}{\frac{\Delta\rho}{\rho} g a_1} - \dfrac{u_2^2}{\frac{\Delta\rho}{\rho} g a_2}} \tag{2.27}$$

Eqs. 2.26 and 2.27 allow backwater computations to be performed for two-layer flows with a difference in velocity between the upper layer and the lower layer. A discussion of two-layer backwater curves is given by Rigter (1970). Examples are given in Section 7.

For homogeneous flow the corresponding backwater curve equation reads

$$\frac{dh}{dx} = \frac{S - \dfrac{\tau_b}{\rho g h}}{1 - \dfrac{u^2}{gh}} \tag{2.28}$$

6. Long waves, concept of critical flow

6.1 Homogeneous flow

Flow properties do not vary in time when observed by a spectator who moves at the same velocity as the long wave. For homogeneous flow this means that

$$\frac{dh}{dt} = \frac{\partial h}{\partial t} + c\,\frac{\partial h}{\partial x} = 0 \qquad\qquad \frac{du}{dt} = \frac{\partial u}{\partial t} + c\,\frac{\partial u}{\partial x} = 0 \tag{2.29}$$

where c: velocity of propagation of long surface wave.

Substituting Eq. 2.29 into Eqs. 2.1 and 2.4, the latter equations may be written as

$$(u-c)\,\frac{\partial h}{\partial x} + h\,\frac{\partial u}{\partial x} = 0 \tag{2.30}$$

and

$$g \frac{\partial h}{\partial x} + (u-c) \frac{\partial u}{\partial x} = - \frac{(\tau_b - \tau_s)}{\rho h} + g\ S \tag{2.31}$$

The velocity of propagation of the long wave, moving over the water surface, can be determined by setting the determinant of this system of equations equal to zero. This gives

$$c = u \pm \sqrt{gh} \tag{2.32}$$

Defining the Froude number as

$$Fr = \frac{u^2}{gh} \tag{2.33}$$

in accordance with Eq. 2.32, depending on the magnitude of the Froude number, distinction can be made between sub-critical flow ($Fr < 1$, one wave propagating in the direction of u and one in the opposite direction), critical flow ($Fr = 1$, one wave propagation in the direction of u and the other one stationary) and super-critical flow ($Fr > 1$, both waves propagating in the direction of u).

6.2 Two-layer flow

Schijf and Schönfeld (1953) and Abbott and Torbe (1963) applied the above procedure to the two-layer flow. From Eqs. 2.2,.2.3, 2.9 and 2.12 they found the above velocity of propagation for the long surface wave. In addition they found for long waves, moving over the interface

$$c_i = \frac{u_1 a_2 + u_2 a_1}{a} \pm [\frac{\Delta\rho}{\rho}\ g\ \frac{a_1 a_2}{a} \{1 - \frac{(u_2 - u_1)^2}{\frac{\Delta\rho}{\rho}\ g\ a}\}]^{1/2} \tag{2.34}$$

a = depth $(a_1 + a_2)$
c_i = velocity of propagation of long wave at interface

When the absolute value of the first term at the right hand side of Eq. 2.34 is smaller than that of the second term, one wave velocity is positive and the other negative. This means that there are two waves propagating over the interface in opposite directions. Both wave velocities have the same sign as the first term at the right hand side, when it is larger than the absolute value of the second term at the right hand side. Then both waves propagate in the direction imposed by the first term at the right hand side.

Therefore, defining internal Froude numbers as

$$Fr_1 = \frac{u_1^2}{\frac{\Delta\rho}{\rho} g a_1} \qquad\qquad Fr_2 = \frac{u_2^2}{\frac{\Delta\rho}{\rho} g a_2} \tag{2.35}$$

where Fr_1, Fr_2: densimetric Froude number of upper- and lower layer

in accordance with the magnitude of (Fr_1+Fr_2), the following distinction can be made

For $(Fr_1+Fr_2) < 1$ the two-layer flow is sub-critical. Then the absolute value of the first term at the right hand side of Eq. 2.34 is smaller than that of the second term. Hence, there are two waves propagating over the interface in opposite directions.

For $(Fr_1+ Fr_2) > 1$ the two-layer flow is super-critical. Then the absolute value of the first term at the right hand side of Eq. 2.34 is larger than that of the second term and both interfacial waves propagate in the direction indicated by the sign of the first term.

For $(Fr_1+Fr_2) = 1$, the two-layer flow is critical. Then the absolute value of the first term at the right hand side of Eq. 2.34 is equal to that of the second term. Then, one wave is propagating over the interface in the direction indicated by the sign of the first term and the other one is stationary $(c_i = 0)$.

6.3 Internal hydraulic jump

For homogeneous flow the transition from super-critical flow to sub-critical flow is associated with a hydraulic jump. In a similar way the transition from super-critical stratified flow to sub-critical stratified flow is associated with an internal hydraulic jump.

The homogeneous flow hydraulic jump causes mixing between the water in the jump and the supernatant air. In a similar manner an internal hydraulic jump causes mixing between the upper layer and the lower layer fluid. (Macagno and Macagno, 1975).

An example of an internal hydraulic jump is given in Fig. 2.4. This figure shows the internal hydraulic jump and the long internal wave, moving over the interface, induced by a sudden inflow of lower layer fluid into a basin in which it has been accumulated.

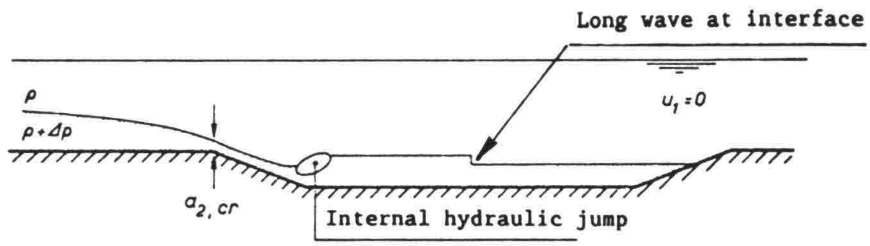

Fig. 2.4 Lower layer fluid being accumulated in deep pit (upper layer at rest)

A detailed description of the internal hydraulic jump is given by Yih and Guha (1955) and by Yih (1980).

7. Application of critical flow concept

7.1 Arrested salt wedge

When a fresh-water river discharges into a saline sea in which the range of tide is zero (e.g. Mediterrenean Sea and Black Sea), an arrested salt wedge results. In the salt wedge the salt water is mostly stagnant (Fig. 2.5).

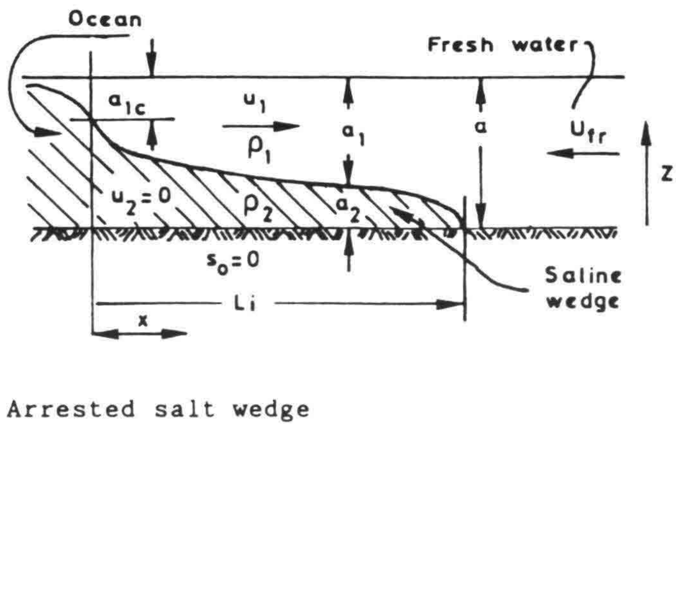

Fig. 2.5 Arrested salt wedge

$$u_2 = 0 \tag{2.36}$$

and

$$a_1 u_1 = - q_{fr} \tag{2.37}$$

where q_{fr} : fresh water flow rate per unit width

In Eq. 2.37 the minus sign is due to the fact that the longitudinal coordinate, x, which is measured from the mouth of the estuary, is taken positive when directed landinwards.

Substituting Eqs. 2.36 and 2.37 into Eq. 2.34 and 2.35 gives that for an arrested salt wedge

$$Fr_1 + Fr_2 = \frac{q_{fr}^2}{\frac{\Delta\rho}{\rho} g\, a_1^3} \tag{2.38}$$

and that the sign of the first term at the right hand side of Eq. 2.34 is negative, meaning that when this stratified flow is super-critical both internal waves propagate in the direction of the river flow, i.e. out of the estuary. Only when the flow is sub-critical, there is one interfacial wave which can propagate in the direction opposite to that of the river flow and hence can penetrate into the river. Thus, salt water penetrates into the river as long as the flow at the mouth of the river is sub-critical.

The larger the quantity of salt which has intruded into the river, the smaller is thickness of the upper layer, a_1, at the mouth of the river. Hence, at a given moment the value of a_1 may become sufficiently small to make $Fr_1 + Fr_2$ equal to one at the mouth of the river, (see Eq. 2.38). Reducing a_1 further requires more salt to penetrate into the river. This is impossible, however, as reducing a_1 further makes the flow super-critical, which for the arrested salt wedge means that internal waves can propagate only out of the river. This means that salt stops to penetrate into the river, when at its mouth

$$\frac{q_{fr}^2}{\frac{\Delta\rho}{\rho} g\, a_1^3} = 1 \tag{2.39}$$

Knowing the value of a_1 at the mouth of the estuary, the length of the arrested salt wedge can be determined using the backwater curve equation for stratified flow (Eq. 2.27) in configuration with Eq. 2.26. Using this procedure Schijf and Schonfeld found the length and the shape of the arrested salt wedge to be given by

$$k_i \, Fr_f \, \frac{L}{a} = \frac{1}{20} - \frac{1}{2} Fr_f + \frac{3}{4} Fr_f^{4/3} - \frac{3}{10} Fr_f^{5/3} \tag{2.40}$$

and

$$k_i \, Fr_f \, \frac{(L_i - x)}{a} = \frac{1}{20} - \frac{1}{4}\left(\frac{a_1}{a}\right)^4 + \frac{1}{5}\left(\frac{a_1}{a}\right)^5 - \frac{1}{2} Fr_f\left(1 - \frac{a_1}{a}\right)^2 \tag{2.41}$$

in which

$$Fr_f = \frac{q_{fr}^2}{\frac{\Delta\rho}{\rho} \, g \, a^3} \ll 1 \tag{2.42}$$

where L_i: length of arrested salt wedge (Fig. 2.5)

Fr_f: densimetric Froude number based on river flow

a: depth of river

x: longitudinal coordinate, measured from mouth of estuary (see Fig. 2.5)

The river flow may be so large that there are no internal waves which can penetrate into the river, even when $a_2 = 0$ and therefore $a_1 = a$. In accordance with Eq. 2.38 this conditions arises when $Fr_f \geq 1$. Then $L_i = 0$.

The velocity of the fresh water, which flows over the arrested salt wedge increases when it comes closer to the sea. The pressure gradient needed for this acceleration is due to the surface slope (Eq. 2.8). The lower layer velocity is zero. This means that, neglecting interfacial shear, the pressure gradient acting on the lower layer is zero. In accordance with Eq. 2.11 this means that for the lower layer the pressure gradient due to the surface slope is balanced by the pressure gradient due to the slope of the interface. As $\Delta\rho/\rho_2 \ll 1$, this requires the slope of the interface to be much larger than that of the water surface.

7.2 Density induced return current

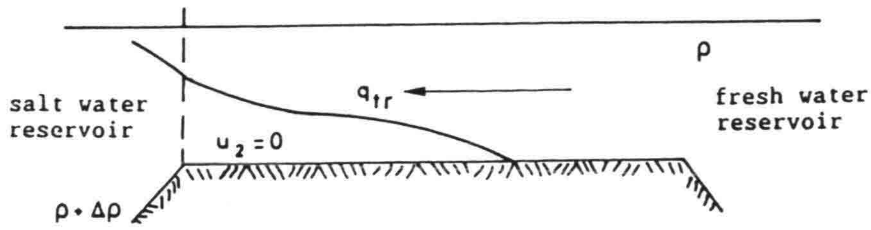

Fig. 2.6[a] Arrested salt wedge above long weir

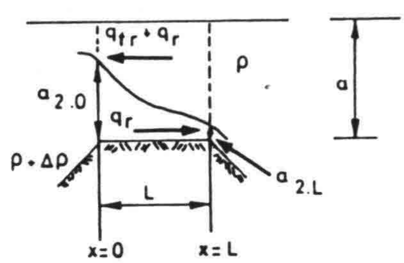

Fig. 2.6[b] Density induced return flow over short weir

For an arrested salt wedge the slope of the interface makes the lower layer velocity equal to zero. If the slope of the interface could be made larger, this would cause a flow of the lower layer in the direction opposite to that of the upper layer flow.

Considering a long weir, connecting a fresh water reservoir with a salt water reservoir, over which there is a net flow q_{fr} from the fresh water reservoir to the salt water reservoir, the length of the weir may be so large that above the weir an arrested salt wedge can be formed (Fig. 2.6[a]). Then the flow above the weir corresponds to the flow described in the preceding section.

When the length of the weir is made smaller than that of the arrested salt wedge, while keeping the net flow q_{fr} the same, salt water starts to flow into the fresh water reservoir, i.e. in the direction opposite to that of the net flow over the weir (Fig. 2.6[b]).

The larger the slope of the interface, the larger is the above density induced return current, q_r. This means that q_r can increase as long as the resulting two-layer flow remains sub-critical over the entire length of the weir.

The slope of the interface and therefore q_r cannot increase further, when the flow at x = 0 and x = L becomes critical. This means that internal waves cannot any longer penetrate into the area above the weir, as both at x = 0 and x = L one of the internal waves is stationary while the other propogates in a direction away from the weir.

The above considerations imply that for a given value of q_{fr} the return flow, q_r, has its maximum value when both at x = 0 and x = L the flow is critical. These critical flow conditions cannot be selected arbitrarily, as the value of a_2 at x = 0 is linked to that at x = L by the backwater curve equation for stratified flow. In formula, this link can be expressed as

$$a_{2,L} = a_{2,0} + \int_0^L \frac{da_2}{dx} dx \tag{2.43}$$

where $a_{2,o}$: value of a_2 at x=0
$a_{2,L}$: value of a_2 at x=L

The problem of determining the critical conditions at x=0 and x=L so that Eq. 2.43 is satisfied has been solved by Rigter (1970), who gives design graphs for the maximum value of q_r as a function of q_{fr}, the length of the weir and the interfacial shear coefficient.

The Strait of Bosporus (length 25 km, depth between 30 and 50 m) separates the Black Sea from the Marmara Sea. Because of the fresh water inflow into it the density of the Black Sea is lower than that of the Marmara Sea, while there is a net flow through the Strait of Bosporus from the Black Sea to the Marmara Sea. Bayazit and Anil (1979) observed a density induced return current in the Strait of Bosporus with an upper layer flow rate of 9000 m^3/s from the Black Sea to the Marmara Sea and a lower layer flow rate of 8000 m^3/s in the opposite direction. They found the two-layer flow to be critical at both ends of the Strait of Bosporus.

A first estimate of the density induced flow through the Cochin-Gut (Chapter 1, Section 7.4) could be made using the theory of the density induced return currents (Chandramohan, 1989).

When $q_{fr} = 0$ the flow over the weir is referred to as a density induced exchange flow. This means that the flow of the upper layer and lower layer are in opposite directions and have the same absolute value. For the density induced exchange flow over a very short weir (L=0) both at x=0 and x=L the thickness of the upper layer and lower layer is about half the water depth above the weir, a. Under these conditions the flow being critical at both x=0 and x=L implies

$$q_{ex} = \frac{1}{4} a \left[\frac{\Delta\rho}{\rho} g a\right]^{1/2} \tag{2.44}$$

where q_{ex}: density induced flow rate per unit width

u_{ex}: velocity of density induced flow (fig. 2.7)

Eq. 2.44 applies to the density induced exchange flows produced when the gate between a fresh water reservoir and a salt water reservoir of equal depth is removed (Fig. 2.7). This exchange flow is given by Eq. 2.44 during a short initial period after removal of the gate.

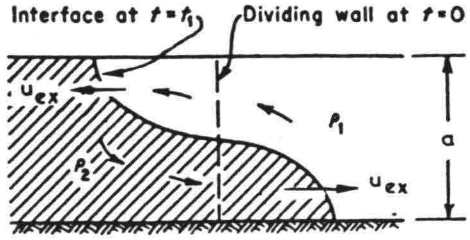

Fig. 2.7 Density induced exchange flow

7.3 Selective withdrawal

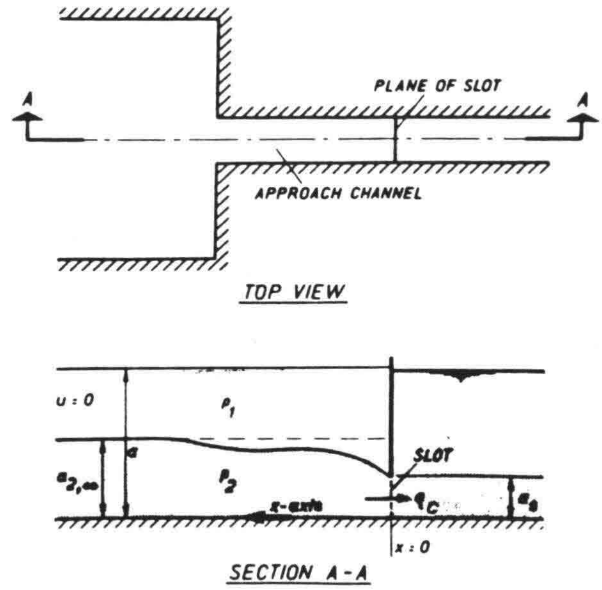

Fig. 2.8 Selective withdrawal; definition sketch

We consider a narrow channel which at one of its ends is in open connection with a wide two-layer reservoir. In this reservoir the thickness of the lower layer is kept constant and equal to $a_{2,\infty}$. At the other end the channel is separated from another reservoir by a gate. Both reservoirs and the channel have the same depth (Fig. 2.8).

A flow from the two-layer reservoir to the other reservoir can be maintained through the channel by regulating the height of a slot and the pressure head over it. The problem to be solved is determining the maximum quantity of lower layer fluid, which can be withdrawn selectively (i.e. without simultaneous withdrawal of upper layer fluid) through the channel from the two-layer reservoir to the other reservoir. This maximum quantity must be given as a function of $a_{2,\infty}$ and the height of the slot a_s for steady conditions.

The selective withdrawal implies $u_1 = 0$. This means that the water surface is horizontal, except for the influence of the interfacial shear. Consequently, the flow of lower layer fluid through the channel is activated by the pressure gradient induced by the slope of the interface.

Before opening the gate, the interface is horizontal over the entire length of the channel. After opening the gate, the interface is lowered near the slot in order to create the lower layer flow. Only when near the slot the flow is subcritical, long internal waves can propagate from the slot towards the stratified reservoir. This means that the lower layer flow has its maximum value when near the slot the two-layer flow is critical.

As $u_1 = 0$, the critical flow condition implies

$$\frac{q_{2,max}^2}{\frac{\Delta\rho}{\rho} g\, a_{2.s}^3} = 1 \qquad (2.45)$$

where $q_{2,max}$: maximum lower layer flow rate per unit width
$a_{2.s}$: thichness of lower layer near slot.

The value of $q_{2,max}$, given by Eq. 2.45, must be selected so that $a_{2.s}$ is linked to $a_{2.\infty}$ by the backwater curve equation.

In the following text we assume the length of the channel so small that the effect of shear may be neglected. Then $a_{2.s}$ is linked to $a_{2.\infty}$ by the Bernoulli equations for two layer flow.

For <u>homogeneous</u> steady flow, the Bernoulli equation is obtained by integrating Eq. 2.4 with respect to x, neglecting the effect of shear. The Bernoulli equation obtained by this procedure reads

$$\frac{u^2}{2g} + h = C(\text{onstant}) \qquad (2.46)$$

where h_b: distance from bottom to horizontal reference plane
C : constant.

Eq. 2.46 implies that the sum of the kinetic energy ($\frac{1}{2}\rho u^2$) and the potential energy (ρgh) per unit volume of fluid is constant.

Integrating Eq. 2.9 with respect to x, neglecting the effect of shear, gives the Bernoulli equation for the <u>upper layer</u>

$$\frac{u_1^2}{2g} + (a_1 + a_2) = C_1 \tag{2.47}$$

and integrating Eq. 2.12 with respect to x that for the <u>lower layer</u>

$$\frac{u_2^2}{2g} + (a_1 + a_2) - \frac{\Delta\rho}{\rho} a_1 = C_2 \tag{2.48}$$

where C_1, C_2: constant for upper and lower layer.

Eqs. 2.47 and 2.48 imply that the sum of the kinetic energy and the potential energy remains constant per unit volume of upper layer and lower layer fluid, when the effect of shear is neglected.

Subtracting Eq. 2.47 from Eq. 2.48 and substituting Eq. 2.26 and $u_1 = 0$ (selective withdrawal) into the equation obtained by this procedure gives

$$\frac{1}{2} \frac{q_2^2}{a_{2.s}^2} + \frac{\Delta\rho}{\rho_2} g\, a_{2.s} = \frac{\Delta\rho}{\rho_2} g\, a_{2.\infty} \tag{2.49}$$

where q_2: lower layer flow rate per unit width.

Substituting Eq. 2.45 into Eq. 2.49 shows that

$$a_{2.s} = \frac{2}{3} a_{2.\infty} \qquad \text{when } q_2 = q_{2,max} \tag{2.50}$$

and that

$$q_{2,max} = [\frac{\Delta\rho}{\rho_2} g \left(\frac{2}{3} a_{2.\infty}\right)^3]^{1/2} \tag{2.51}$$

Eq. 2.51 gives the maximum flow through the channel for conditions of selective withdrawal. However, in order to obtain selective withdrawal it is necessary that the interface passes through the upper edge of the slot or remains above it. This means that Eq. 2.51 applies only when the pressure head over the slot is so large that the height of the slot, a_s, is equal to or smaller than the value of $a_{2.s}$ given by Eq. 2.50. Hence

$$\frac{q_c}{[\frac{\Delta\rho}{\rho} \partial g\, a_s^3]^{1/2}} = [\frac{2}{3} \frac{a_{2.\infty}}{a_s}]^{3/2} \qquad \text{for } a_s \leq \frac{2}{3} a_{2.\infty} \tag{2.52}$$

where q_c: maximum value of q_2 with selective withdrawal for given value of a_s.

For $a_s \geq \frac{2}{3} a_{2.\infty}$ selective withdrawal requires $a_{2.s} = a_s$. The latter condition implies that for these values the interface passes through the upper edge of the slot. Then the maximum value of q_s with selective withdrawal can be obtained by substituting $a_{2.s} = a_s$ into Eq. 2.49. This gives

$$\frac{q_c}{[\frac{\Delta\rho}{\rho} g\, a_s^3]^{1/2}} = [2(\frac{a_{2.\infty}}{a_s} - 1)]^{1/2} \qquad \text{for } a_s \geq \frac{2}{3} a_{2.\infty} \tag{2.53}$$

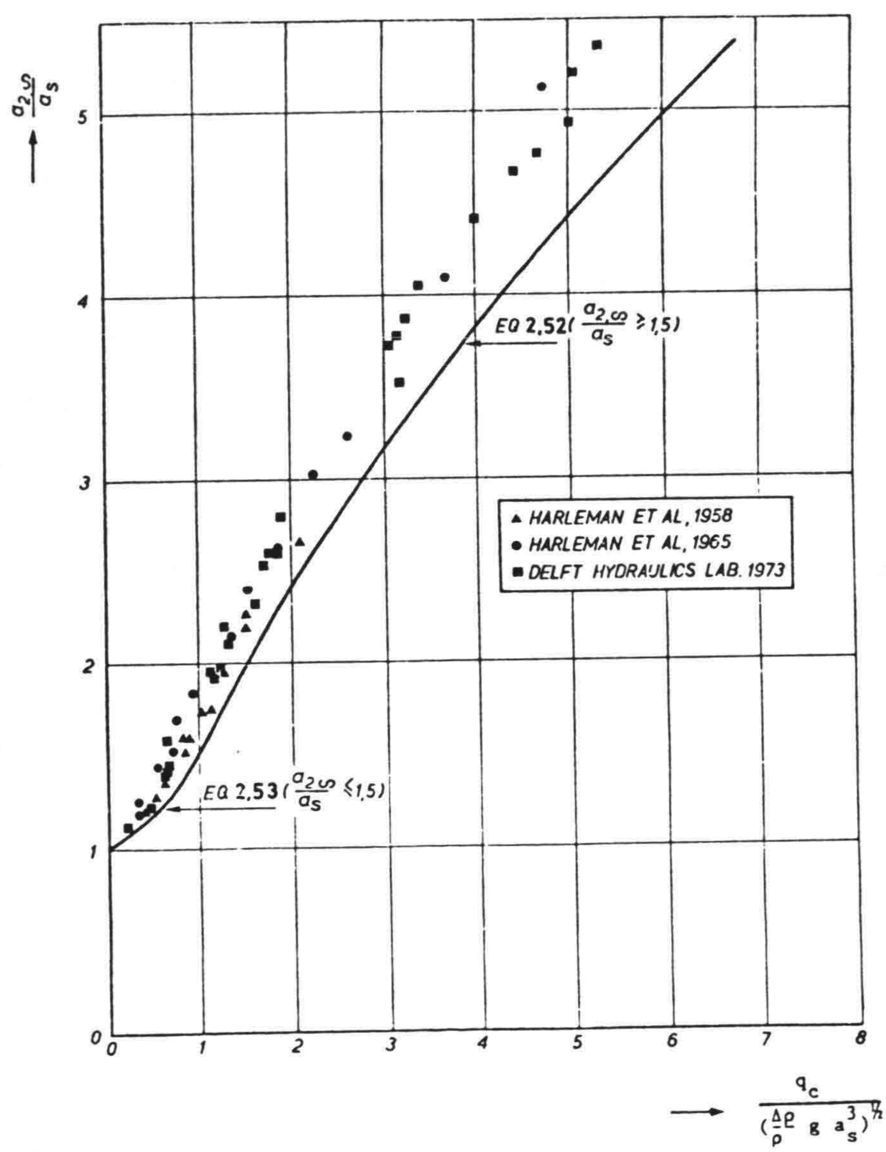

Fig. 2.9 Selective withdrawal; experimental results.

Both Eqs. 2.52 and 2.53 are derived neglecting deviations from the uniform distribution of velocity in the lower layer. Therefore the values of q_c given by these equations represent an upper limit of the actual values of q_c. Taking this into consideration, there is a satisfactory agreement between the above theory (Harleman and Elder, 1965) and the experimental results given in Fig. 2.9. The experimental value of $a_{2.\infty}/a_s$ needed to obtain a given value of $q_c/(\frac{\Delta\rho}{\rho}\, g\, a_s^3)^{1/2}$ is larger than the theoretical value, meaning that the theory gives an upper limit of q_c indeed.

In a similar manner Jirka (1979) treats the problem of incomplete selective withdrawal, assuming that a small fraction of upper layer fluid is withdrawn simultaneously with the lower layer fluid.

7.4 Summary

Sections 6.1 - 6.2 give examples of sub-critical stratified flows for which $Fr_1 + Fr_2 \leq 1$, except at those points where the flow is critical. At these points the values of a_1 (or a_2) can be determined from the condition that $Fr_1 + Fr_2 = 1$. Knowing these values of a_1 (or a_2) the considered flows could be solved integrating the backwater curve equation for stratified flow with respect to x.

This chapter shows the similarities between homogeneous flows and the considered type of density currents, and shows the possibility of solving actual problems by schematising the stratified flows as a two-layer system.

8. References

8.1 Wind shear stress

Smith, S.D. and Banke, E.G., Variation of the sea surface drag coefficient with wind speed, Quart. J.R. Met. Soc, 101, pp. 665-673.

8.2 Long internal waves

Abbott, M.B. and Torbe, I., On flows and fronts in a stratified fluid, Proceedings of the Royal Society, A, Volume 273, pp. 12-40, 1963.

Schijf, J.B. and Schönfeld, J.C., Theoretical considerations on the motion of salt and fresh water, Proceedings of the Minnesota International Hydraulics Convention, Joined Meeting, I.A.H.R. and Hydr. Div. A.S.C.E., Sept. 1953, pp. 321-333.

8.3 Internal hydraulic jumps

Macagno, E.O. and Macagno, E.C., Mixing in interfacial hydraulic jumps,, Proceedings 16th Congress of Intern. Assoc. of Hydraulic Research, Volume 3, paper C 43, pp. 373-381, Sao Paulo, 1975.

Stefan, H. and Hayakawa, N., Mixing induced by internal hydraulic jump, Water Resources Bulletin, Volume 8, no. 3, pp. 531-545, 1972.

Yih, C.S. and Guha, C.R., Hydraulic jump in a fluid system of two layers, Tellus, VII, 1955.

Yih, C.S., Stratified flows, Academic Press, New York (1980).

8.4 Arrested salt wedge

Harleman, D.R.F., Stratified flow, chapter 26, Handbook of Fluid Dynamics, Edited by V.L. Streeter, Mc Graw-Hill, New York, (1961).

Schijf, J.B. and Schönfeld, J.C., Theoretical considerations on the motion of salt and fresh water, Proc. Minn. Intern Hydr. Conv. September, 1953, pp. 321-333.

8.5 Density induced return currents

Bayazit, M. and Anil, A., Mathematical model of the two-layer system in the Bosporus Strait, Proceedings 18th Congress of International Association for Hydraulic Research, 3, Cagliari 1979, pp. 287-293.

Chandramohan, P.V., Density currents and siltation with particular reference to Cochin, Master of Science thesis, International Institute for Hydraulic Engineering, 1989.

Rigter, B.P., Density induced return currents in outlet channel, Proc. A.S.C.E., 96, Journ. of Hydr. Div. No. HY2, Febr. Paper no. 7086, pp. 529-546, 1970.

8.6 Selective withdrawal

Delft Hydraulics, Two-dimensional investigations of selective withdrawal (in Dutch), Report no. M1204, July 1973

Harleman, D.F.R., R.S. Gooch and A.T. Ippen, Submerged sluice control of stratified flow, Proc. A.S.C.E. vol. 84, no. Hy 2, pt 1, April 1958.

Harleman, D.F.R. and R.A. Elder, Withdrawal from two-layer stratified flows, Proc. A.S.C.E., vol. 91, no. HY 4, July 1965.

Jirka, G.H., Supercritical withdrawal from two-layered fluid systems, Part 1: Two-dimensional skimmer wall, Journal of Hydraulic Research vol. 17, no. 1, 1979, pp. 43-51.

Additional reading

Imberger, J., Selective withdrawal: a review, Proceedings, 2nd International symposium on stratified flows, vol. 1, pp 381-400, Tapir, Trondheim, 1980.

Monismith, S. and Imberger, J., Shear waves and unsteady selective withdrawal, Journal of Hydraulic Engineering, A.S.C.E., vol. 114, no. 9, 1988, pp 1134-1152.

Appendix A: Experimental data on interfacial shear

This appendix gives experimental information on the following two-layer flows which are sub-critical over their entire length, except at the points indicated in Fig. 2.A.1, where they are critical.

- arrested salt wedge (Fig. 2.A.1.a) (Section 7.1)
- density induced return current (Fig. 2.A.1.b) (Section 7.2)
- temperature surface wedge (Fig. 2.A.1.c) (Bata, 1957, Polk et al 1971)

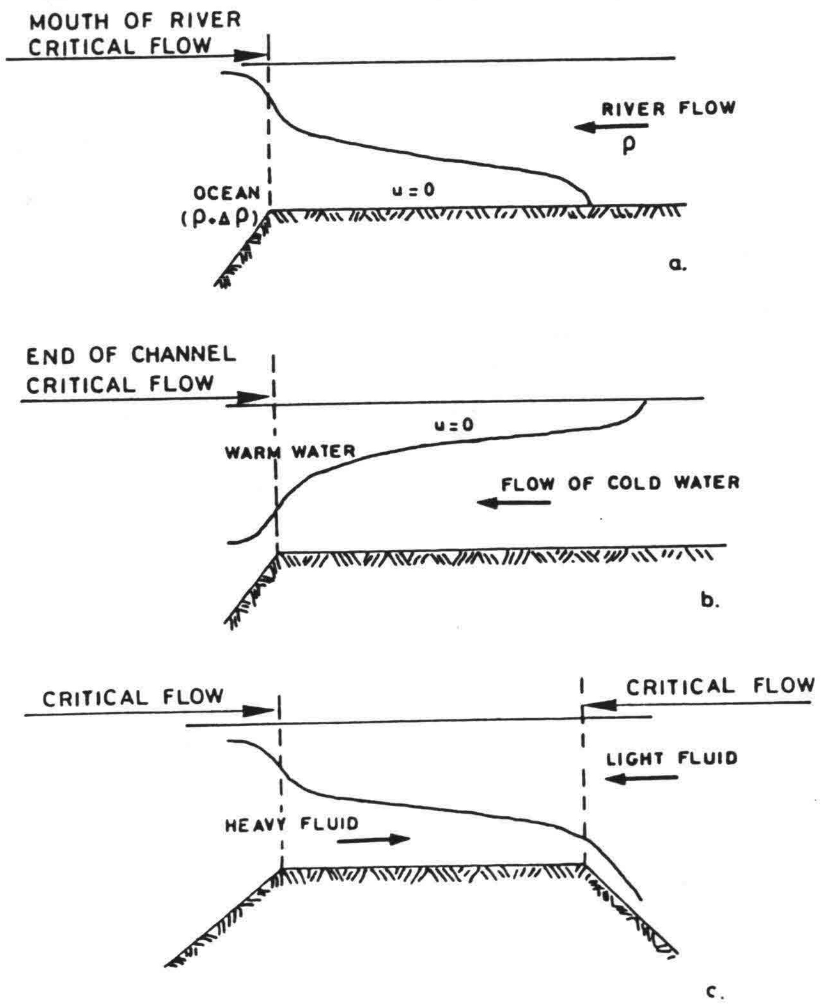

Fig. 2.A.1 Considered sub-critical stratified flows

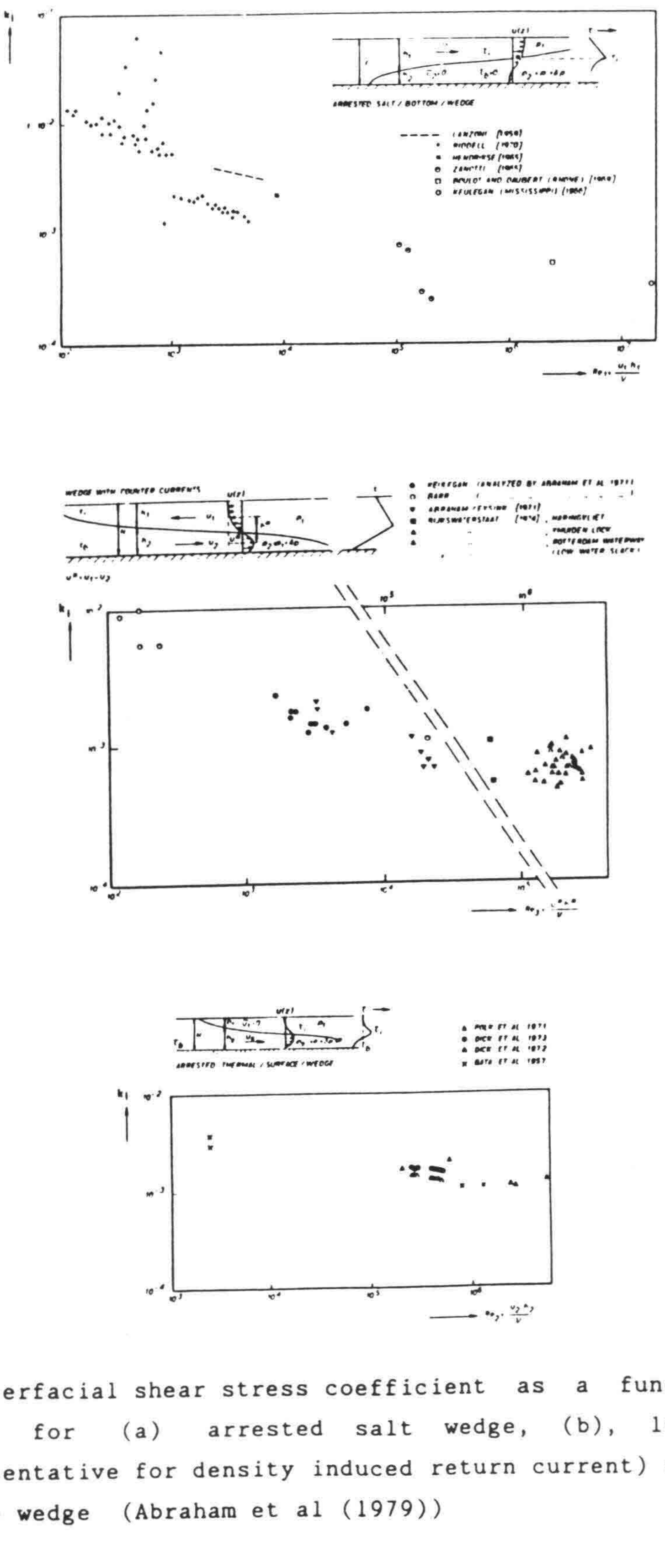

Fig. 2.A.2 Interfacial shear stress coefficient as a function of Reynolds number for (a) arrested salt wedge, (b), lock exchange flow (representative for density induced return current) and (c) temperature surface wedge (Abraham et al (1979))

From the measurements it can be concluded that k_i decreases with increasing Reynolds number, tending to a constant value for large values of Re, the constant values being

<u>a</u> arrested salt wedge $k_i \approx 4.10^{-4}$

<u>b</u> lock exchange flow $k_i \approx 7.10^{-4}$

<u>c</u> temperature surface wedge $k_i \approx 15.10^{-4}$

The above values of k_i vary with the type of flow as turbulence is generated both at the interface and at the bottom.

Abraham et al (1979) therefore conclude that the interfacial shear should satisfy an equation like

$$\tau_i = k_{i,i}\rho\,(u_1-u_2)\,|u_1-u_2| + k_{i,b}\rho\, u_2|u_2| \cdot \left(\frac{a_1}{a_1+a_2}\right) \qquad (2.A1)$$

where

$k_{i,i}$ = interfacial shear coefficient, expressing the effect of turbulence generated at the interface

$k_{i,b}$ = interfacial shear coefficient, expressing the effect of turbulence generated at the bottom

For large values of Re the values of $k_{i,i}$ and $k_{i,b}$ then will be

$k_{i,i} \approx 4.10^{-4}$

$k_{i,b} \approx 24.10^{-4}$

References

Abraham, G., Karelse, M. and Van Os, A.G. On the magnitude of interfacial shear of subcritical stratified flows in relation with interfacial instability. Journal of Hydraulic Research, Vol. 17, no. 4, 1979, pp. 273-287.

Bata, G.L., 1957. Recirculation of cooling water in rivers and canals. Journ. of Hydr. Div., Proc. A.S.C.E., 83, HY3, paper 1265.

Delft Hydraulics, 1974. Momentum and mass transfer in stratified flows, Report R 880, Chapter 2.

Polk, E.M., B.A. Benedict and F.L. Parker, 1971. Cooling water and density wedges in streams. Proc. A.S.C.E., 97, HY10, pp. 1639-1652.

Chapter 3, Salt intrusion into estuaries; basic physical phenomena

1. Introductory remarks

"An estuary is a semi-closed coastal body of water which has a free connection with the open sea and within which sea-water is measurably diluted with fresh water derived from land drainage" [Cameron and Pritchard].

"An estuary is where a river meets the sea" [Fischer et al, 1979, Section 7.1].

An estuary flow is complex, unsteady and spatially varying, driven by the tide and often affected by internal density effects (after Fischer et al, 1979, Section 7.1).

Many studies of individual estuaries are available in the literature and there are several texts that produce the relevant general principles. These include Cameron and Pritchard (1963), Lauff (1967), Ippen (1966), Dyer (1973), McDowell and O'Connor (1977), Fischer et al (1979, Section 7.1) and Dronkers and Van Leussen (1988). An overview is given by Fischer (1976).

2. Stratification of estuaries

The density difference between sea water and fresh river water tends to make estuaries stratified. Energy is needed to overcome the stratification. In estuaries the mixing is effectuated by turbulence, and the required energy is supplied by the tidal flow. Therefore, stratification is most pronounced in estuaries, through which a river issues into a non-tidal sea and stratification is the weaker the stronger the tidal action is.

On this basis, Cameron and Pritchard (1963) and Dyer (1973) have classified estuaries by their stratification and their salinity distributions. They define the following types of estuaries:

- highly stratified salt wedge type estuaries
- partly mixed estuaries, and
- well mixed estuaries.

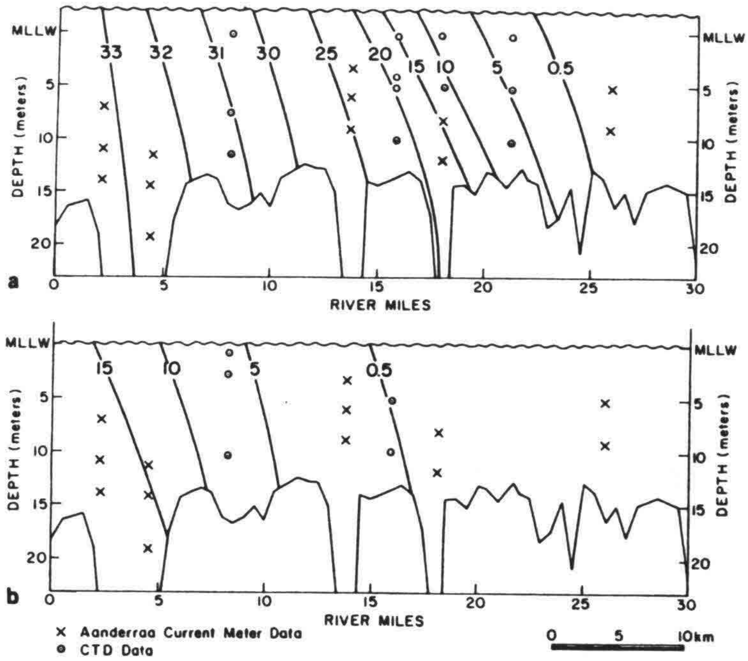

FIG. 3.1 Salinity sections for a end of flood and b end of ebb for the spring tide of October 24–26, 1980. The horizontal salinity gradient is nearly uniform and the stratification is weak. Model results (Jay 1987) show that the ebb-flood variation in the horizontal salinity gradient is caused by the along-channel decrease in tidal transport associated with the presence of large tidal flats

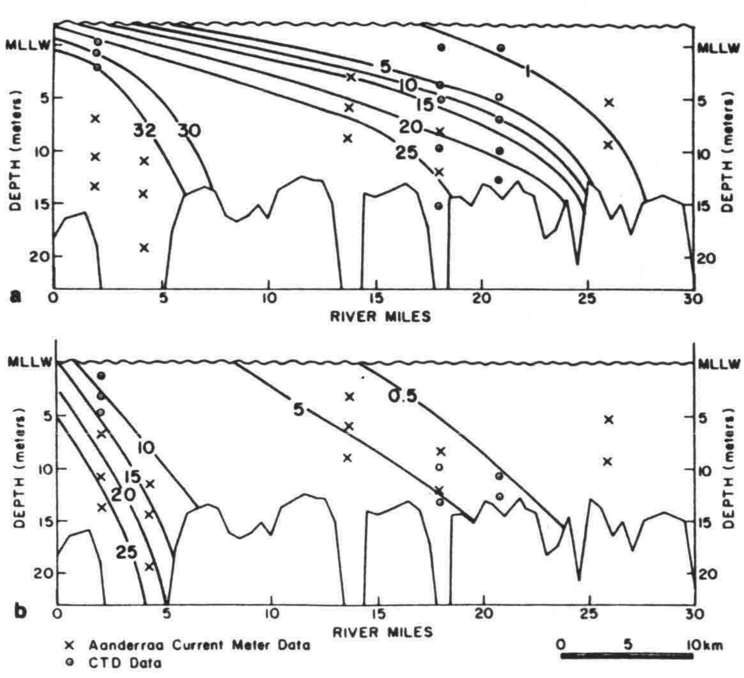

FIG. 3.2 Salinity sections for a end of flood and b end of ebb for the neap tide of October 16–17, 1980. The flood shows a two-layer advance, with strong horizontal and vertical gradients at the head of the saline water mass. The salt water is both advected and mixed out of the estuary on ebb

Figs. 3.1 and 3.2 Salinity sections of Columbia River estuary, (Jay and Smith, 1988)

In the salt wedge type estuary fresh water flows over virtually non-diluted sea water towards the sea. In well mixed estuaries the density varies primarily in the horizontal direction and hardly over the depth of the estuary (Fig. 3.1). A partly mixed estuary is in the intermediate position (Fig. 3.2).

Fig. 3.1 refers to the Columbia River estuary, United States of America, for the spring tide of October 24-26, 1980 (tidal range 3.4 m). Fig. 3.2 refers to the neap tide of October 16-17, 1980 (tidal range 2.0 m). For both tidal conditions the fresh water flow rate was 4000 m^3/s (Jay and Smith, 1988). Figs. 3.1 and 3.2 illustrate that the Columbia River estuary shows a clear pattern of tidal monthly changes in density distribution during the low-flow season. It shares this pattern with several other estuaries.

Fig. 3.3 gives an example of highly stratified conditions, obtained from the Fraser River Estuary, Canada (Geyer, 1988).

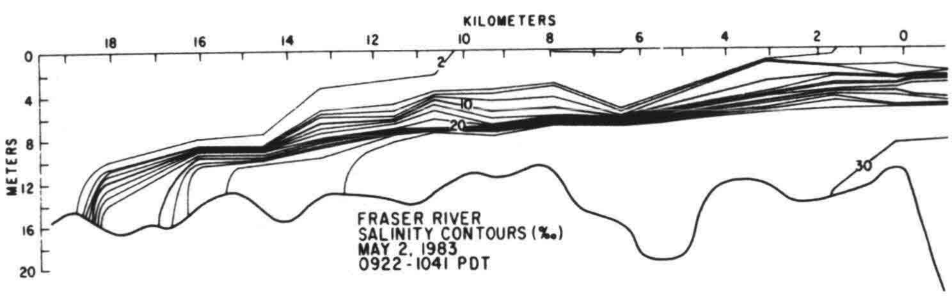

Salinity section at the end of the flood, at the time of maximum intrusion. The upper and lower layers are nearly homogeneous, and isopycnal slope is weak. Note the change in horizontal scale from Fig. 1

Fig. 3.3 Salinity section of Fraser River estuary (Geyer, 1988)

3. Stratification parameters

Stratification parameters are used to classify estuaries on stratification. The stratification parameters themselves are expressed in the volumetric ratio, α, and the estuary densimetric Froude number, Fr_o, respectively defined as

$$\alpha = \frac{Q_{fr}\ T}{P_t} = \pi \frac{u_{fr}}{\hat{u}_{1.0}} \tag{3.1}$$

and

$$Fr_o = \frac{\hat{u}^2_{1.0}}{\frac{\Delta\rho}{\rho}\ g\ h_o} \tag{3.2}$$

where: α : ratio of volume of river water coming down the estuary per tidal cycle over the flood volume, introduced by Simmons (1955)

Fr_o : estuary densimetric Froude number

Q_{fr} : river flow rate

T : duration of tidal cycle

P_t : volume of sea water entering the estuary on the flood tide

g : acceleration by gravity

$\hat{u}_{1,0}$: amplitude of profile averaged tidal velocity at mouth of estuary

u_{fr} : river velocity, i.e. river flow rate over cross-sectional area at mouth of estuary

h_o : depth at mouth of estuary

$\Delta\rho$: difference in density between sea water an river water

ρ : density of either sea water or river water, which are about equal

Simmons (1955) gives a classification, relating the stratification to α. Thatcher and Harleman (1981) relate the stratification to the "estuary number", E_D, defined as

$$E_D = \frac{1}{\pi}\ \frac{\rho\ \hat{u}^3_{1.0}}{\Delta\rho\ g\ h_o\ u_{fr}} = \alpha^{-1} Fr_o \tag{3.3}$$

where: E_D : estuary number, introduced by Thatcher and Harleman (1981)

The energy input by the tidal current per unit area and per unit time is proportional to the product of bottom shear and the tidal velocity, i.e. to the tidal velocity cubed. This energy input controls the stratification of an estuary. The buoyancy flux into an estuary is proportional to the product of the river flow per unit width and the density difference between sea water and river water. Therefore, the estuary number is a measure for the ratio of the energy input by the tidal current and the energy needed for mixing.

Fischer (1976) relates the stratification to an "estuary Richardson number", which is inversely proportional to the estuary number.

Table 3.1 gives a classification on stratification parameters, derived from Simmons (1955) for the classification on α and from Ippen and Harleman (1967) for the classification on E_D. The latter classification coincides approximately with the one given by Fischer et al (1979, p 243).

Table 3.1 Classification of estuaries on stratification parameters

type of estuary	α	E_D
highly stratified	$\alpha > 1.0$	$E_D < 0.2$
partly mixed	$\alpha \approx 0.25$	$0.2 < E_D < 8$
well mixed	$\alpha < 0.1$	$E_D > 8$

4. Gravitational circulation

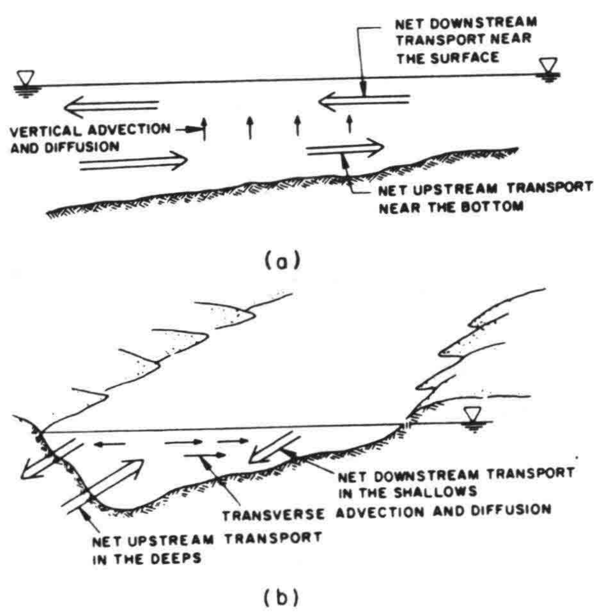

Fig. 3.4 Two views of a salt balance maintained by gravitational circulation
a: the vertical circulation envisaged by Pritchard in the James;
b: a three-dimensional circulation in a non-rectangular channel.
(after Fischer, 1976)

Gravitational circulation is the driving mechanism for salt intrusion into estuaries, as is explained for well mixed estuaries in Section 2.3 of Chapter 1.

Two views on a salt balance maintained by gravitational circulation are presented by Fischer (1976): a vertical circulation in an estuary of rectangular cross-section (Fig. 3.4.a) and a three-dimensional circulation in an irregularly shaped channel (Fig. 3.4.b).

In Section 2.3 of Chapter 1 it has been shown (Eq. 1.9, term c) that for a well mixed estuary the gravitational circulation is caused by a force per unit mass of fluid, F_p, given by

$$F_p = -\frac{1}{\bar{\rho}} \left(\frac{1}{2}h + h_b - z\right) g \frac{\partial \bar{\rho}}{\partial x} \tag{3.4}$$

where: F_p : net force per unit mass of fluid caused by a longitudinal gradient of hydrostatic pressure

h : water depth

h_b : vertical coordinate of bottom (see Fig. 1.4)

z : vertical coordinate (see Fig. 1.4)

$\partial\bar{\rho}/\partial x$: longitudinal density gradient, averaged over the depth

Hence, $|\partial\bar{\rho}/\partial x|$ is a measure for the strength of the gravitational circulation. Therefore, the strength of the gravitational circulation increases with increasing distance from the sea until $|\partial\bar{\rho}/\partial x|$ reaches its maximum value at about half the salt intrusion length. Further landinward $|\partial\bar{\rho}/\partial x|$ decreases to become zero in the river water zone of the estuary. Because of continuity considerations, this variation of the strength of the gravitational circulation in the horizontal direction is associated with a relatively small vertical flow. Near the mouth of the estuary this is a downward flow. Near the tip of the zone of salt intrusion it is an upward flow, as shown in Fig. 3.5.

The longitudinal density gradients have a considerable effect on the variation of the time averaged velocity over the depth. In the zone of salt intrusion this velocity is in the landward direction at the bed and in the seaward direction at the water surface. This is explained in Section 2.3 of Chapter 1 and illustrated by the field data which are represented in Fig. 3.13.

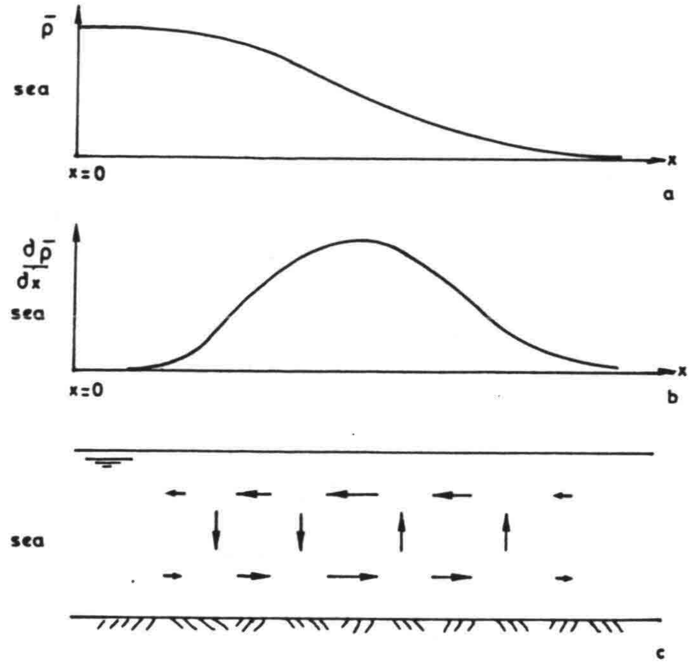

Fig. 3.5 a: longitudinal variation of $\bar{\rho}$, b: longitudinal variation of $|\partial\bar{\rho}/\partial x|$ c: variation of longitudinal and vertical velocity components over length of estuary

The longitudinal density gradients also have a considerable effect on the variation of the instantaneous velocity over the depth. During ebb, at the bottom the ebb flow is slowed down both by the bottom shear and the pressure gradient induced by the density differences, while at the surface the ebb flow is accelerated by this pressure gradient. This means that in the zone with salt intrusion ($\partial\rho/\partial x \neq 0$) the ebb flow varies more strongly over the depth than outside this zone. During flood, at the bottom the flood flow is slowed down by the bottom shear and accelerated by the pressure gradient induced by the density differences. At the surface the flood flow is slowed down by this pressure gradient. Hence, in the zone of salt intrusion the flood flow is distributed more homogeneously over the depth than outside that zone. The above effects are represented schematically in Fig. 3.6 and illustrated further by the field data given in Fig. 3.12.

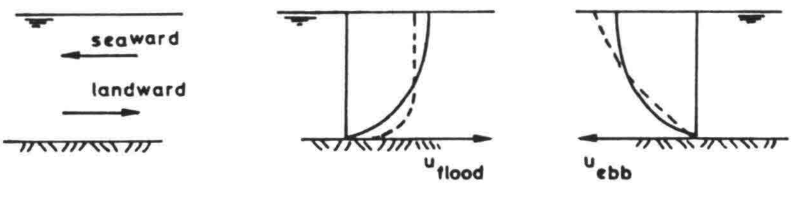

—— : homogeneous flow ($\partial\rho/\partial x = 0$)

---- : ($\partial\rho/\partial x \neq 0$)

: direction of force per unit mass of fluid induced by density gradients

Fig. 3.6 Effect of longitudinal density gradients on variation of instantaneous velocity over depth

Summarizing, the following phenomena are important in salt intrusion:

- tidal movement,
- the effect of differences in density on the hydrostatic pressure leading to gravitational circulation,
- the vertical flow caused by the variation of the strength of the gravitational circulation with increasing distance from the sea, and
- turbulent mixing induced by the tidal flow.

Because of the differences in density, near the bottom the landinward flow is stronger than if there were no differences in density. Near the water surface, the position is reversed. This causes salt water to intrude over the bottom further up the river than if there were no differences in density. Factors which limit the distance the salt water can intrude inland are the vertical turbulent mixing and the vertical flow, which near the tip of the zone of salt intrusion is directed upward. By these mechanisms salt from the bottom layers with a predominantly landward flow is brought into the upper layers with a predominantly seaward flow.

5. Field data on gravitational circulation

5.1 Chao Phya estuary, Thailand

The Chao Phya estuary comprises the tidal stretch of the Chao Phya river and the adjacent part of the Gulf of Thailand. The Chao Phya river is a meandering river with in the area of salt intrusion a width of about 500 m and a mean depth of about 8 m. It extends into the Gulf of Thailand, where an artificial channel is maintained. Some features of the estuary are given in Fig. 3.7.

The salt intrusion and sedimentation in the Chao Phya estuary have been the subject of a 2 years' field survey made by the Netherlands Engineering Consultants (Nedeco) in combination with Delft Hydraulics (Nedeco, 1965). The survey provided a rather complete set of field data, which is presented here to illustrate some of the relevant issues.

The river flow varies from 25 to 250 m^3/s in the dry season up to a maximum of about 4000 m^3/s in the wet season. The smaller the flow, the further the salt penetration into the estuary. The salinity regime varies from well mixed in the dry season to stratified in the wet season.

Table 3.2 Characteristic parameters of the Chao Phya Estuary

	June 1962	December 1962
average width (m)	530	530
average depth (m)	8	8
wet cross section (m^2)	4250	4250
$\Delta\rho$ (kg/m^3)	25	25
riverdischarge (m^3/s)	85	800
flood volume (m^3)	90.10^6	90.10^6
maximum ebb velocity (m/s)	1.5	1.5
<u>Stratification parameters:</u>		
α	0.04	0.36
Fr_o	1.11	1.37
E_D	26.36	3.84

Table 3.2 gives some characteristic parameters of the Chao Phya estuary during two measuring periods, one with a low river discharge (June 1962) and one with higher discharges. The figures in the table show that this estuary will be completely mixed in a dry period ($\alpha = 0.04$, $E_D = 26$), while in the wetter period it will be partly stratified ($\alpha = 0.36$, $E_D = 3.8$).
This is confirmed by Fig. 3.8. This figure shows the effect of the river flow on the salt intrusion length and the stratification of the estuary. It gives the variation of the river discharge over the year. For 5 locations in the estuary it gives the mean density, averaged over the tidal cycle and the cross-section. Positive distances are measured from the mouth of the river in the upstream direction; negative distances in the downstream direction along the navigation channel in the Gulf of Thailand. The figure further shows the salinity ratio at the river mouth, a ratio of the order one indicating well mixed conditions. (See also Fig. 3.17 on page 3.27).

Fig. 3.9 gives the relation between the mean density (salinity), averaged over the tidal cycle and the cross-section, at the mouth of the estuary and river discharge. This relationship is a unique feature of the Chao Phya estuary. A relationship of this type must be available, whenever making an one-dimensional tidally-averaged salt intrusion model for a given estuary (Section 5, Chapter 5).

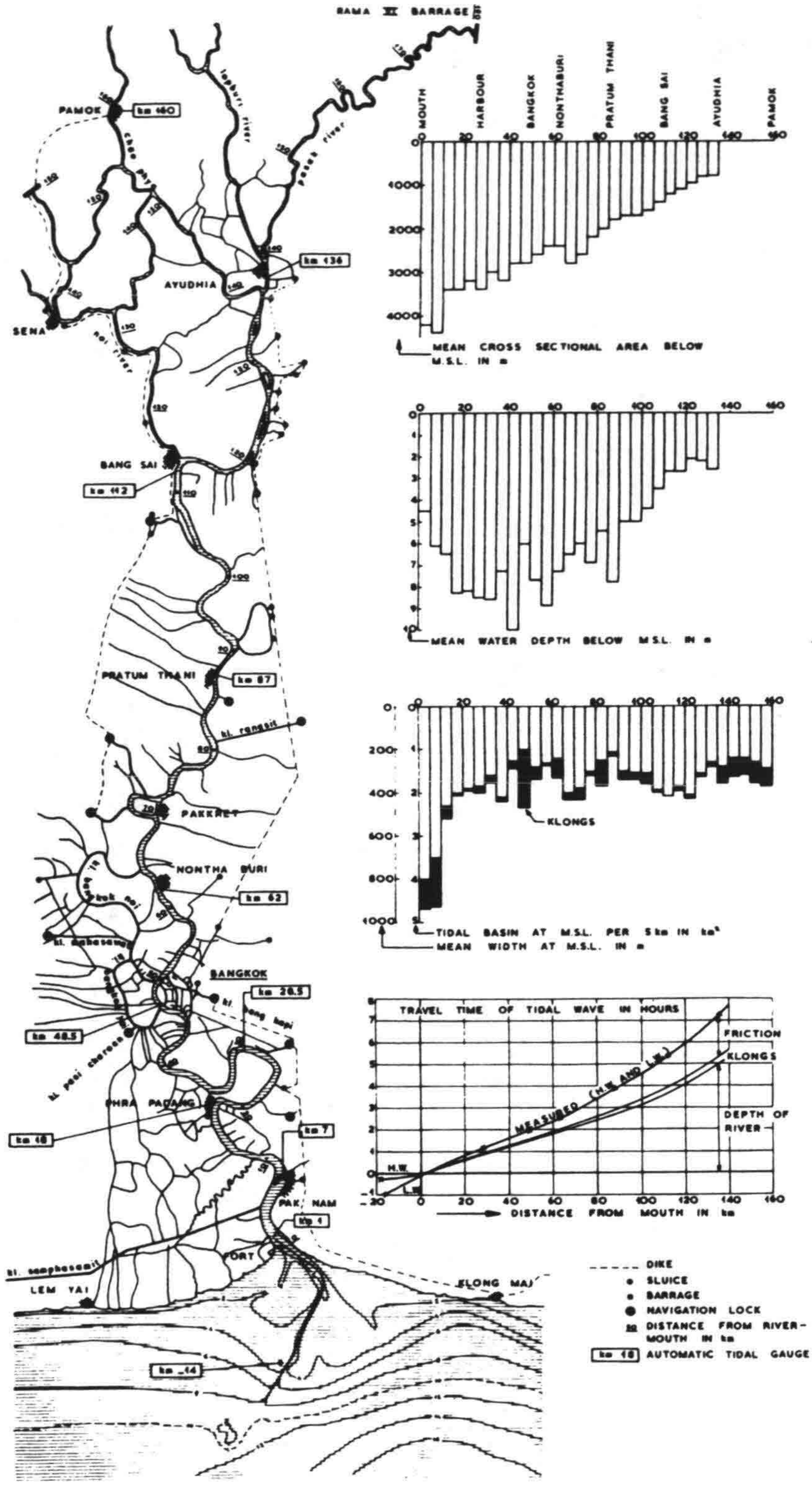

Fig. 3.7 The Chao Phya Estuary

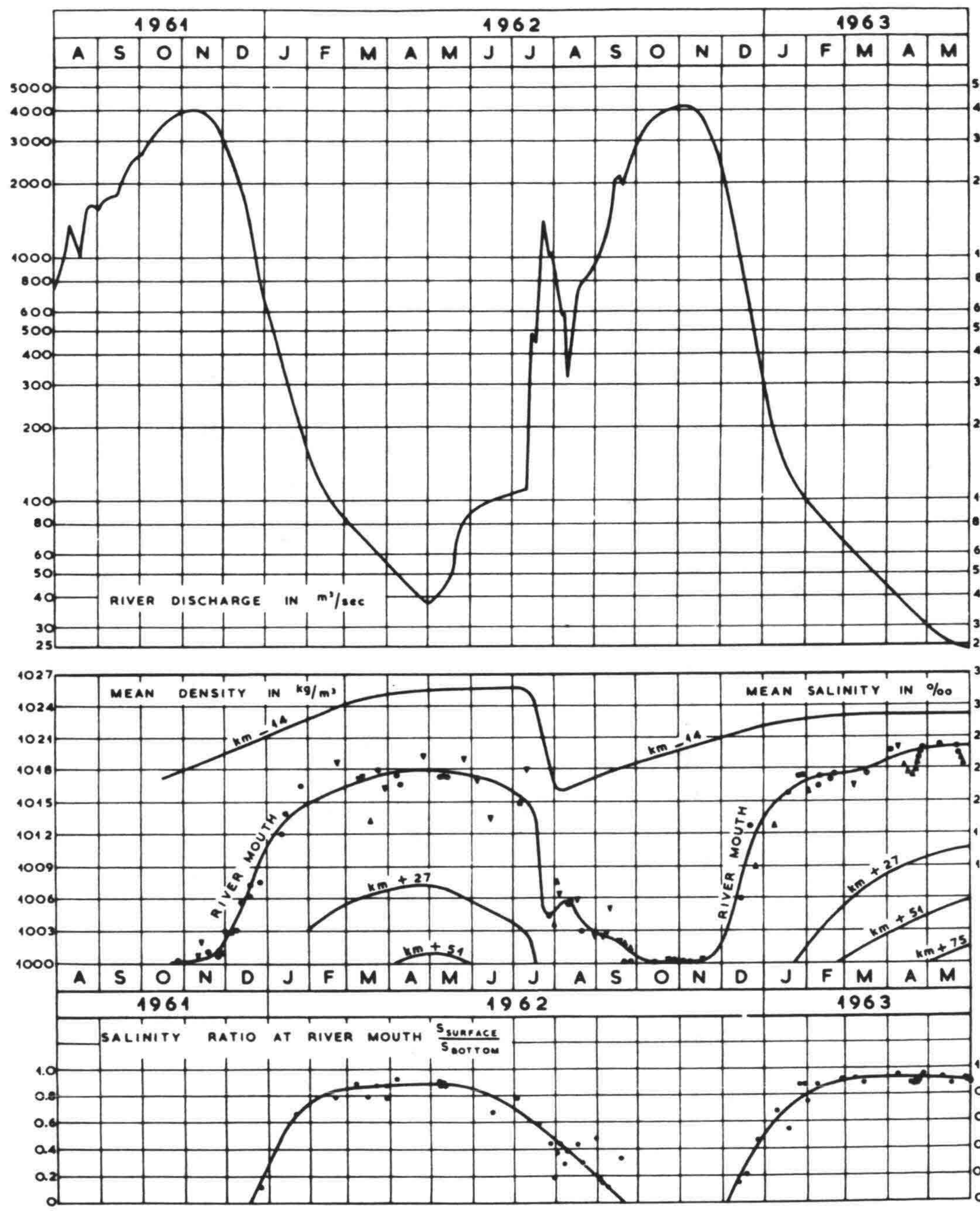

Fig. 3.8 Salinities at five locations in the estuary and the salinity ratio at the river mouth, compared with the discharge of the Chao Phya

Some observations at a discharge of about 900 m^3/s show a relatively large deviation from the relationship drawn in Fig. 3.8. These data were obtained in the short period of relatively small discharges of the river around August 10, 1962 (Fig. 3.7). The response of the density (salinity) to these changes of the discharge was not fast enough to follow the rapid variation of the discharge. In this respect, Fig. 3.9 shows the necessity of being aware of transient conditions when analyzing field data. This subject is elaborated upon in Section 11 of this Chapter.

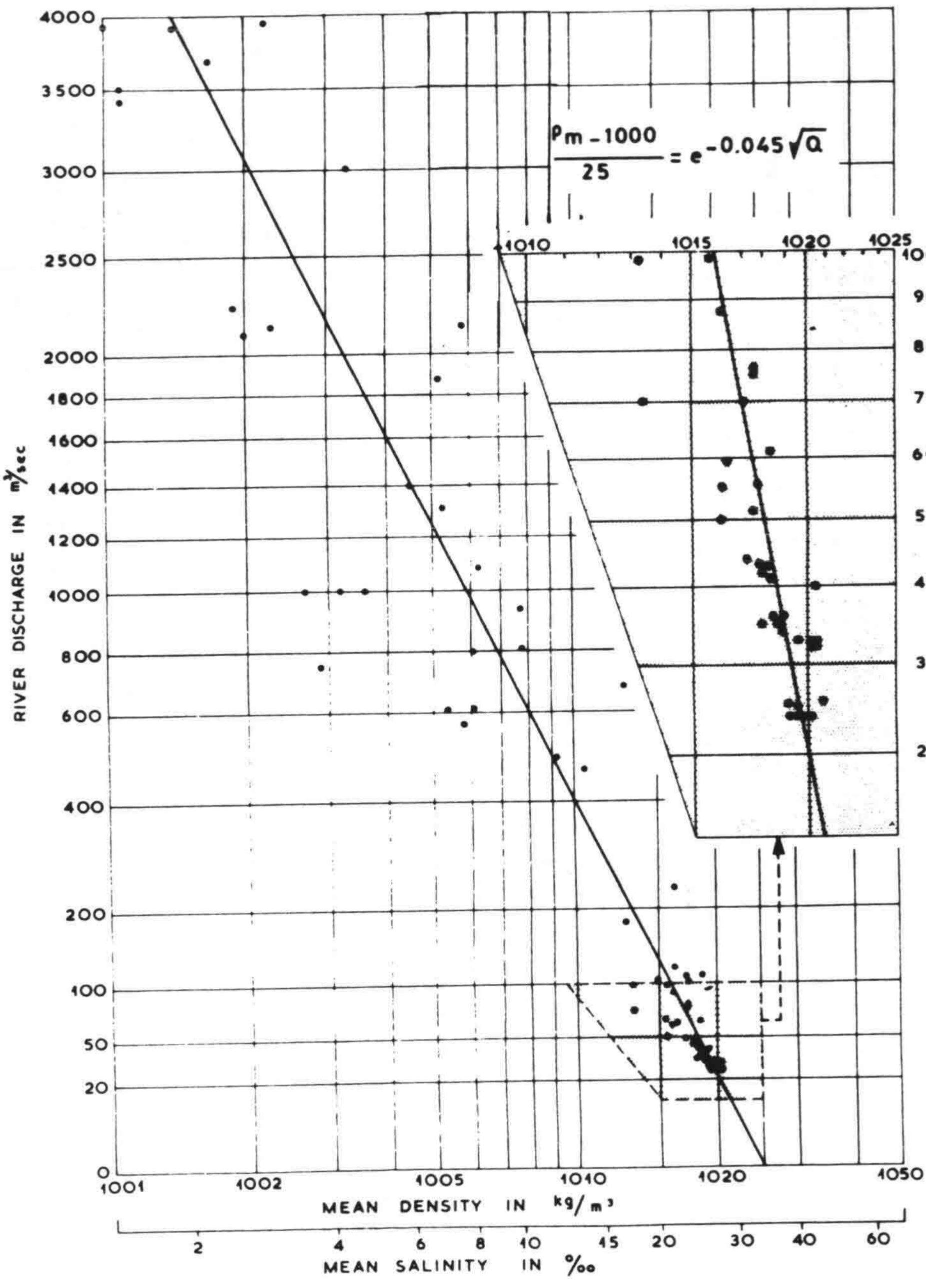

Fig. 3.9 Mean density (salinity) at the river mouth vs. discharge of the Chao Phya

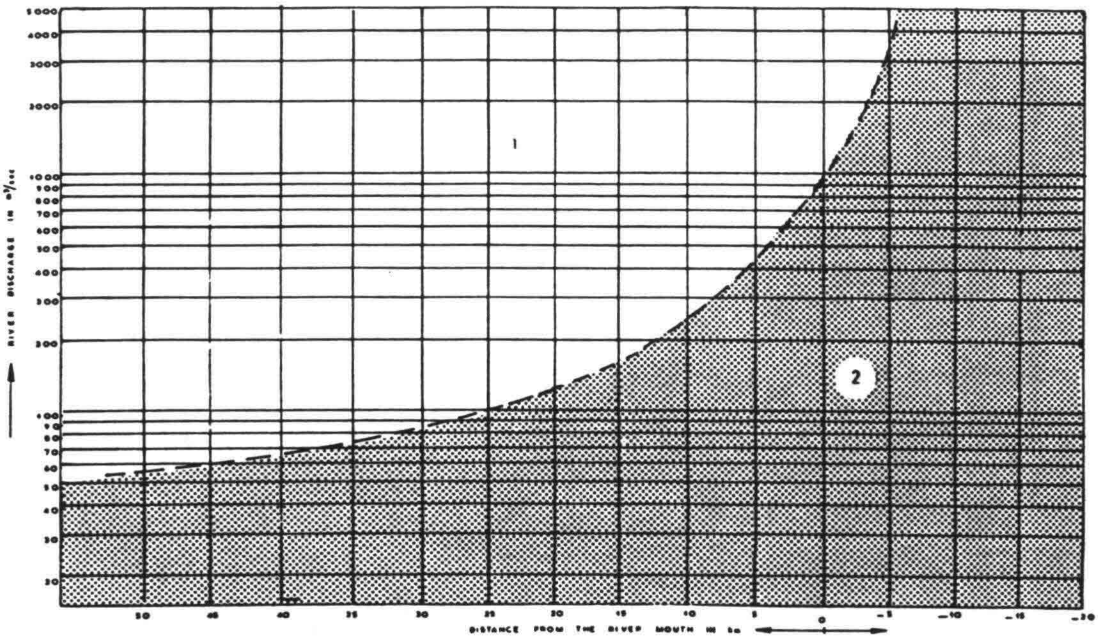

Fig. 3.10 Location of null point against the river discharge and the distance from the river mouth

1: tidally averaged velocity near bottom in downstream direction

2: tidally averaged velocity near bottom in upstream direction

Fig. 3.10 shows that for river discharges below 1000 m^3/s the null point is located in the Chao Phya river (e.g. at a distance of 25 km from the mouth for a discharge of 100 m^3/s). For discharges above 1000 m^3/s the null point is pushed into the Gulf of Thailand. This feature is reflected in the seasonal sediment transports in the Chao Phya estuary. During the dry season, the river supplies very little sediment and there is an inward transport induced by the gravitational circulation. During the wet season the gravitational circulation does not occur in the river, and therefore there is no inward transport of sediment during the wet season (Fig. 3.11).

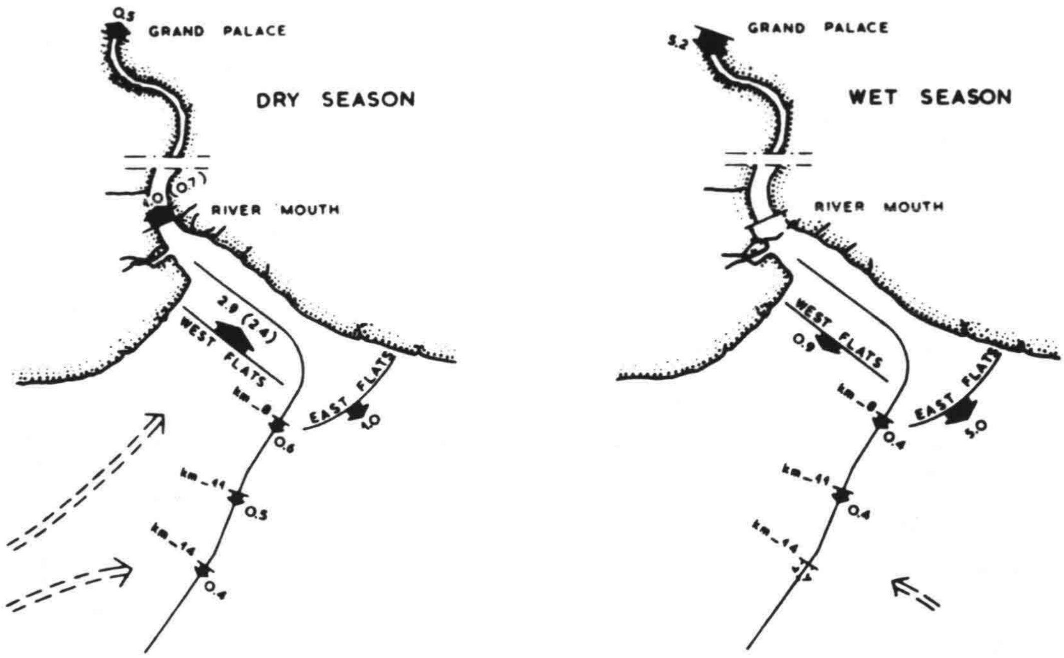

Fig. 3.11 Seasonal residual silt transports in Chao Phya Estuary (Allersma et al, 1966)

5.2 Rotterdam Waterway estuary, The Netherlands

The Rotterdam Waterway is a man-made estuary of approximately rectangular cross-section, having a width of about 410 m and a depth of about 16 m. The estuary has been continuously deepened to provide sufficient sailing depth. This leads both to increased salinity intrusion and maintenance dredging. Both these problems are the subject of extensive study. Within this context a substantial programme of field measurements has been performed in conjunction with both mathematical model and hydraulic model studies. One of the functions of the field measurements has been to provide field data for the calibration and verification of a hydraulic model of the Rotterdam Waterway estuary (Breusers and Van Os, 1981) and a series of mathematical models.

Table 3.3 gives the characteristic parameters of the Rotterdam Waterway during the various stages of the development of this estuary from 1874 when the construction took place (width of 141 m, depth of 7.7 m, Q_{fr} = 358 m^3/s, Flood volume P_t = $25.10^6 m^3$, α = 0.64, E_D = 2.08) up to 1982 (width = 410 m, depth = 15.8 m, Q_{fr} = 1190 m^3/s, P_t = 98.10^6 m^3, α = 0.55 and E_D = 0.52). From this table it can be concluded that this estuary is partly stratified, which did not change during the various constructional changes.

Table 3.3 Characteristic parameters of the Rotterdam Waterway

YEAR	1874	1908	1956	1913	1971	1982
average width (m)	141	375	375	410	410	410
average depth (m)	7.7	7.0	10.8	11.8	15.8	15.8
wet area (m^2)	1089	2626	4048	4846	6478	6478
$\Delta\rho$ (kg/m^3)	25	25	25	25	25	25
river discharge (m^3/s)	358	649	738	895	1550	1190
flood volume (Pt) (10^6 m^3)	25	47	69	83	94	98
maximum ebb velocity (m/s)	1.61	1.24	1.20	1.21	1.02	1.06
<u>Stratification parameters</u>:						
α	0.64	0.62	0.48	0.48	0.73	0.55
Fr_o	1.34	0.88	0.54	0.49	0.27	0.28
E_D	2.08	1.42	1.13	1.03	0.36	0.52
characteristic change	constr.	incr. width incr. Qf	incr. depth	incr. depth incr. width	incr. Qf incr. depth	decr. Qf

Fig. 3.12 gives velocity and concentration profiles observed at different stages of the tidal cycle. The variation of the ebb tide velocities over the depth is much stronger than that of the flood velocities, confirming the schematized picture given in Fig. 3.6.

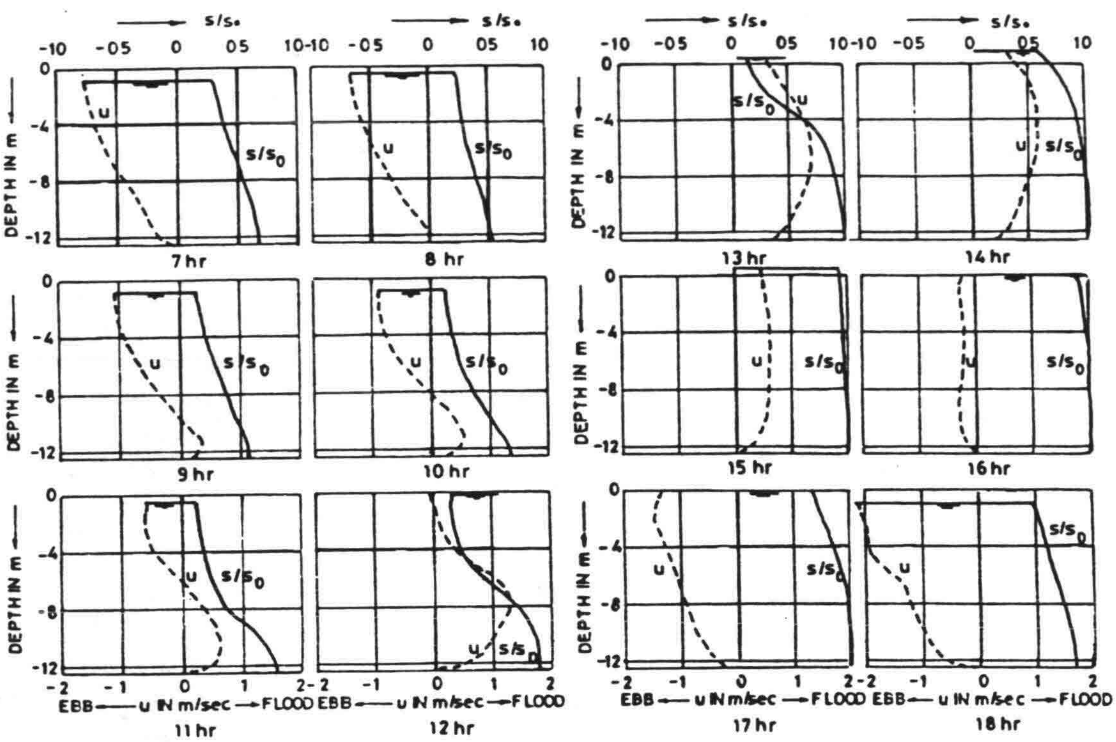

Fig. 3.12 Velocity and salinity profiles Rotterdam Waterway (s_o: salinity of sea water)

<u>5.3 Mersey River estuary, United Kingdom</u> (Bowden and Sharaf El Din, 1966)

Fig. 3.13 gives velocities and salinities as measured in the Narrows of the Mersey River estuary. The figure gives the values of these parameters, averaged over the tidal cycle. It shows how these tidally averaged parameters vary over cross-section C. The velocities u are in the longitudinal direction, the velocities v in the transverse direction.

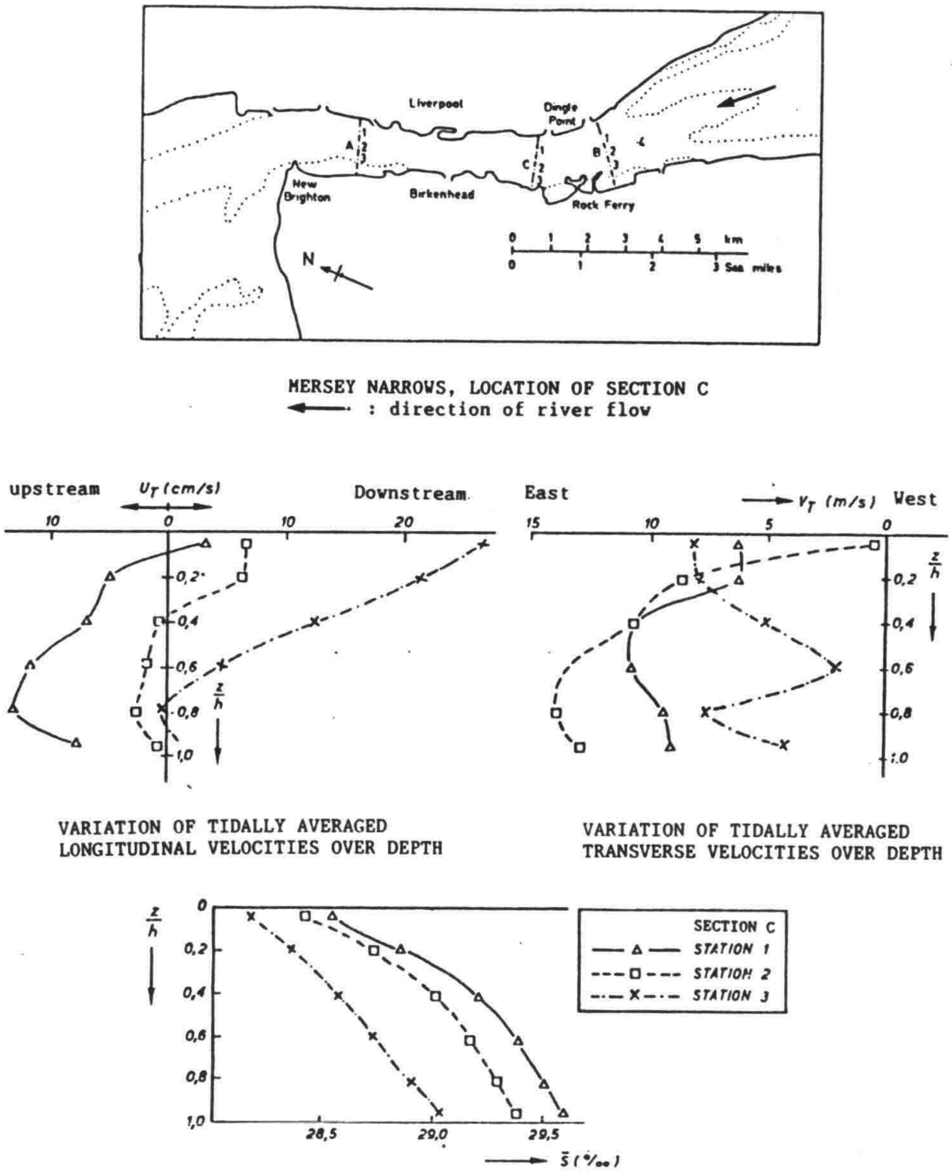

MERSEY NARROWS, LOCATION OF SECTION C
⟵ : direction of river flow

VARIATION OF TIDALLY AVERAGED LONGITUDINAL VELOCITIES OVER DEPTH

VARIATION OF TIDALLY AVERAGED TRANSVERSE VELOCITIES OVER DEPTH

VARIATION OF TIDALLY AVERAGED SALINITIES OVER DEPTH

Fig. 3.13 Mersey Narrows, Section C, variation of tidally averaged velocities and salinities over depth (Bowden and Sharaf El Din, 1966)

Tidally averaged near the bottom the longitudinal flow tends to be in the landward direction and at the surface in the seaward direction. This is due to the gravitational circulation in the longitudinal direction.

Averaged over the depth and the tidal cycle the transverse velocity component tends to be in the Eastern direction. This is due to the curvature of the channel. This means that averaged over the depth there is a circulation in the horizontal plane. In addition, there is a circulation in the transverse direction with tidally averaged transverse velocity components in the Western direction at the surface and in the Eastern direction at the bottom.

Summarizing, Fig. 3.13 gives evidence of circulations in the horizontal plane as well as in the vertical plane, while the circulation in the vertical plane occurs both in the longitudinal and transverse direction. These circulations are closely related to the geometric features of the Mersey River estuary.

6 Rotation of earth

Because of the rotation of the earth with respect to well-mixed estuaries distinction must be made between laterally inhomogeneous and laterally homogeneous estuaries (Dyer, 1973).

(a) Laterally inhomogeneous estuaries
When the estuary is sufficiently wide Coriolis force will cause a horizontal separation of the flow. The seaward net flow will occur at all depths on the right-hand side in the northern hemisphere and the compensating landward flow on the left. Thus the circulation would be in a horizontal plane rather than in the vertical sense as found in the other estuarine types. The increase of salinity towards the mouth will be regular on both sides of the estuary.

(b) Laterally homogeneous estuaries
When the width is smaller, lateral shear may be sufficiently intense to create laterally homogeneous conditions. Salinity increases evenly towards the mouth and the mean flow is seawards throughout the cross-sections.

7. Large scale advective mixing

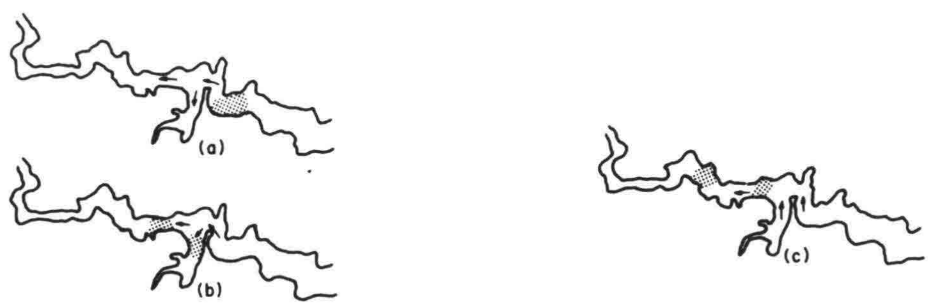

Fig. 3.14 The phase effect in a branching channel. (a) A cloud of tracer being carried upstream on flooding tide. (b) At high water some of the particles are trapped in the branch. (c) During the early stages of the receding tide the flow in the main channel is still upstream. The particles trapped in the branch re-enter the main channel, but are separated from their previous neighbours

The interaction between the tidal flow and the large-scale geometry of the estuary induces large-scale advective mixing. Fig. 3.14 shows the example of temporary storage of a constituent in a side arm. (Pritchard, 1959 and Fischer et al, 1979, Section 7.2.2). In the main channel the velocities are larger than in the side arm. Consequently the momentum of the flow in the main channel is larger than that in the side arm. This causes a phase difference between the tidal flows in the main channel and the side arm. In the side arm the current direction changes at high water, in the main channel some time after high water. This phase difference acts as a "chopping mechanism" separating fluid particles which at a given moment in time were neighbours. Temporary storage in shallow basins or above tidal flats has a similar effect as long as there is a phase difference between the main flow and the flow to and from the areas of storage.

An example which is related to the above temporary storage mechanism can be found at the junction of two tidal rivers. In this case chopping occurs if there is a phase difference between both rivers, i.e. when the ebb flow in the one tidal river begins earlier than it does in the other tidal river. (Abraham et al, 1986).

Chopping may also take place when a flood channel (or ebb channel) divides itself into two channels with different times of current reversal (slack). This is illustrated by Fig. 3.15, which is derived from Dronkers et al (1981).

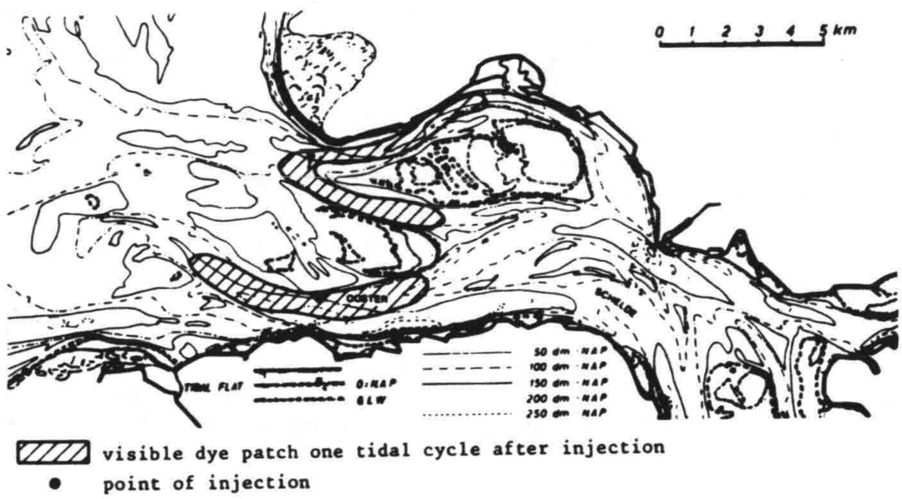

Figure 3.15 Concentration distribution primarily controlled by large scale advection induced by combined influence of tidal flow and bathymetry; dye patch separated into two parts

The large scale transports discussed thusfar are due to tidal currents. In addition one has to distinguish those due to wind and residual currents (Fischer et al, 1979, Sections 7.2.1 and 7.2.2.2). In wide estuaries residual currents may be caused by the Coriolis force (see Section 6) and by the interaction of the tidal flow with the irregular bathymetry.

8. Independent variables

Table 3.4 lists the main independent variables, which govern the salt intrusion and their effect. Fig. 3.16 gives quantitative information, derived from an extensive flume study performed by Delft Hydraulics (Rigter, 1973). This figure gives the effect of the separate independent variables on the maximum and minimum salt intrusion length, which occur at the end of the flood and the ebb, respectively.

Table 3.4 Effect of main independent variables

effect of increasing independent variable on:	stratification	salt intrusion
independent variable:		
water depth	+	+
river discharge	+	-
driving density difference	+	+
bed roughness	-	-
tidal amplitude (a)	-	- when (a) is small + when (a) is large

+: stratification or salt intrusion increases with increasing value of independent variable
-: stratification or salt intrusion decreases with increasing value of independent variable

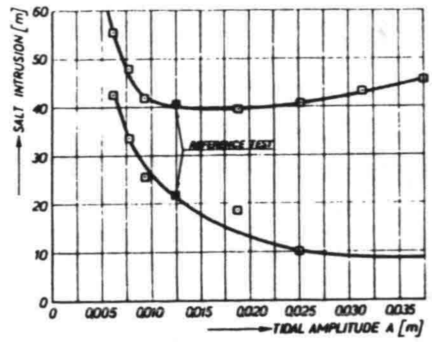

FIG. a -Maximum and Minimum Salt Intrusion Versus Tidal Amplitude

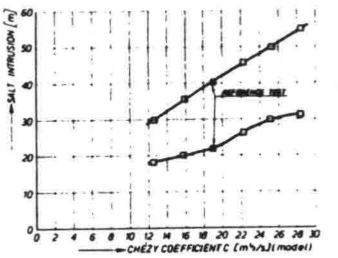

FIG. b -Maximum and Minimum Salt Intrusion Versus Chézy Coefficient

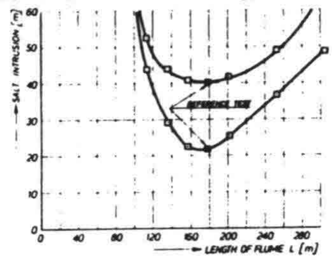

FIG. c -Maximum and Minimum Salt Intrusion Versus Length of Flume

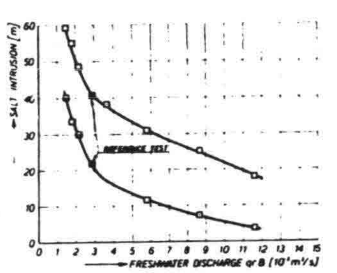

FIG. d -Maximum and Minimum Salt Intrusion Versus Freshwater Discharge

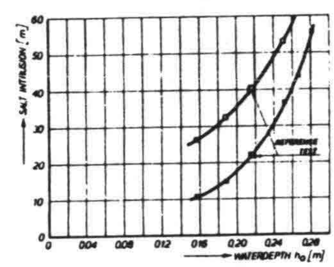

FIG. e -Maximum and Minimum Salt Intrusion Versus Water Depth

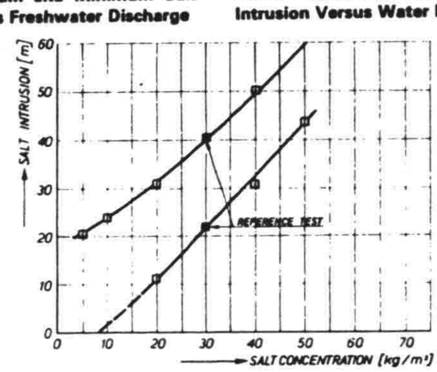

FIG. f -Maximum and Minimum Salt Intrusion Versus Salt Concentration at Sea

Fig. 3.16 Maximum and minimum salt intrusion as observed in systematic series of Delft Hydraulics' experiments (Rigter, 1973)

Turbulent energy is needed to cause vertical mixing. The amount of energy needed increases with increasing water depth, increasing river discharge and increasing driving density differences, i.e. the density difference between sea water and fresh water. The amount of energy available for mixing increases with increasing bed roughness and increasing tidal amplitude. These observations explain the effect of these independent variables on the stratification as listed in Table 3.4.

The fresh water velocity, i.e. the river discharge devided by the cross-section of the estuary decreases with increasing water depth, while it increases with increasing river discharge. Therefore, the salt water intrusion increases with increasing water depth, Fig. 3.16.e, while it decreases with increasing river discharge (Fig. 3.16.d). The strength of the gravitational circulation and therefore the salt intrusion increases with increasing driving density difference (Fig. 3.16.f).

Vertical mixing is a factor, which limits salt intrusion (see Section 4). Because of this reason the salt intrusion decreases with increasing bed roughness, i.e. decreasing Chézy coefficient (Fig. 9.16.b).

The effect of the tidal amplitude is determined by two counteracting effects. Large tidal amplitudes at the mouth of the estuary are associated with strong tidal currents, and hence with strong turbulent mixing and weak stratification. The stronger the turbulent mixing, the smaller salt intrusion tends to be. Because of this effect salt intrusion tends to become smaller with increasing tidal amplitude, in particular when the estuary is stratified.
Large tidal amplitudes at the mouth of the estuary are further associated with large tidal excursion paths. The larger the tidal excursion path, the larger salt intrusion tends to be at high water slack. Because of this effect, the salt intrusion tends to become larger with increasing tidal amplitude, in particular when the estuary is mixed.
Which of the above counteracting mechanisms prevails varies with the stratification, i.e. with the strength of the tide. For the flume, studied by Rigter (1973), this is clearly demonstrated by the fact that salt intrusion at high water slack decreases with increasing tidal amplitude when the latter is relatively small, while salt intrusion at high water slack increases with increasing tidal amplitude when the latter is relatively large. For

intermediate tidal amplitudes salt intrusion at high water slack is found to have its smallest magnitude (Fig. 3.16.a).

A further factor to be considered is the amplification of the tidal motion within the estuary channel. There is a maximum amplification of the tidal motion when the channel length corresponds to a quarter of the tidal wave length. There is a minimum amplification of the tidal motion when the channel length corresponds to half of the tidal wave length (Pugh, 1987, Section 5.2.2.).

Fig. 3.16.c shows that the salt intrusion has its minimum value for a length of the flume of 180 m, which is about 10% smaller than the length with maximum amplification and therefore with largest tidally induced mixing. Apparently for this length of the flume turbulent mixing is the prevailing mechanism.

9. Time scales

The independent variables, which govern the salt intrusion, vary with time. Therefore, several time scales can be distinguished in the variation of the salt intrusion with time.

- from year to year (because of a variation of the river flow from wet years to dry years)
- within the year from season to season (because of a variation of the river flow from a wet season to a dry season)
- over a month (because of the spring neap-tide cycle)
- within a tidal cycle (which may be either diurnal or semi-diurnal)
- at special events (e.g. a temporary increase of mean sea level because of a landward wind or a storm surge at sea).

During a tidal cycle the water moves a distance E_E outward during ebb and a distance E_F inward during flood-tide. Because of the river discharge the water gradually shifts seaward over a distance E_E-E_F. In a state of equilibrium the salinity at a certain point is the same after each whole tidal cycle. The downstream shift of the water is compensated by the upward "diffusion" of the salt. The tidal excursion of the salt E is estimated to be the mean of E_E and E_F and the motions of the salt can be supposed to be symmetric with respect to the mean situation.

The maximum and minimum of the salt intrusion occur when the currents reverse their direction at the times of slack water. At a certain point the maximum salinity, at high water slack, is equal to the mean salinity at a distance ½E downstream. In the same way the minimum salinity is related to the mean salinity at ½E upstream from the point. Fig. 3.17 illustrates how the extreme densities can be obtained from the time averaged values.

The tidal displacement of the longitudinal salt distribution, as shown in Fig. 3.17, is a direct response to the longitudinal tidal displacement of the water in the estuary. Therefore, the salt intrusion reacts immediately to changes in the longitudinal displacement of the water. These changes may be due to changes of the tidal range or by temporary changes of the mean sea-level.

The longitudinal salt distribution itself is affected by gravitational circulation and vertical mixing (Section 4 of this Chapter). The vertical mixing is a relatively slow process, in particular when the estuary is partly mixed or stratified. Hence, it may take the longitudinal salt distribution some days to adapt to changes in the gravitational circulation or vertical mixing. These changes may be induced by changes in the tidal range or water depth. They also may be due to a variation of the river discharge, which causes the downward shift E_E-E_F to change and therefore requires a change of the upward diffusion of salt, by which the downward shift of the water is compensated.

The relative slow response of the longitudinal salt distribution to a variation of the river discharge made it impossible for the density at the mouth of the Chao Phya estuary to follow the rapid variation of the discharge around August 10, 1962, as represented by Fig. 3.9.

Because of the same reason the response of the salt intrusion to a short term variation of the mean sea-level (e.g. during a day) is primarily controlled by its effect on the longitudinal displacement of water.

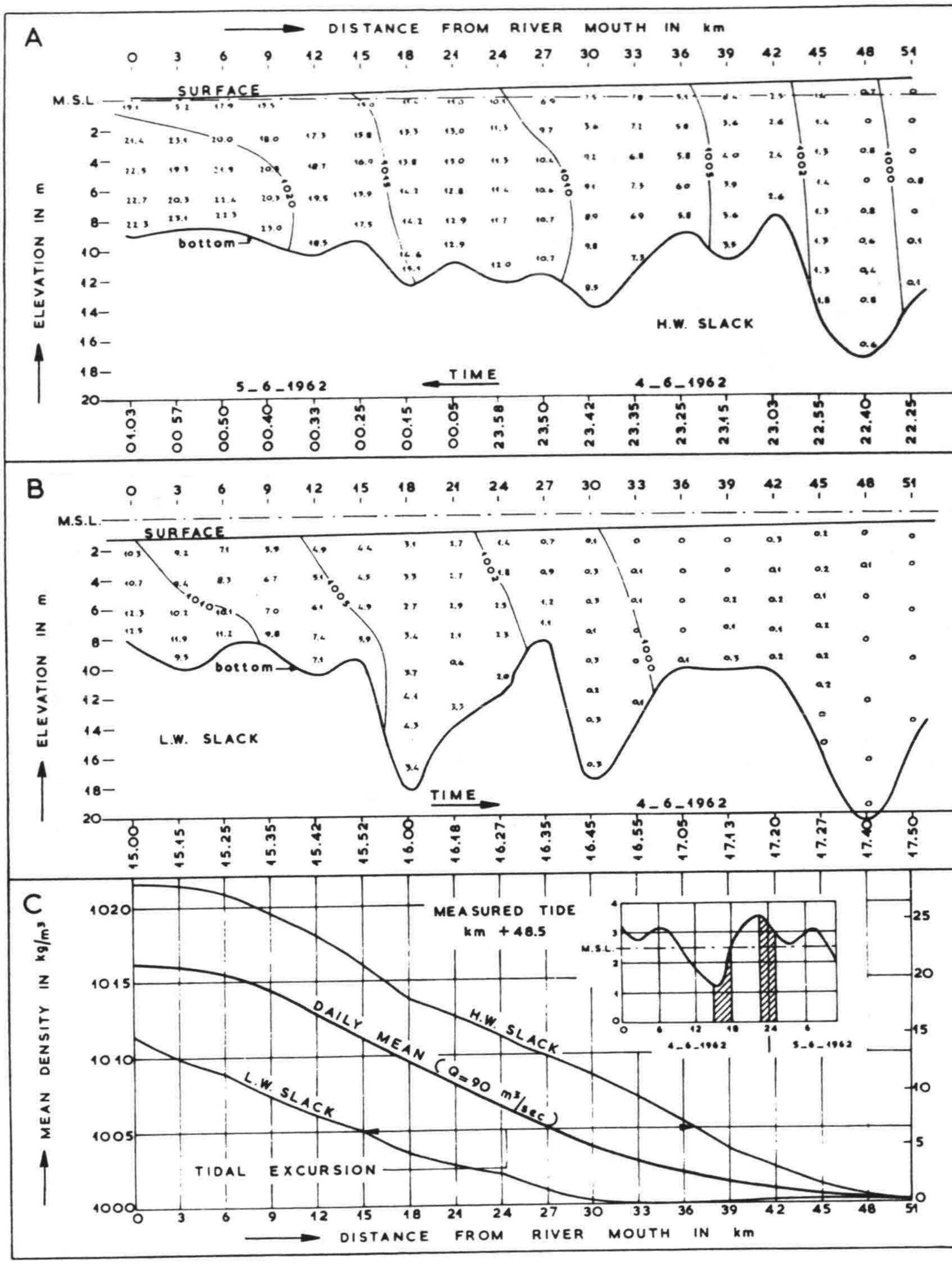

Fig. 3.17 Results of two sampling tours in the southern part of the Chao Phya river a) Around high water slack; b) Around low water slack; c) Comparison of the results

The Delft Hydraulics flume study, referred to in Section 9 of this chapter, includes experiments on the response of the salt intrusion to an increase of the time-mean water depth at sea. In a series of experiments the initial time-mean water depth at sea was 21.5 cm. After equilibrium conditions were obtained it was increased to become 24.7 cm. The time used for this increase ranged from 1 to 6 tidal cycles (n=1 to n=6). Fig. 3.18 shows some results. At the vertical axis this figure gives the difference between the maximum salt intrusion length measured at HW slack in a given tidal cycle and the maximum salt intrusion length measured in the original equilibrium condition. This difference is given in m as measured in the flume. At the horizontal axis Fig. 3.18 gives time (t) expressed in number of tidal cycles (T).

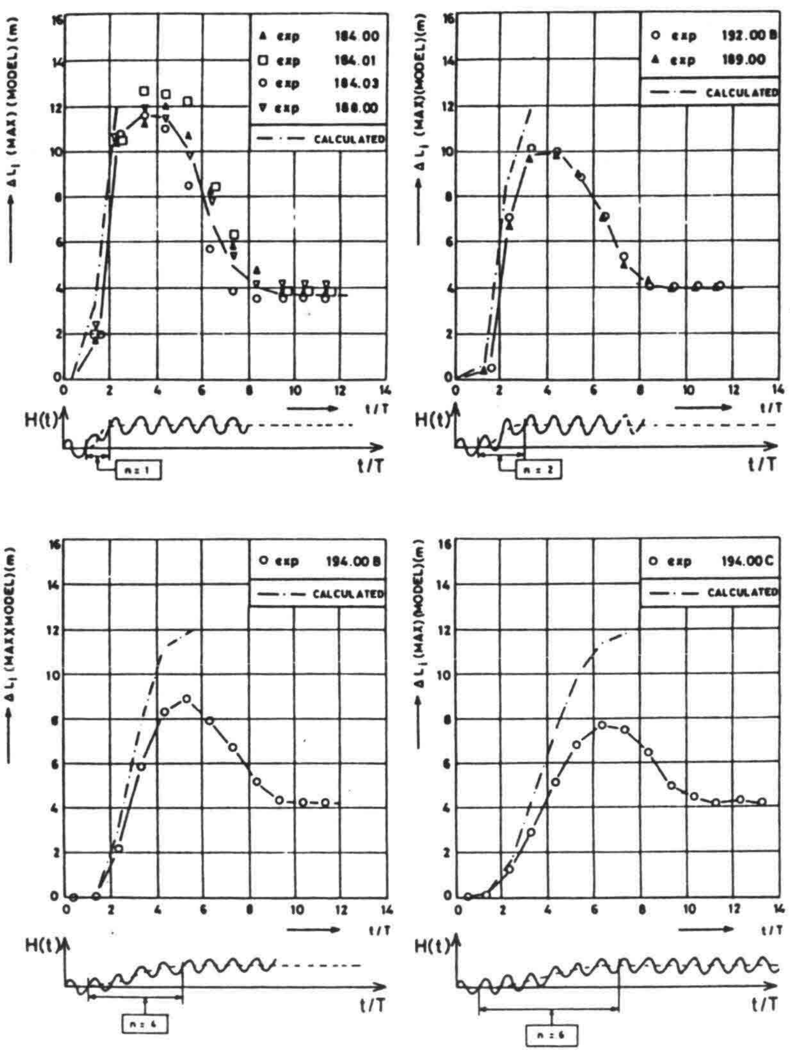

Fig. 3.18 Effect of increase of depth on salt intrusion length

Fig. 3.18 shows that it takes 8 to 10 tidal cycles to obtain a new equilibrium condition. In the new equilibrium condition the water depth and therefore the salt intrusion is larger than in the original equilibrium condition. In the transition period ($t/T < 8$ to 10) there is an overshoot, the salt intrusion being larger than in both the original and the final equilibrium condition. The overshoot decreases with increasing n.

To explain the overshoot it must be realized that a rise of the water level at sea must be followed by a rise of the water level in the river, which is in open connection with the sea. This requires an increase of the volume of water stored in the river, e.g. at high water slack. When the rise of the water level at sea is a relatively fast process (n=1), initially this increase of volume is primarily supplied from the sea. This is due to the fact that only a limited amount of water flows down the river. Eventually part of the increase of volume is supplied by the river, the river water gradually replacing part of the sea water. This explains the overshoot. When the rise of the water level at sea is a relatively slow process (n=6), part of the increase of volume can be supplied by the river. This implies that the overshoot becomes smaller.

Fig. 3.18 also gives calculated values of the increase of the salt intrusion length. This increase was calculated as the increase of E_F (i.e. the distance over which the water moves inward during the flood tide), assuming that the whole increase of volume was supplied from the sea. The faster the rise of the water level at sea, the better the calculations agree with the experiments. This finding confirms that the response of the salt intrusion to a short variation of the mean sea-level (e.g. during a day) is primarily controlled by its effect on the longitudinal displacement of the water.

The salt intrusion may increase considerably, when during the dry season the river discharge drops below a critical value. When the river discharge remains below this critical value for an extended period of time, the salt intrusion increases steadily during this period. Fig. 3.19 shows this phenomenon for the Gambia estuary, Gambia, where the discharge varies from 2-2000 m^3/s during the year and salt intrudes 200-250 km from the mouth over a 6 months' period during the dry season (Sanmuganathan and Abernethy, 1975). Similar observations have been made for the Pusur River estuary, Bangladesh, where the salt was found to intrude 135 km over a 4 months' period during the dry season (Delft Hydraulics, 1980).

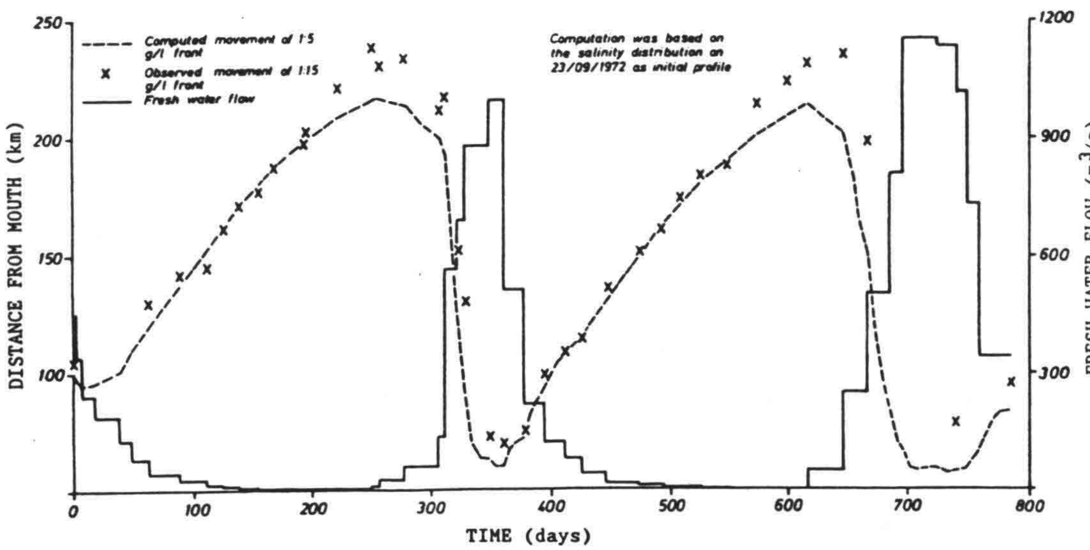

Fig. 3.19 Salinity advance and hydrograph for Gambia estuary (after Sanmuganathan and Abernethy (1975)).

10. Transient conditions versus equilibrium conditions

The factors governing the salt intrusion vary with time. Therefore, analyzing field data it is important to realize that this data may have been collected under

- equilibrium conditions, or
- transient conditions.

Under equilibrium conditions the salt concentration at a given location is the same after a whole tidal cycle. Transient conditions arise when the independent variables governing the salt intrusion vary with time over a sufficiently short preceding period. Then the salt intrusion must follow these changes.

Calibrating a mathematical model using salinities measured in conditions of equilibrium is relatively simple. Then it is sufficient to simulate the tide during which the salinities were measured. When the salinities are measured in transient conditions, the measured salinities are influenced not only by the hydraulic conditions pertaining in the tide of measurement but also by those in the preceding tides. Then, a sufficiently large number of preceding tides must be included in the calibration. Otherwise the "calibration" will result in an incorrectly tuned model.

11. Salt intrusion formulae

From dimensionless correlations for the Delft Tidal Flume and the Waterways Experiment Station flume data Rigter (1973) derived a formula for the minimum salt intrusion:

$$Li_{min} = \left[0.2 \frac{\frac{\Delta\rho}{\rho} g h_o}{u_{fr}^2} \cdot \frac{u_{fr}}{u_{1,0} - u_{fr}} - 1 \right] \cdot (\frac{C^2}{g}) \cdot h_o \tag{3.5}$$

with Li_{min} = minimum salt intrusion length in m, measured from the mouth of the estuary

and C = Chézy coëfficient in $m^{½}/s$

On the basis of the same data Fischer (1974) derived the formula:

$$Li_{min} = 3.7 \left[\frac{h_o^7 \, C^5 (\frac{\Delta\rho}{\rho})^3 \, g^{1/2}}{u_{fr} \, u_{1,0}^5} \right]^{1/4} \tag{3.6}$$

These formulae can be rewritten using the stratification parameters α and Fr_o (or Fr_f). They then read:

$$Li_{min} = 0.2(\frac{C^2}{g}) \left[Fr_f^{-1}\alpha(\frac{1}{\pi-\alpha}) - 5\right] h_o = 2(\frac{C^2}{g}) \left[Fr_o^{-1}\alpha^{-1}(\frac{1}{\pi-\alpha}) - 0.5\right] h_o \tag{3.7}$$

and

$$Li_{min} = 0.9(\frac{C^2}{g})^{5/8} Fr_f^{-3/4} \alpha^{5/4} h_o = 5(\frac{C^2}{g})^{5/8} Fr_o^{-3/4} \alpha^{-1/4} h_o \tag{3.8}$$

In chapter 2 of these lecture notes a formula for the stagnant salt wedge is given (Eq. 2.40) which in first approximation reads ($Fr_f << 1$):

$$L_i = 0.05 \, (\frac{1}{k_i}) \cdot Fr_f^{-1} \cdot h_o \tag{3.9}$$

where k_i^{-1} is the roughness parameter of the interface equivalent to C^2/g for the bottom roughness.
Therefore a formula for the salt intrusion length with $Fr_f^{-1} \cdot h_o$ or $Fr_o^{-1} \cdot h_o$ as (3.7) is, seems not unrealistic as a first approximation.

On this basis the Delft Tidal Flume experiments and prototype measurements of the Rotterdam Waterway and Chao Phya were re-examined giving the following simple formula for the minimum salt intrusion length:

$$Li_{min} \approx 0.055\left(\frac{C^2}{g}\right) Fr_f^{-1} \alpha h_o = 0.55\left(\frac{C^2}{g}\right) Fr_o^{-1} \alpha^{-1} h_o \qquad (3.10)$$

In table 3.5 a comparison is given of the observed intrusion lengths and those calculated by Eq. 3.7, 3.8 and 3.10, for tidal flume, Rotterdam Waterway and Chao Phya.

Table 3.5 Salt intrusion formulae compared with observations

Estuary	Delft tidal flume		Rotterdam Waterway				Chao Phya	
Characteristic	test 119	test 111	1908	1956	1963	1971	June 1962	Febr. 1970
Q_f (m^3/s)	$11.6 \cdot 10^{-3}$	$2.9 \cdot 10^{-3}$	430	960	1440	1550	85	150
h_o (m)	0.216	0.216	7.7	13.0	13.8	15.8	8.0	8.0
C ($m^{1/2}/s$)	19	19	65	60	60	60	60	60
α	1.64	0.75	0.42	0.65	0.86	0.73	0.04	0.07
Fr_o	0.51	0.15	0.44	0.23	0.25	0.27	1.11	1.38
Li_{min} observed (km)	**$4 \cdot 10^{-3}$**	**$49 \cdot 10^{-3}$**	**10**	**18**	**15**	**16**	**33**	**17**
Eq. 3.7	$7 \cdot 10^{-3}$	$59 \cdot 10^{-3}$	10	20	15	18.5	37	15
Eq. 3.8	$17 \cdot 10^{-3}$	$56 \cdot 10^{-3}$	4	8.5	8	9	3	2.5
Eq. 3.10	$6 \cdot 10^{-3}$	$44 \cdot 10^{-3}$	10	17	12.5	16	34	15

From these figures the following observations can be made:
- Eq. 3.8 seems to underestimate the intrusion in nature, possibly due to the 5/8 power of C^2/g
- Eq. 3.7 or 3.10 can be used to make a rough estimate of the intrusion length, however they should be used with care since they only give the order of magnitude
- for relative purposes, i.e. to make an estimate of the influence of changes of one of the parameters involved (h_o, Q_{fr}, etc.) all formulae can be used; they will give an indication of the relative importance of the various parameters.

References

Abraham, G., De Jong, P. and Van Kruiningen, F.E., 1986. Large-scale mixing processes in a partly mixed estuary, in Physics of shallow estuaries and bays, Van de Kreeke, J. (ed.), Springer, Berlin.

Allersma, A., Hoekstra, A.J. and Bijker, E.W. Transport patterns in the Chao Phya estuary, paper 5.5, Proceedings 12th Coastal Engineering Conference, Tokyo, 1966, an extending version of which is published as Delft Hydraulics Laboratory Publication no. 47, March 1967.

Bowden, K.F. and Sharaf El Din, S.H. Circulation, salinity and river discharge in the Mersey Estuary, Geophysical Journal of the Royal Astronomical Society, Vol. 10, 1966, pp. 383-399.

Breusers, H.N.C. and Van Os, A.G. Physical Modeling of the Rotterdamse Waterweg estuary, Proc. ASCE, Journal of Hydraulic Division, 107, No. HY 11, 1981, pp. 1351 - 1370.

Cameron, W.M. and Pritchard, D.W. Estuaries in the Sea. Hill, M.N., editor, Vol. 2, Wiley, New York, 1963, pp. 306 - 324.

Delft Hydraulics Laboratory. Tidal estuary studies - Bangladesh, Interim-report on Planning Phases I and II(A), Report on Identification Mission October 31st - November 29th, 1979, in Bangladesh, prepared for Bangladesh Ministry of Flood Control, Water Resources and Power, and Bangladesh Water Development Board, March 1980.

Dronkers, J., Van Os, A.G., and Leendertse, J.J., 1981. Predictive salinity modeling of the Oosterschelde with hydraulic and mathematical models, in Transport models for inland and coastal waters, Fischer, H.B. editor, Academic Press.

Dronkers, J. and Van Leussen, W. (eds.), (1988). Physical processes in estuaries, Springer, Berlin.

Dyer, K.R. Estuaries, a physical introduction, Wiley, London, 1973.

Dyer, K.R. The salt balance in stratified estuaries. Estuarine and Coastal Marine Science, Vol. 2, 1974, pp. 273-281.

Dyer, K.R. Lateral circulation effects in estuaries. Estuaries, Geophysics and the Environment, National Academy of Science, 1977, pp. 22-29.

Fischer, H.B. Mass transport mechanisms in partially stratified estuaries. Journal of Fluid Mechanics, 53, part 4, 1972, p. 671.

Fischer, H.B. Mixing and dispersion in estuaries. Annual Review of Fluid Mechanics, 8, 1976, pp. 107-133.

Fischer, H.B. Discussion of minimum length of salt intrusion in estuaries, by B.P. Rigter, J. Hydr. Div., Proc. ASCE, 100, HY5, 1974, pp. 708-712.

Fischer, H.B., List, E.J., Koh, R.C.Y., Imberger, J. and Brooks, N.H. Mixing in inland and coastal waters, Academic Press, New York, 1979.

Geyer, W.R., 1988. The advance of a salt wedge front; observations and dynamical model, in Physical processes in estuaries, Dronkers, J. and Van Leussen, W. (eds.), Springer, Berlin.

Harleman, D.R.F. and Ippen, A.T., 1967. Two-dimensional aspects of salinity intrusion in estuaries; analysis of salinity and velocity distributions. Committee on Tidal Hydraulics, Corps of Engineers, U.S. Army, Technical Bulletin no. 13.

Hughes, F.W. and Rattray, M. Salt flux and mixing in the Columbia River - Estuary, Estuarine and Coastal Marine Science, Vol. 10, 1980, pp. 479-493.

Ippen, A.T. (editor). Estuary and coastline hydrodynamics, Mc Graw-Hill, New York, 1966.

Jay, D.A. and Smith, J.D., 1988. Residual circulation in and classification of shallow, stratified estuaries, in Physical processes in estuaries, Dronkers, J. and Van Leussen, W. (eds.), Springer, Berlin.

Lauff, G.H. Estuaries, Publ. 83, American Association for the Advance of Sciences, 1967.

Mc. Dowell, D.M. and O´Connor, B.A. Hydraulic behavior of estuaries, Mc. Millan, London, 1977.

Nedeco. Siltation Bangkok port channel, Volume 2, Netherlands Engineering Consultants, the Hague, the Netherlands, 1965.

Pritchard, D.W. The movement and mixing of contaminants in tidal estuaries. Proc. 1st International conference on waste disposal in the marine environment, University of California, Berkeley, 1959, pp. 512-525.

Pugh, D.T. Tides, surges and mean sea-level, John Wiley Chichester, 1987.

Rigter, B.P. Minimum length of salt intrusion in estuaries. Proc. ASCE, Journal of Hydraulics Division, 99, No. HY 9, September 1973, pp. 1475-1496.

Sanmuganathan, K. and Abernethy, C.L. A Mathematical model to predict long term salinity intrusion in estuaries, Proceedings Second World Congress, International Water Resources Association, New Delhi, December 1975, Vol. 3, pp. 313-324.

Simmons, H.B. Some effects of upland discharge on estuarine hydraulics. Proc. ASCE, 81, 1955, paper no. 792, see also
Simmons, H.B. Field experience in estuaries, chapter 16 of Estuary and coastline hydrodynamics, Ippen, A.T., editor, Mc. Graww-Hill, New York, 1966.

Thatcher, M.L. and Harleman, D.R.F. Long-term salinity calculation in Delaware Estuary, Proc. ASCE, Journal Environmental Engineering Division, 107, No. EE1, February 1981, pp. 11-27.

Chapter 4. One-dimensional real-time intrusion models

1. Introduction

For several technical problems it is of interest to know how the salt intrusion is affected by modifications of the estuary conditions such as a reduction of the river flow (e.g. when using the river water for irrigation) and an artificial increase of the depth (e.g. by dredging for navigation). Both a reduction of river flow and an increase of depth are associated with an increasing length of the zone with salt intrusion. Predictive models for salt intrusion can be used to answer these questions. Dependent on the accuracy needed, the available data and, of course, the time and research budgets available, one of the following models can be chosen:

- hydraulic scale models, which are very reliable and accurate, if skillfully built and operated, but also very expensive

- mathematical models, where the extent of schematization in dimensions and time determines the reliability and cost:
  - three-dimensional real-time models, where turbulence is parameterized, but all other phenomena are taken into account; they are expensive too
  - two-dimensional width integrated models, where the vertical dimension, and thus the gravitational circulation is taken into account, but the lateral phenomena should be parameterized
  - two-dimensional depth integrated models, where the equations are averaged over the depth, thus parameterizing the gravitational circulation
  - two-layer models (width integrated or not), where the vertical variations are schematized in two layers (see chapter 2)
  - one-dimensional, cross-sectional averaged models, where real-time models, as well as time integrated long term models can be distinguished; these models are relatively simple and cheap to use, they can easily be applied on a personal computer.

The stratification of an estuary is an important factor, determining the applicability of a model: in a stratified situation, depth averaged models cannot reliably be used, where as in a completely mixed situation these models are very useful. Then one-dimensional real-time salt intrusion models can be used to answer questions as mentioned above on the basis of the profile averaged salt concentration.

One-dimensional real-time solutions are obtained by solving

(i) the continuity for water,

(ii) the equation of motion in the longitudinal direction, and

(iii) the continuity equation for salt,

all averaged over the cross-section of the considered channel.

The solution of these equations gives the profile averaged velocity, the profile averaged salt concentration and the water depth as a function of the distance from the mouth of the estuary and the time.

One-dimensional real-time salt intrusion models give the variation of the above parameters with time within a tidal cycle. In this respect they differ from one-dimensional time-averaged salt intrusion models, which give the variation of these parameters with time over the tidal cycles.

The one-dimensional continuity equation for salt contains the dispersive transport of salt. Understanding this transport is essential to understand the capabilities and limitations of the one-dimensional salt intrusion models.

2. Notation; basic relationships

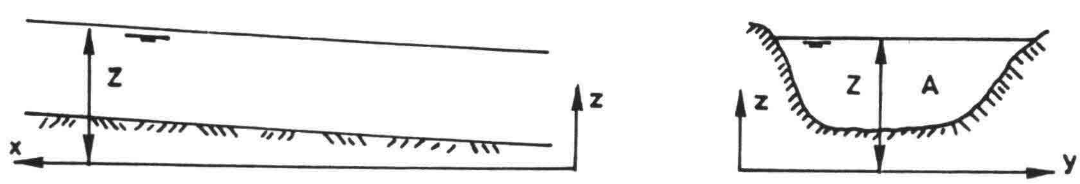

Fig. 4.1 Notation: longitudinal section and cross-section of considered water course

It is convenient to use the following notation in this chapter.

- Z : elevation of water surface with respect to a horizontal datum ($z=0$) (see Fig. 4.1) ($Z = h + h_b$ in notation of Chapter 1)
- x : longitudinal coordinate, measured from mouth of estuary and positive when directed inward
- z : vertical coordinate (see Fig. 4.1)
- y : transverse coordinate
- A : wet cross-sectional area.

From the geometry of the considered channel the following relationships can be found

$$A = f_1(Z) \qquad\qquad h = f_2(Z) \tag{4.1}$$

where

h : water depth, averaged over width

f_i: functional dependence

For a well mixed estuary (see Section 2.3, Chapter 1)

$$p = \bar{\rho}\, g(Z-z) \tag{4.2}$$

where
p : hydrostatic pressure
ρ : density
g : acceleration by gravity
$=$: symbol denoting profile averaged value.

and

$$F_p = -\frac{1}{\rho}\frac{\partial p}{\partial x} = -g\frac{\partial Z}{\partial x} - \frac{1}{\bar{\rho}}\, g\,(Z-z)\,\frac{\partial \bar{\rho}}{\partial x} \tag{4.3}$$

where F_p : net inward force per unit mass of fluid caused by a variation of p with x

Knowing the shape of the cross-section, one can determine the profile averaged value of F_p, i.e.

$$\bar{\bar{F}}_p = \frac{1}{A} \int_A F_p \, dA = - g \frac{\partial Z}{\partial x} - \frac{1}{\bar{\rho}} g \, d_c \frac{\partial \bar{\rho}}{\partial x} \tag{4.4}$$

where d_c : distance from water surface to centroid of cross-section

For a channel with rectangular cross-section $d_c = \frac{1}{2}$ h, where h is the water depth, averaged over the width.

The first term at the righthand side of Eq. 4.4 represents the effect of the slope of the water surface on the net force acting on a unit mass of fluid. The second term represents the relatively small effect of the density differences on the profile averaged tidal flow. The second term is of the order $\Delta\rho/\rho$, compared with the first term.

As the effect of the second term is small it is justified to approximate d_c by $\frac{1}{2}$ h and to apply Eq. 4.4 also to partially mixed estuaries, although it is derived for well mixed estuaries.

3. Governing equations

3.1 Continuity equation for water

The continuity equation for water reads

$$\frac{\partial A}{\partial t} + \frac{\partial A\bar{\bar{u}}}{\partial x} = 0 \tag{4.5}$$

where $\bar{\bar{u}}$: longitudinal velocity component

3.2 Momentum equation

Substituting Eq. 4.4, approximating d_c by $\frac{1}{2}$ h and the hydraulic radius by h, the momentum equation is given by

$$\frac{\partial \bar{\bar{u}}}{\partial t} + \bar{\bar{u}} \frac{\partial \bar{\bar{u}}}{\partial x} + g \frac{\partial Z}{\partial x} + \frac{1}{2} \frac{1}{\bar{\rho}} g \, h \frac{\partial \bar{\rho}}{\partial x} + g \frac{\bar{\bar{u}}|\bar{\bar{u}}|}{C^2 \, h} = 0 \tag{4.6}$$

where C : Chézy coefficient

The density ρ has to be related to the salt concentration using the equation of state

$$\bar{\rho} = f_3(\bar{c}) \qquad (4.7)$$

where c : concentration of salt

The equation of state can be derived from the appendix of Chapter 1.

3.3 Continuity equation for salt

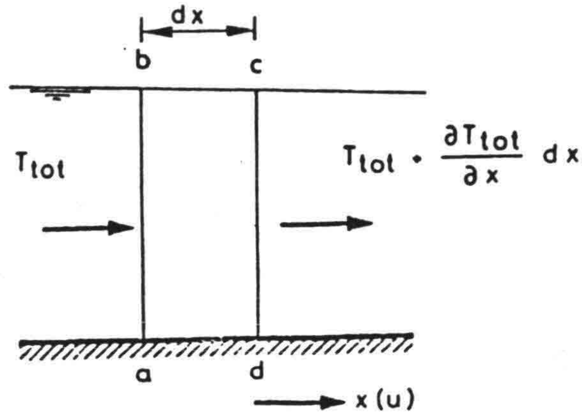

Fig. 4.2 Derivation of one-dimensional continuity equation for salt

Inflow of salt through plane ab into the space between planes ab and cd, which are a distance dx apart, (See Fig. 4.2) is

$$T_{tot}\, dt \qquad \text{(a)}$$

where T_{tot} : total transport of salt through cross section of channel.

Inflow of salt through plane cd is

$$- (T_{tot} + \frac{\partial T_{tot}}{\partial x} dx)\, dt \qquad \text{(b)}$$

Increase of quantity of salt between planes ab and cd is

$$\frac{\partial A \bar{c}}{\partial t} dt\, dx \qquad \text{(c)}$$

The continuity equation for salt expresses the increase of the quantity of salt between planes ab and cd to be equal to the net inflow of salt through these planes. This means (a) + (b) = (c) or

$$\frac{\partial\, A\, \bar{\bar{c}}}{\partial t} + \frac{\partial\, T_{tot}}{\partial x} = 0 \tag{4.8}$$

4. Total transport of salt

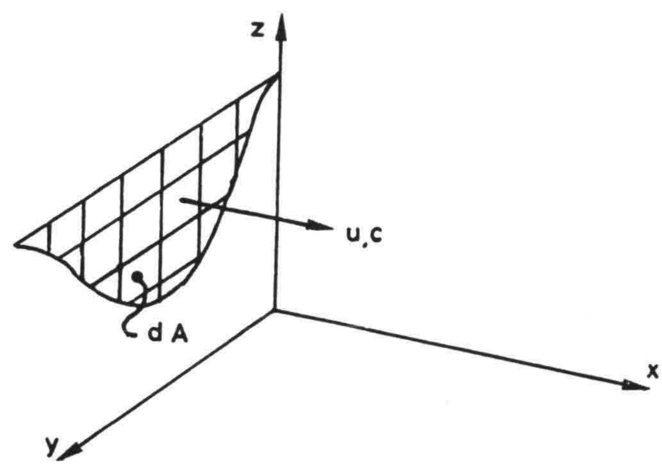

Fig. 4.3 Cross-section A divided into elements dA

The cross-section of a channel can be divided into different elements, each having an area dA. The elements can be taken so small that in each point of them the velocity, the salt concentration and the turbulent transport of salt have the same value.

Under these conditions the flux of volume through an element, i.e. the volume of water flowing through it per unit time, amounts to udA. This implies that the discharge through the considered cross-section amounts to A $\bar{\bar{u}}$.

The volume of water flowing through an element dA may have a salt concentration c. If so, the transport of salt through the element, induced by the flow amounts to ucdA per unit time. In addition there is a turbulent transport of salt through the element, which per unit time amounts to $T_{turb,x}dA$, where $T_{turb,x}$ represents the turbulent transport per unit area of the cross-section and per unit time.

Therefore, the total transport of salt through the cross-section is given by

$$T_{tot} = \int_A (u.c + T_{turb,x})\, dA = A\,(\overline{\overline{uc}} + \overline{\overline{T}}_{turb,x}) \qquad (4.9)$$

where $T_{turb,x}$: turbulent transport of salt in x-direction per unit area of cross-section

5. Dispersive transport; dispersion coefficient

In problems of salt intrusion u and c vary over the cross-section, e.g. due to the stratification and the gravitational circulation. Under these conditions

$$\overline{\overline{uc}} \neq \overline{\overline{u}}\,.\,\overline{\overline{c}} \qquad (4.10)$$

This is illustrated by Fig. 4.4 where schematized triangular distributions of salt concentration and velocity over the depth are given.

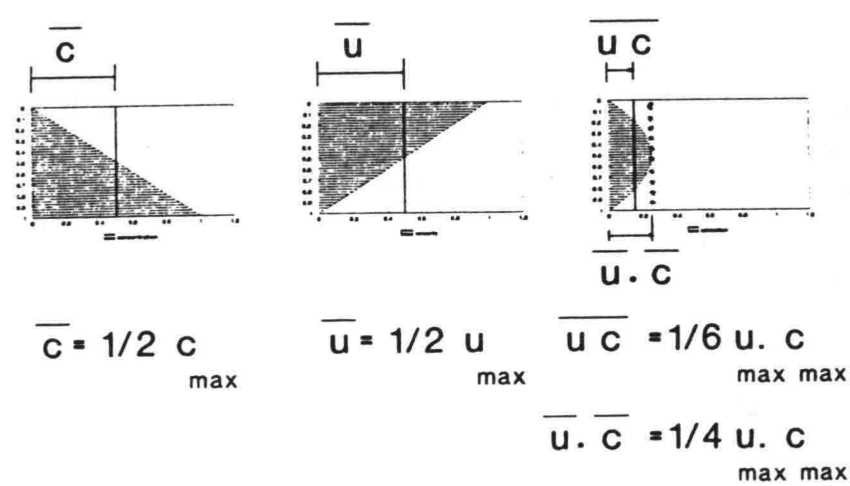

Fig. 4.4 Schematized illustration of dispersive transport

These distributions give as average values for concentration and velocity respectively

$\bar{c} = \frac{1}{2} c_{max}$ and $\bar{u} = \frac{1}{2} u_{max}$, and consequently

$\bar{u} \cdot \bar{c} = \frac{1}{4} u_{max} \cdot c_{max}$

However $\overline{uc} = \frac{1}{6} u_{max} \cdot c_{max} \neq \bar{u}.\bar{c}$

These schematized distributions are not unrealistic as can be seen in Fig. 4.5 (page 4.10), 7 hr.
In the same figure at 11 hr. another example of inequality (4.10) can be seen.

At high water slack, $\bar{u} = 0$. Hence $\bar{u}.\bar{c} = 0$. Yet, there is a net inward transport of salt trough the cross-section induced by the flow, i.e. $\overline{uc} \neq 0$, when the salt concentration of the water flowing in over the bottom is larger than that of the water flowing out at the surface.

The purpose of one-dimensional modelling is to determine $\bar{u}$, $\bar{c}$ and A as a function of x and t. Therefore, the total transport must be expressed in these quantities. Eq. 4.10 implies that this cannot be accomplished by simply substituting $\bar{u}.\bar{c}$ for $\overline{uc}$.

To overcome this difficulty, the total transport is devided into the following parts

$$T_{tot} = A\ \bar{u}.\bar{c} + T_{disp} \tag{4.11}$$

where $T_{disp.}$: dispersive transport of salt, defined as

$$T_{disp.} = A\ [\underbrace{(\overline{u.c} - \bar{u}.\bar{c})}_{(1)} + \underbrace{\bar{T}_{turb,x}}_{(2)}] = \int_A [\underbrace{(u - \bar{u})\ (c - \bar{c})}_{(1)} + \underbrace{T_{turb,x}}_{(2)}]dA \tag{4.12}$$

The unknown quantities $\overline{uc}$ and $T_{turb,x}$ are included in the dispersive transport. In the example of Fig. 4.4 term (1) is equal to $-\frac{1}{12} u_{max} \cdot c_{max}$, i.e. half as much as $\overline{u.c}$ and with opposite sign.

The dispersive transport is the salt transport into the estuary through a reference plane moving at velocity $\bar{u}$. Salt would not penetrate further into the estuary from its mouth than the tidal excursion length, if the dispersive transport were zero. If so, salt water which enters into the estuary from the sea on the flood tide, would return to the sea before the end of the following ebb tide. This is because, when moving at velocity $\bar{u}$, the river flow makes the seaward displacement on the ebb tide larger than the land-inward displacement on the flood tide.

The first part of the dispersive transport represents the contribution by the variation of the velocity and concentration over the cross section. The second part represents the contribution by turbulent transport. The first part is zero when the velocity or concentration is completely homogeneously distributed over the cross section. Then the inequality given by Eq. 4.10 does not apply.

In order to express the total transport in $\bar{c}$ the dispersion coefficient is introduced. By definition

$$T_{disp} = - A D \frac{\partial \bar{c}}{\partial x} \tag{4.13}$$

where D : dispersion coefficient.

When the variation of c over the cross-section is small, the magnitude of D can be derived from theory (Fischer et al, 1979. Sections 4.2, 4.3, 5.2, 7.2.2). For salt intrusion into estuaries, the magnitude of D can not be derived from theory. Therefore, for each separate estuary it must be derived from field measurements. This is discussed further in Section 9 of this chapter.

Substituting Eqs. 4.11 and 4.13 into Eq. 4.18, the continuity equation for salt may be written as

$$\frac{\partial \bar{c}}{\partial t} + \bar{u} \frac{\partial \bar{c}}{\partial x} - \frac{1}{A} \frac{\partial}{\partial x} A D \frac{\partial \bar{c}}{\partial x} = 0 \tag{4.14}$$

6. Field data on dispersive transport

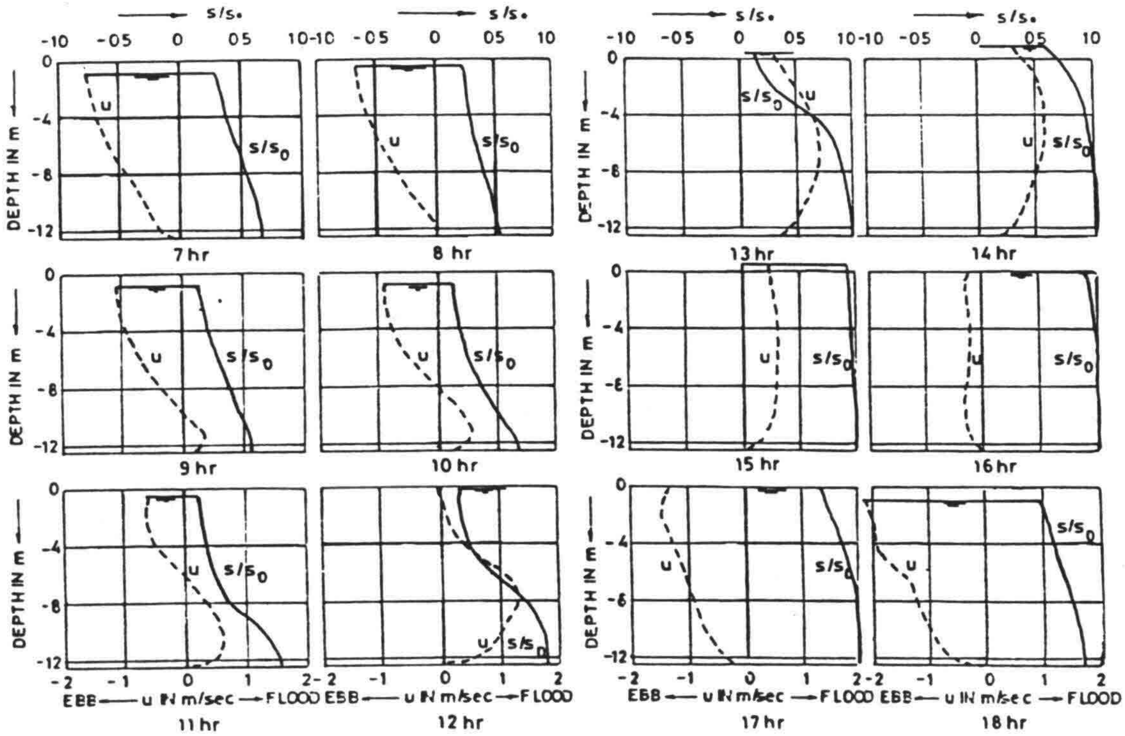

Fig. 4.5 Rotterdam Waterway estuary, station 1030 km; variation of velocity and salinity over depth (top) and associated dispersive transport (bottom).

Fig. 4.5 gives the variation of velocity and salinity over the depth as observed at the Rotterdam Waterway estuary in station 1030 km close to the mouth of the estuary. Fig. 4.6.b gives the associated dispersive transport. Because of the gravitational circulation the variation over the depth of ebb velocities (around 7 hr) and low water slack velocities (around 11 hr) is much larger than that of flood velocities (around 14 hr). Therefore, at the considered station during the ebb tide and at low water slack the dispersive transport tends to be larger than during the flood tide.

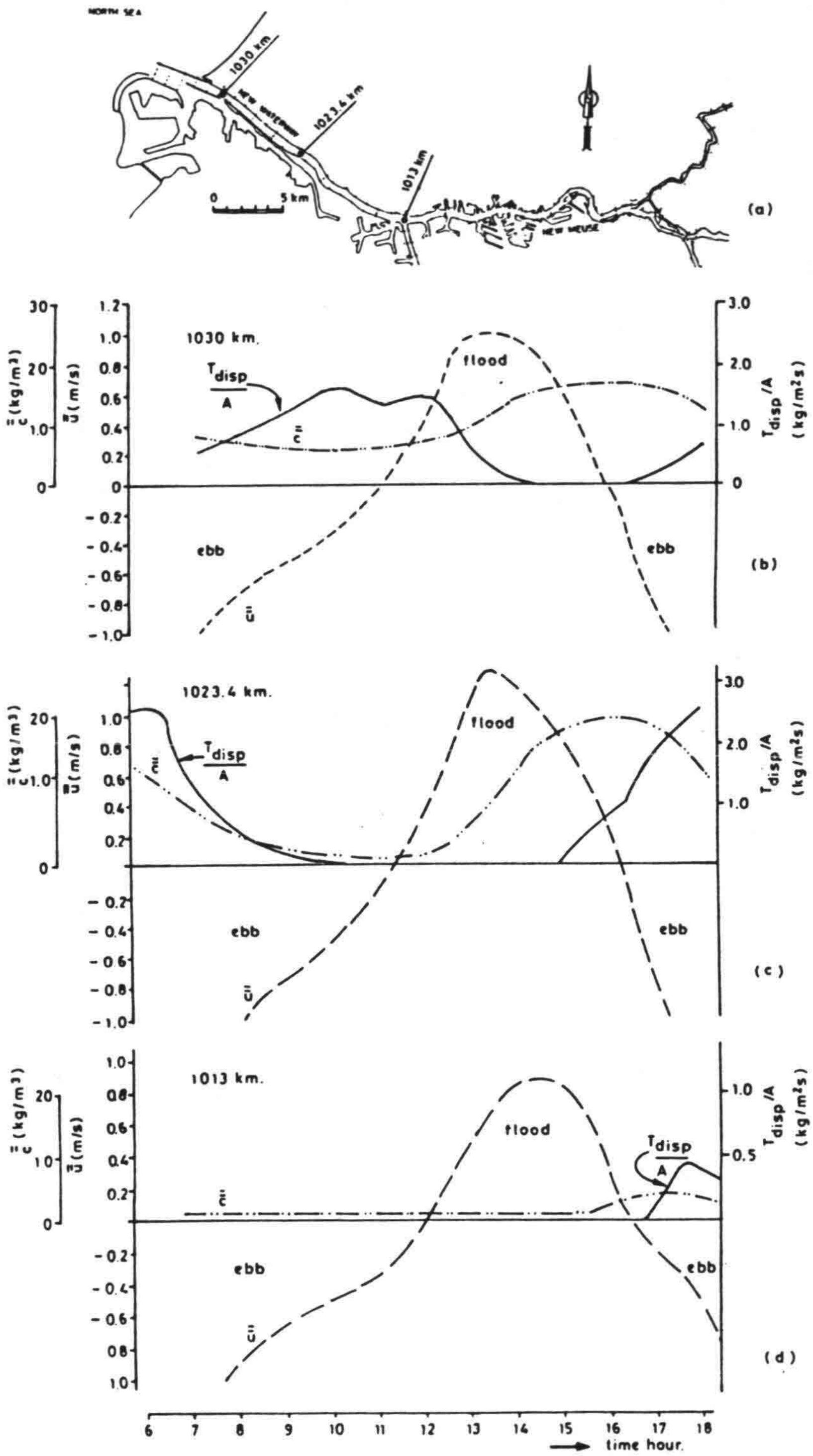

Fig. 4.6 Rotterdam Waterway estuary, variation of dispersive transport over tidal cycle for stations 1030 km, 1023.4 km and 1013 km

Minimum salt intrusion occurs at the end of the ebb, i.e. at low water slack. For stations far from the mouth this implies that around low water slack the salt content is about zero. Therefore, for stations further upstream in the zone of salt intrusion the dispersive transport tends to have its largest value during maximum ebb rather than at low water slack (see Fig. 4.6.c for station 1023.4 km). For stations near the end of the zone of salt intrusion the dispersive transport, if any, only can occur at high water slack, i.e. when maximum salt intrusion occurs (Fig. 4.6.d for station 1013 km).

Summarizing, the dispersive transport varies with time during the tidal cycle. Ebb values tend to be larger than flood values. Close to the mouth of the estuary peak values occur at low water slack, half way the zone of salt intrusion at maximum ebb and near the end of the zone of salt intrusion at high water slack.

The above findings imply that the dispersion coefficient varies both with time during the tidal cycle and with the longitudinal coordinate.

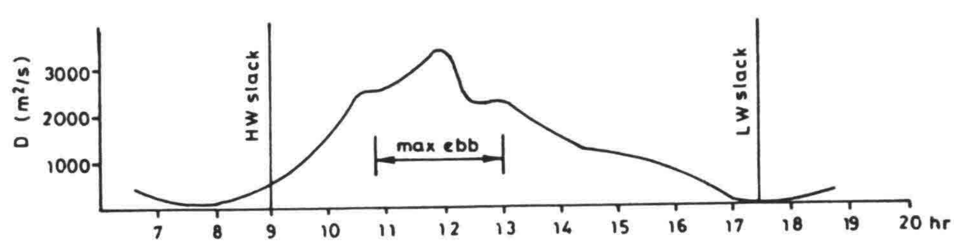

Fig. 4.7 Variation of D with time over a tidal cycle, Rotterdam Waterway estuary, station 1025 km, april 11, 1985

Fig. 4.7 gives the variation of the dispersion coefficient, D, with time for the Rotterdam Waterway estuary for station 1025 km where the peak values of D occur during maximum ebb.

Fig. 4.8 (Thatcher and Harleman, 1983) gives a typical instantaneous longitudinal distribution of D for the Delaware estuary (solid line), showing the contribution of geometric effects and density effects, D_g and $D_{\Delta\rho}$ respectively. In the region of salt intrusion (x < 90 miles) density effects account for about two-third of the total dispersion coefficient. In the fresh water portion of the estuary (x > 90 miles) geometric effects provide the entire dispersion coefficient.

The D values given for the Rotterdam Waterway estuary are substantially larger than those given for the Delaware estuary (D of the order of 1000 m^2/s versus D of the order of 100 m^2/s)). This seems due to a difference in stratification as the Rotterdam Waterway is a partly mixed estuary while the Delaware estuary is well mixed.

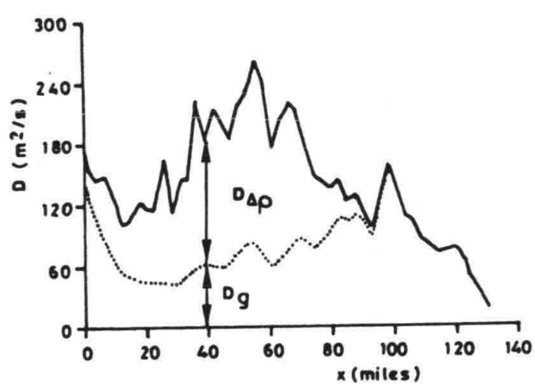

Fig. 4.8 Instantaneous distribution of $D = D_g + D_{\Delta\rho}$, Delaware estuary (Thatcher and Harleman, 1983)

7. Number of equations versus number of unknown

The continuity equation for water, the momentum equation, the continuity equation for salt and the equation of state form a system of four equations, which contain four unknown parameters ($\bar{u}$, $\bar{c}$, $\bar{\rho}$, Z) and two characteristics of the channel geometry (A, h), which can be given as a function of Z. Hence, the four unknown parameters can be solved from this system of four equations.

equations	unknowns	coeffi- cients	functions of Z	
continuity equation for water (Eq. 4.5)	$\bar{\bar{u}}$, Z		A	
momentum equation (Eq. 4.6)	$\bar{\bar{u}}$, $\bar{\bar{c}}$, $\bar{\bar{\rho}}$, Z	C		h
continuity equation for salt (Eq. 4.14)	$\bar{\bar{u}}$, $\bar{\bar{c}}$, Z	D	A	
equation of state (Eq. 4.7)	$\bar{\bar{c}}$, $\bar{\bar{\rho}}$			
4 equations	4 unknowns			

The above system of four equations contains two coefficients, the Chezy coefficient C and the dispersion coefficient D. These coefficients have to be given as input data. This, however, is the critical issue of one-dimensional real-time salt intrusion modelling since no empirical relationships between the magnitude of the dispersion coefficient and determining conditions generally applicable to any arbitrary estuary is available as yet.

8. Boundary conditions

For the continuity equation for water and the momentum equation, the same boundary conditions can be used as for homogeneous tidal computations.

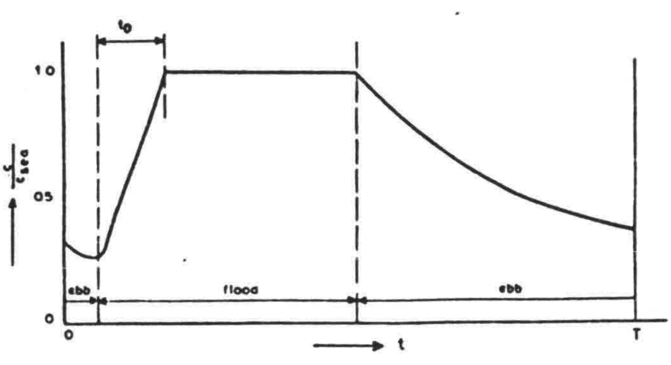

Fig. 4.9 Prescribing boundary conditions at mouth by prescribing transition time, t_o, and concentration of water entering from sea, c_{sea}.

For the continuity equation for salt, boundary conditions must be given both upstream and at the mouth of the estuary.

The upstream boundary condition for salt is relatively simple. The salt concentration can be set equal to zero, when the upstream boundary is outside the zone of salt intrusion.

Specifying the boundary condition at the mouth of the estuary is a more delicate problem. Doing so, one has to indicate how the value of the concentration averaged over the cross-section varies with time. This can be solved by assuming that during flood this concentration coincides with the concentration at sea. During ebb it is controlled by the river. Then it is equal to the salt concentration of the water flowing out of the estuary passing the mouth. This concentration is governed by the conditions upstream from the mouth, and hence it can be computed. At the end of the ebb the concentration of the water flowing out of the estuary is lower than the concentration at sea. Hence, at the beginning of the flood there is a gradual transition from the concentration occurring at the end of the ebb to the concentration as found at sea, c_{sea}. How this transition proceeds depends upon the the conditions at sea, and hence cannot be computed. This has to specified by prescribing the duration of the period of transition, t_o, (see Fig. 4.9) as a fraction of the tidal cycle, T. (Thatcher and Harleman, 1981).

The necessity to prescribe the duration of the transition period, introduces an arbitrary element not only in the formulation of the boundary conditions, but also in the magnitude of the dispersion coefficient. The smaller t_o, the larger the salt concentration of the water entering the estuary from the sea at the beginning of the flood tide and hence the larger the transport of salt into the estuary from the sea at the beginning of the flood tide. Consequently, the smaller t_o, the larger the salt intrusion, unless compensated by adjusting the magnitude of the dispersion coefficient. The smaller the dispersion coefficient, the smaller the dispersive transport of salt into the estuary from the sea. Hence the effect on the salt intrusion of a reduction of t_o can be compensated by a decrease of the magnitude of the dispersion coefficient. For instance, for the Rotterdam Waterway it was found that a reduction of t_o/T from 0.15 to 0.05 could be compensated by a decrease of D from 100% to about 60%. (Delft Hydraulics project M896). Consequently the dispersion coefficient to be applied depends on the formulation of the boundary conditions and vice versa.

9. Dispersion coefficient

The dispersion coefficient depends on the variation of u and c both with the transverse coordinate y and the vertical coordinate z (Eq. 4.12, Fig. 4.3). This implies that the dispersion coefficient depends on

- the stratification of the estuary,
- the gravitational circulation,
- the geometry of the estuary.

The gravitational circulation tends to make the dispersive transport large during the ebb-tide and small during the flood-tide. Therefore the ebb values of the dispersion coefficient tend to be larger than the flood values.

The geometry of the estuary influences the variation of u and c over the depth and in the transverse direction. Because the cross-section of most estuaries is not rectangular, the gravitational circulation is unevenly distributed over the width of the channel (Fig. 3.4). Bends have changes in cross-sectional form associated with them and cause the thread of the maximum current to swing towards the outside of the bend. The changes in cross-sectional form may lead to circulations in the horizontal plane (Fig. 3.13). Hence, the dispersion coefficient depends both on the shape of the cross-section and the curvature of the estuary and the variation of these features with the longitudinal coordinate. This means that the dispersion coefficient depends on the unique geometric features of an individual estuary.

10. Implications for one-dimensional real-time modelling

A dispersion relationship, which is used in one-dimensional real-time salt intrusion modelling must satisfy contradictory requirements. In order to represent the main mechanisms, it must account for the geometric features of the considered estuary, its vertical stratification and the variation of the dispersion over the tidal cycle from the ebb-tide to the flood-tide. However, in order to be applicable in an one-dimensional context, it must be expressed in profile averaged parameters without knowing precisely how u and c vary over the cross-section. Therefore, the dispersion relationship cannot be obtained from theory. Instead, for each considered estuary it represents an empirical relationship to be derived from field measurements or from a calibrated physical or three-dimensional numerical model when available for other purposes.

The only method available in the literature, which attempts to solve this problem is given by Thatcher and Harleman (1972, 1981), who account for the effects of geometry and vertical stratification on D separately, introducing a dispersion relationship which reads

$$D = D_{\Delta\rho} + D_g \tag{4.15}$$

with

$$D_{\Delta\rho} = m_1 \, E_D^{-1/4} \, \hat{u}_{1.0} \, L \, \frac{\partial \, \frac{\bar{\rho}(x,t)}{\Delta\rho}}{\partial \, \frac{x}{L}} \tag{4.16}$$

and

$$D_g = m_2 \, 20 \, R(x,t) \, u_*(x,t) \tag{4.17}$$

where $D_{\Delta\rho}$: contribution to dispersion coefficient by density effects,
D_g : same by geometric effects
m_i : dimensionless coefficient
$\hat{u}_{1.0}$: amplitude of profile averaged tidal velocity at mouth of estuary
u_* : shear velocity
$\Delta\rho$: difference in density between sea water and fresh water
L : length of estuary from mouth to head of tide
R : hydraulic radius
E_D : estuary number, a dimensionless stratification parameter (Section 3, Chapter 3), defined as

$$E_D = \frac{1}{\pi} \frac{\rho \, \hat{u}_{1.0}^3}{\Delta\rho \, g h_o \, u_{fr}} \tag{4.18}$$

where E_D : estuary number
u_{fr}: river velocity, i.e. river flow rate over cross-sectional area at mouth of estuary
h_o : water depth at mouth of estuary.

The relationship represented by Eqs. 4.16-4.18 is widely used and is presented as being generally valid (Thatcher and Harleman, 1983). This claim for general validity must be questioned, however.

Eq. 4.16 sets $D_{\Delta\rho}$ proportional to $\partial\bar{\rho}/\partial x$, in order to account for the effect of the gravitational circulation on D. A proportionality to the square of $\partial\bar{\rho}/\partial x$ is also used for this purpose (Fischer, 1981). The gravitational circulation is induced by a force per unit mass, which is proportional to $g \, h \, \partial\bar{\rho}/\partial x$.

This suggests setting $D_{\Delta\rho}$ proportional to $h\ \partial\bar{\bar{\rho}}/\partial x$ rather than to $L\ \partial\bar{\bar{\rho}}/\partial x$ as in Eq. 4.16.

The proportionality of D to $E_D^{-1/4}$ is derived from data collected in the field, in a hydraulic scale model and in a flume (Fig. 4.10).

$$\frac{D_{\Delta\rho}}{\hat{u}_{1.0}L\ \dfrac{\dfrac{\partial\ \bar{\bar{\rho}}}{\partial\ x}}{\partial\ \dfrac{x}{L}}}$$

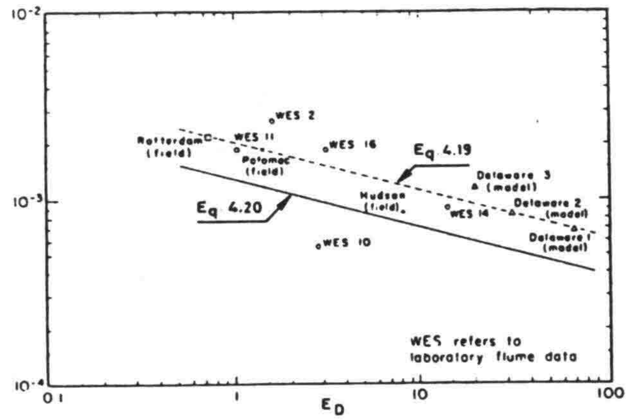

Fig. 4.10 $D_{\Delta\rho}$ as a function of E_D.

The coefficient m_2 is treated as a calibration parameter for dispersive effects due to the geometric features of the considered estuary, including dispersion due to channel irregularities and due to the transverse velocity and concentration. The coefficient m_2 is assumed not to be influenced by stratification (Thatcher and Harleman, 1983). On this basis the density effects and the geometric effects are accounted for separately. This procedure is not valid for geometric influences caused by the uneven distribution of the gravitational circulation over the cross-section (Fig. 3.4).

Whether for a given estuary the above conceptual limitations make it necessary to modify the dispersion relationship of Thatcher and Harleman (Eqs. 4.16-4.18) is a question to be answered on the basis of field data collected in the specific estuary (Abraham et al 1975, Odd 1981).

11. Examples

Harleman and Thatcher (1974) applied the dispersion relationship represented by Eqs. 4.16-4.18 to the well mixed Delaware estuary. In this early application they set t/T_o = 0.05 and used

$$m_1 = 0.0025 \qquad\qquad m_2 = 1 \qquad\qquad (4.19)$$

These values of the coefficients m_1 and m_2 were derived from the data of various sources as shown in Fig. 4.10.

As the dispersion coefficient depends on the unique geometric features of an individual estuary, in a later study (Thatcher and Harleman, 1981) the coefficients m_1 and m_2 were determined from data from the Delaware estuary only. On this basis they found

$$m_1 = 0.0013 \qquad\qquad m_2 = 25 \tag{4.20}$$

These more precise coefficients lead to well documented accurate predictions of the long term salt intrusion.

It is by no means sure that for an arbitrary estuary D is proportional to $E_D^{-1/4}$, nor that the coefficients m_1 and m_2 are constant over the entire length of the estuary when this proportionality is adopted. The latter item is illustrated by a study of the salt intrusion in the Lower Corantijn.

In the Corantijn study (Ministry of Public Works and Traffic, 1980), Eqs. 4.16 to 4.18 were adopted to correlate the dispersion coefficient with conditions pertaining in the estuary. The coefficients m_1 and m_2 were adjusted to give a best-fit between mathematical simulations and observations of salinity. In this process it was found that satisfactory agreement between simulations and observations required the coefficient m_1 to vary with x to account for the individual geometric features of the Corantijn estuary. The following values were adopted.

$$\begin{array}{lcl} m_1 = 0.0013 & x < 20 \text{ km} & m_2 = 25 \\ m_1 = 0.0010 & 20 \text{ km} < x < 30 \text{ km} & m_2 = 25 \\ m_1 = 0.0007 & x > 30 \text{ km} & m_2 = 25 \end{array} \tag{4.21}$$

Notwithstanding the variation of m_1 with x the agreement between simulations and observations could not be perfect (see Fig. 4.11).

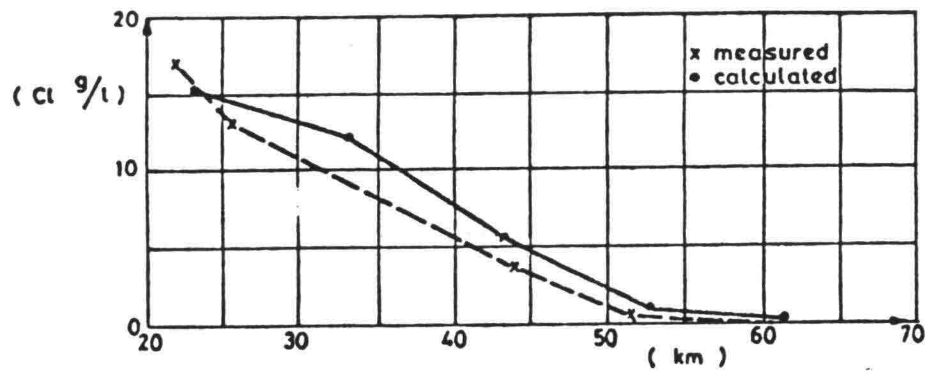

Fig. 4.11 Lower Corantijn; comparison of measured and calculated chlorinities at high water slack. August 16, 1965. (E_D = 12)

In the Corantijn study the effect of small variations of m_1 on the computed salt concentrations was determined. Fig. 4.12 shows the results of this sensitivity analysis.

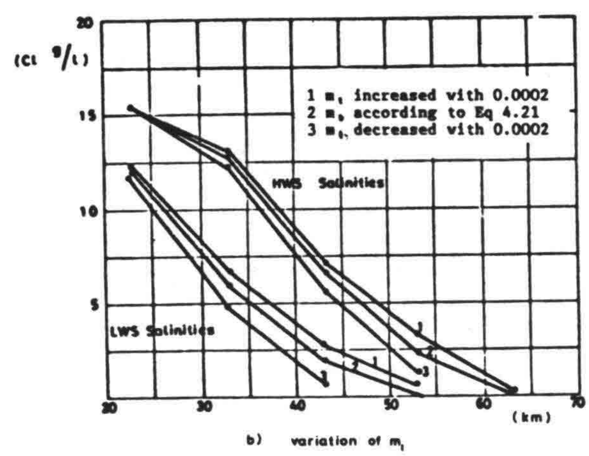

Fig. 4.12 Lower Corantijn; sensitivity of mathematical simulations

12. Concluding remarks

The dispersive transport and the dispersion coefficient describe the combined effect of separate salt intrusion processes such as gravitational circulation, circulations in the horizontal plane and large scale advective mixing. The flow and salt transport processes as observed in a given estuary form an unique blend of these basic transport processes, depending on the unique individual properties of this estuary, such as its geometric features, the characteristics of its tributary rivers, etc. Therefore, dispersion relationships which work well to describe the combined effect of the different basic transport processes in a given estuary do not necessarily work in another estuary (after Fischer et al, 1979, Section 7.1). Therefore, one-dimensional real time salt intrusion models must be calibrated on the basis of field data obtained in the considered estuary itself.

The one-dimensional real-time salt intrusion models PENPAS, DUFLO and MIKE 11 are available at I.H.E.

13. References

Abraham G., Karelse, M. and Lases, W.B.P.M. Data requirements for one-dimensional mathematical modelling of salinity intrusion in estuaries, Proc. 16th Congress of the IAHR, Sao Paulo, 1975, Vol. 3, pp 275-283.

Fischer H.B., List, E.J., Koh, R.C.I., Imberger, J. and Brooks, N.H. Mixing in inland and coastal waters, Academic Press, New York (1979).

Fischer, H.B., Discussion of Thatcher and Harleman (1981), Journal of Environmental Engineering Division, Vol. 107, no. EE4, Aug. 1981, pp. 874-876.

Harleman, D.R.F. and Thatcher, M.L. Longitudinal dispersion and unsteady salinity intrusion in estuaries. La Houille Blanche, no. 1/2, 1974, pp. 25-33.

Ministry of Public Works and Transport , Hydraulic Research Division. A study of the salt intrusion in the Lower Corantijn, report no. P 80-60, May 1980, Paramaribo, Suriname.

Odd, N.V.M. The predictive ability of one-dimensional estuary models. Chapter 2 of Transport models for inland and coastal waters, Fischer H.B., editor, Academic Press, New York. (1981).

Thatcher, M.L. and Harleman, D.R.F. A mathematical model for the prediction of unsteady salinity intrusion in estuaries. Report 144, Ralph M. Parsons Laboratory, Department of Civil Engineering, Massachusetts Institute of Technology, Cambridge, Febr. 1972.

Thatcher, M.L. and Harleman, D.R.F. Long term salinity calculation in Delaware Estuary, Journal of Environmental Engineering Division, Vol. 107, no. EE1, Febr. 1981, pp. 11-27.

Thatcher, M.L. and Harleman, D.R.F. Closure of discussion by Fischer (1981), Journal of Environmental Engineering Division, vol. 109, no. 1, Febr. 1983, pp. 253-257.

Chapter 5. One-dimensional long term salt intrusion models

1. Introduction

The following long term salt intrusion models can be found in the literature.

- tidally averaged one-dimensional models, which give the salt concentration averaged over the tidal cycle
- high water slack one-dimensional models, which give the salt concentration at high water slack
- low water slack one-dimensional models, which give the salt concentration at low water slack.

The long term salt intrusion models require less computational effort than real time models. However, the formulation of their boundary conditions at the mouth of the estuary is more difficult than it is for real time models. Also determining the dispersion coefficient is more difficult than it is for real time models.

The long term models can be applied to study conditions of equilibrium or to determine the long term variation of salt intrusion as in estuaries with long well defined wet and dry periods.

2. Tidal variations of salt concentration in conditions of equilibrium

As described in Section 10 of Chapter 3, in a tidal estuary the water moves a distance F_E outward during ebb and a distance E_F inward during the flood-tide. Because of the river discharge, in each tidal cycle averaged over the cross section the water gradually moves seaward over a distance $E_E - E_F$. In a state of equilibrium the salt concentration at a certain point is the same after each whole tidal cycle. The downward shift of the water is compensated by the upward dispersion of the salt. The tidal excursion of the salt E is estimated to be the mean of E_E and E_F and the motions of the salt can be supposed to be symmetric with respect to the mean situation.

The maxima and the minima of the salt concentration occur when the currents reverse their direction at the times of slack water. At a certain point the maximum salt concentration, at high water slack, is equal to the time-averaged salt concentration at a distance ½ E downstream. In the same way the minimum salinity is related to the mean salinity at ½ E upstream from the point. See Fig. 5.1.

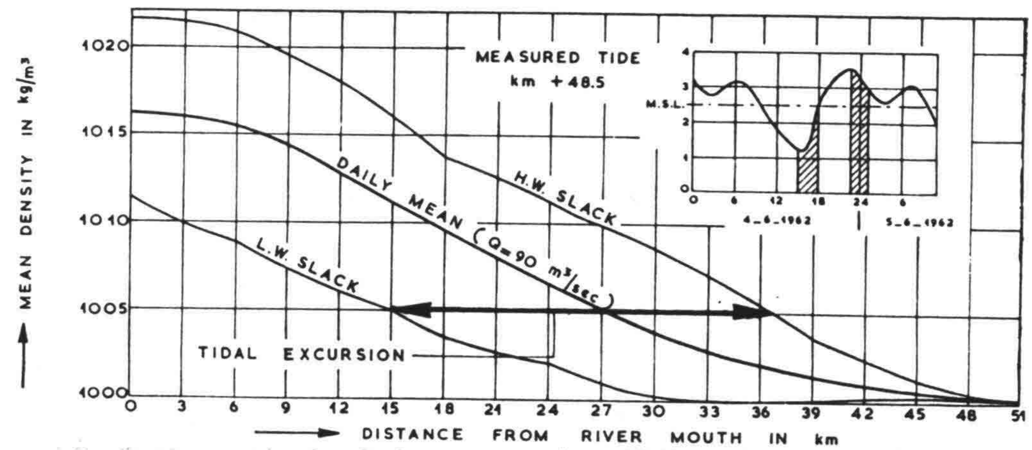

Fig. 5.1 Chao Phya estuary; comparison of high water slack and low water slack densities averaged over cross section (Nedeco, 1965)

Ippen and Harleman (1961) - see also Ippen (1966, chapter 13) - express the mechanics behind the above picture as follows in mathematical terms.

In a tidal estuary the velocity $\bar{\bar{u}}$ is composed of two parts, one due to the tidal motion and one due to the fresh water flow. In formula

$$\bar{\bar{u}} = \bar{\bar{u}}_T - \bar{\bar{u}}_{fr} \tag{5.1}$$

with

$$\langle u_T \rangle = 0 \quad \text{and} \quad \bar{\bar{u}}_{fr} = \frac{Q_{fr}}{\langle A \rangle}$$

where u : longitudinal velocity component, positive when in upstream direction

u_T : contribution due to tidal motion, positive when in upstream direction

u_{fr} : contribution due to fresh water flow, positive when in <u>downstream</u> direction

Q_{fr} : fresh water discharge

A : cross sectional area

$=$: symbol denoting profile averaged value

$\langle\ \rangle$: symbol denoting tidally averaged value.

In Eq. 5.1 the negative sign is due to the fact that x, $\bar{u}$ and $\bar{u}_T$ are positive when directed in the upstream direction, while $\bar{u}_{fr}$ is defined to be positive when directed in the downstream direction.

Substituting Eq. 5.1 into Eq. 4.14 gives

$$\frac{\partial \bar{c}}{\partial t} + \bar{u}_T \frac{\partial \bar{c}}{\partial x} - \bar{u}_{fr} \frac{\partial \bar{c}}{\partial x} - \frac{1}{A} \frac{\partial}{\partial x} (A\ D \frac{\partial \bar{c}}{\partial x}) = 0 \qquad (5.2)$$

where x : longitudinal coordinate, measured from mouth of estuary and positive when in the upstream direction

t : time

c : concentration of salt

D : dispersion coefficient in real time model

In the state of equilibrium it may be assumed that the longitudinal distribution of the salt concentration is essentially determined by a balance between the upward longitudinal dispersion and the downward advection due to the fresh water flow. This means that in first approximation the relatively fast tidal variations of the salt concentration due to the displacement of the longitudinal salt concentration profile over the tidal excursion (Fig. 5.1) are governed by the equation.

$$\frac{\partial \bar{c}}{\partial t} + \bar{u}_T \frac{\partial \bar{c}}{\partial x} = 0 \qquad (5.3)$$

3. One-dimensional long term continuity equation for salt

3.1 Equilibrium condition

For conditions of equilibrium, the long term continuity equation for salt reads

$$- \bar{u}_{fr} \frac{\partial \bar{c}_i}{\partial x} - \frac{1}{A_i} \frac{\partial}{\partial x} (A_i\ D_i \frac{\partial \bar{c}_i}{\partial x}) = 0 \qquad (5.4)$$

where index i refers either to tidally averaged, high water slack or low water slack values of the parameters involved.

For the tidally averaged model, Eq. 5.4 is obtained by averaging Eq. 5.2 over the tidal cycle, after substituting Eq. 5.3. This procedure gives

$$- u_{fr} \frac{\partial \tilde{c}}{\partial x} - \langle \frac{1}{A} \frac{\partial}{\partial x} (A\ D \frac{\partial \bar{c}}{\partial x}) \rangle = 0 \tag{5.5}$$

where $\tilde{}$: symbol denoting averaging over both the cross-sectional area and the tidal cycle

The purpose of one-dimensional modelling is to determine $\tilde{c}$. Therefore, the tidally averaged model uses a dispersion coefficient, D_t, which is related to the dispersion coefficient of the real time model by the equation

$$\frac{1}{\langle A \rangle} \frac{\partial}{\partial x} (\langle A \rangle\ D_t \frac{\partial \tilde{c}}{\partial x}) = \langle \frac{1}{A} \frac{\partial}{\partial x} (A\ D\ \frac{\partial \bar{c}}{\partial x}) \rangle \tag{5.6}$$

where D_t : dispersion coefficient of tidally averaged model

As both $\partial \bar{c}/\partial x$ and D vary with time

$$\langle D \rangle \neq D_t \tag{5.7}$$

The dispersion coefficient D_t expresses not only the effect of spatial averaging over the cross-section but also the effect of temporal averaging over the tidal cycle. Therefore it is more difficult to be determined than D.

For the tidally averaged model Eq. 5.4 is obtained with $\bar{c}_i = \tilde{c}$, $A_i = \langle A \rangle$ and $D_i = D_t$ by substituting Eq. 5.6 into Eq. 5.5.

The salt concentration distribution, represented in Fig. 5.1, has its maximum or minimum intrusion when $\bar{u}_T = 0$. The corresponding concentration distributions are referred to as the high water slack or low water slack distribution. For conditions of equilibrium the high water slack and low water slack distributions can be obtained from Eq. 5.2 by setting simultaneously $\partial \bar{c}/\partial t$ and $\bar{u}_T$ equal to zero. For the high water slack model this procedure gives Eq. 5.4 with $\bar{c}_i = \bar{c}_{HW}$, $A_i = A_{HW}$ and $D_i = D_{HW}$, where index HW refers to high water slack. For the low water slack model Eq. 5.4 is found with $\bar{c}_i = \bar{c}_{LW}$, $A_i = A_{LW}$ and $D_i = D_{LW}$, where index LW refers to low water slack.

As these coefficients result from different procedures

$$D_t \neq D_{HW} \neq D_{LW} \tag{5.8}$$

where D_{HW} : dispersion coefficient of high water slack model

D_{LW} : dispersion coefficient of low water slack model

3.2 Long term variation of salt concentration

Suppose that the fresh water discharge starts to increase gradually after a period of equilibrium. Then the upward dispersion and the downward advection become gradually out of balance. Then the concentration $\bar{c}_i$ changes gradually over the tidal cycle. This gradual change is governed by the equation

$$\frac{\partial \bar{c}_i}{\partial T} - \bar{u}_{fr} \frac{\partial \bar{c}_i}{\partial x} - \frac{1}{A_i} \frac{\partial}{\partial x} (A_i \; D_i \frac{\partial \bar{c}_i}{\partial x}) = 0 \tag{5.9}$$

Where T : time measured in tidal cycles while time t (Eq. 5.2) is measured in hrs or seconds

Eq. 5.9 states that the increase of the salt concentration $\bar{c}_i$ over a tidal cycle is due to a difference between the upward dispersion and the downward advection.

4. Number of equations versus number of unknown

The continuity equation for salt is the only equation solved in the long term salt intrusion models. The salt concentration is the only unknown parameter, while the dispersion coefficient, the cross-sectional area and the fresh water velocity must be given as input data.

equation	unknown parameter	coefficient	input data
continuity equation for salt (Eq. 5.4 or Eq. 5.9)	$\bar{c}_i$	D_i	$A_i, \bar{u}_{fr}$

Under conditions of equilibrium the longitudinal coordinate is the only independent variable. Then, for simple dispersion coefficient relationships it is possible to find an analytical solution.

As for one-dimensional real time models the magnitude of the long term dispersion coefficients D_t, D_{HW} and D_{LW} must be determined from field data collected in the studied estuary.

5. Boundary conditions

Solving Eqs. 5.4 and 5.9 $\bar{\bar{c}}_i$ must be known at the mouth of the estuary to determine the magnitude of the integration constant for the integration involved. This implies that $\bar{\bar{c}}_i$ must be given at the mouth ($x = 0$) as a boundary condition.

Applying Eqs. 5.4 and 5.9 to find $\tilde{c}$ as a function of x for new values of Q_{fr}, it is necessary to know $\tilde{c}$ at $x = 0$ for these new values of Q_{fr}. This limits the applicability of the time averaged model for extrapolations to new fresh water discharges in comparison with the real time model. For the real time model the boundary conditions at the mouth of the estuary can be schematized by specifying the duration of the transition period t_o (see Fig. 4.5) as boundary condition at $x = 0$. The time averaged model, however, requires experimental information on the relationship between $\tilde{c}$ at $x = 0$ and Q_{fr}. This is in particular a disadvantage in studies to determine the effect on the salinity intrusion of technical measures, such as deepening the navigation channel at the mouth of the estuary. Then for the new situation the relationship between $\tilde{c}$ at $x = 0$ and Q_{fr} cannot be derived from measurements in the existing situation.

Similar arguments hold with respect to $\bar{\bar{c}}_{HW}$ and $\bar{\bar{c}}_{LW}$.

Studying the salt intrusion during a dry season of extended duration, it may be justified to assume that $\bar{\bar{c}}_{HW}$ is equal to the salt content of sea water. If so, the boundary conditions for the high water slack model can be formulated in this manner.

6. Dispersion coefficient; application

6.1 Equilibrium conditions

For equilibrium conditions Prandle (1981) reproduced the tidally averaged longitudinal concentration distribution by one-dimensional tidally averaged modelling. He did so for various estuaries ranging from partially mixed to well mixed, deriving the boundary condition $\tilde{c}$ at the mouth of the estuary from field observations. He compared calculated and observed concentration distributions, where for each estuary the value of D_t in the calculated distribution was chosen to produce the best agreement with the observed distribution.

Prandle examined the following dispersion relationships

$$D_t = \text{constant} \qquad D_t \sim \partial\tilde{\rho}/\partial x \qquad D_t \sim (\partial\tilde{\rho}/\partial x)^2 \tag{5.10}$$

These three forms give different solution $\tilde{c} = f(x)$, i.e. different shapes of the longitudinal tidally averaged concentration distribution (Fig. 5.2). The latter two forms were selected to account for the effect of the gravitational circulation on D_t. They are based on similar approximations as with the dispersion coefficient, D, of the real time model (Section 10, Chapter 4).

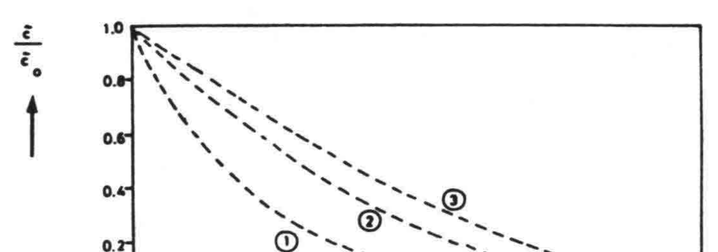

Fig. 5.2 Shapes of longitudinal tidally averaged concentration distribution, D_t = constant (curve 1). $D_t \sim \partial\tilde{\rho}/\partial x$ (curve 2) and $D_t \sim (\partial\tilde{\rho}/\partial x)^2$ (curve 3); L_i: length of salt intrusion, $\tilde{c}_o$: value of $\tilde{c}$ at x = 0.

For D_t constant over the entire zone of salt intrusion, Prandle obtained the best agreement between calculated and observed concentration distributions for the values of D_t, listed in Table 5.1. The table gives an indication of the order of magnitude of D_t.

Table 5.1 D_t values determined by Prandle (1981)

Estuary	$D_t (m^2/s)$	Source
Thames	87	Prandle (1981)
Potamac	91	
Hudson	111	
Delaware	112	
Bristol Channel	270	
St. Lawrence	510	
Rotterdam Waterway	2740	

The Rotterdam Waterway D_t value, which is listed in Table 5.1, is of the order 3000 m^2/s. This value is of the same order of magnitude as the peak value of D, which is given for the Rotterdam Waterway in Fig. 4.5. In the other six estuaries of Table 5.1, the values of D_t lie in the range 50-500 m^2/s. The Rotterdam Waterway is more stratified than the other estuaries. This stratification may account for the large D_t value of the Rotterdam Waterway.

Table 5.2 D_t values collected by Prandle (1981)

Estuary	$D_t (m^2/s)$	Source
Severn	100-1000	Uncles and Redford (1980)
Severn	54-535	Bowden (1963)
Thames	53-338	
Mersey	161-360	
James River	24	Dyer (1974)
Southampton Water	158	
Tay	50-300	
Columbia	5000	

Table 5.2, which is also derived from Prandle (1981) gives the order of magnitude of D_t values found in other studies. Depending on the size and the

stratification of the estuaries involved, this table gives D_t values in the range of 50-5000 m^2/s.

Savenye (1986) introduces a tidally averaged dispersion relationship for funnel-shaped well-mixed estuaries. He applied this relationship to simulate concentration distributions as observed in some African estuaries (Fig. 5.3), deriving the boundary condition $\tilde{c}_o$, i.e. $\tilde{c}$ at x = 0, from field observations. The dispersion relationship gives D_t as a function of x and gross estuarine parameters. It does not contain a dependency of D_t on $\tilde{c}$ or $\partial\tilde{\rho}/\partial x$. Under these conditions Eq. 5.4 is linear in $\tilde{c}$. This leads to a solution of the form $\tilde{c}/\tilde{c}_o = f(x)$. This solution implies that the length of the zone of salt intrusion does not depend on $\tilde{c}_o$, i.e. on the difference in density between the river and the water at the mouth of the estuary. This finding does not apply, when gravitational circulation is a factor to be considered and density effects influence the velocity distribution over the depth as indicated in Fig. 3.6.

In a subsequent publication Savenye (1989) presents his solution for the HWS-, LWS- and tidally averaged model on spread sheet giving a useful method for quick interpretation of field measurements with a personal computer. Moreover his method illustrates inequality 5.8 as can be seen from table 5.3 which is derived from his results for the Chao Phya estuary.

Table 5.3 Long term dispersion coefficients for a particular Chao Phya situation

Date	D_{HW} (m^2/s)	D_t (m^2/s)	D_{WW} (m^2/s)
5 June 1962	720	530	360

Table 5.4 gives D_t values, listed by Savenye for the well mixed estuaries which he studied.

Table 5.4 D_t values determined by Savenye (1986)

Estuary	$D_t (m^2/s)$	Source
Incomati	30	Savenye (1986)
Maputo	50-170	
Punque	130-200	
Limpopo	290-510	

Summarizing, following Prandle (1981) tidally averaged models can provide a reasonable simulation of actual conditions.

Models of this type cannot be reliably applied

- **to estuaries where observational data are insufficient to determine D_t and/or the seaward boundary condition accurately, and**
- **to estuaries where some major change is proposed which might alter the value of D_t or the seaward boundary condition.**

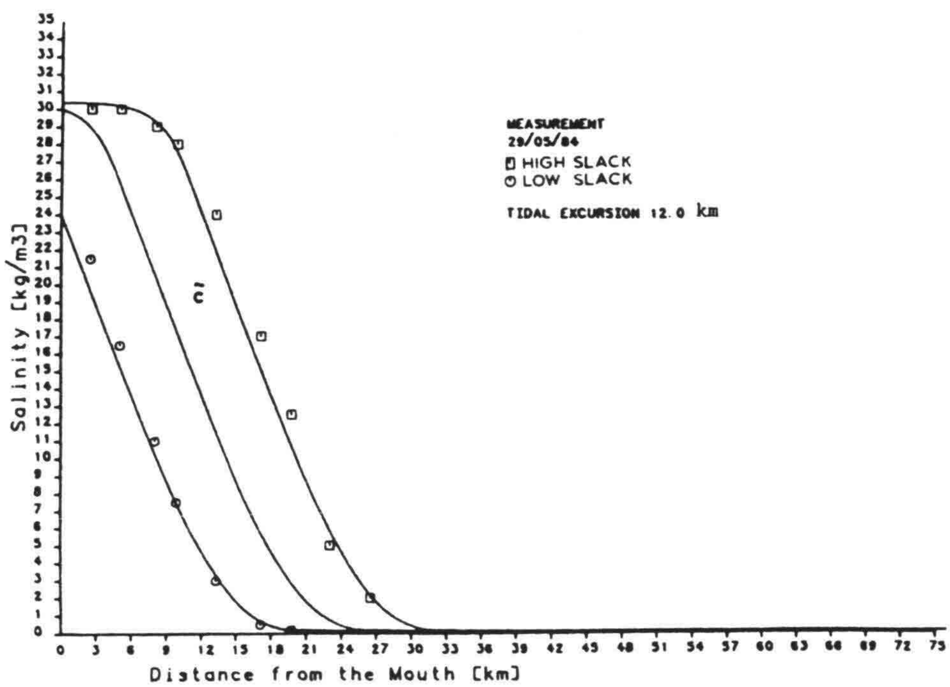

Fig. 5.3 Calculated intrusion versus measured intrusion, Maputo estuary on 29/05/84 (Savenye, 1986)

6.2 Long term variation of salt concentration

Sanmuganathan and Abernethy (1975) developed a high water slack model to study the long term salinity intrusion in the Gambia estuary, Gambia. The dispersion relationship used in the model was obtained by a modification of the real time relationship proposed by Harleman and Thatcher (1974). The coefficients, which are contained in the dispersion relationship were derived from salt concentrations obtained in field measurements over a period of three months. The model was found to give satisfactory results over two extended dry periods with continuously increasing salt intrusion (Fig. 3.19).

Though with other values for the experimental coefficients, the above dispersion relationship was found to work also satisfactorily for the Guyas estuary (Sanmuganathan and Abernethy, 1979 a). Discussing the applicability of the model to new estuaries, Sanmuganathan and Abernethy (1976 b) indicate that there is no theoretical foundation for the model and that the experimental coefficients contained in it must be found from matching the model results to a sequence of field observations. They mention that deriving the coefficients from field observations collected over a period of 2-3 months in the course of the dry season is usually sufficient to get reasonably accurate extrapolations.

Savenye (1988) applied the tidally averaged dispersion relationship, referred to in the previous section, to simulate the salt intrusion into the Gambia estuary over a period of 10 years (Fig. 5.4). In this application it was found necessary taking into account the effect of evaporation during the dry season.

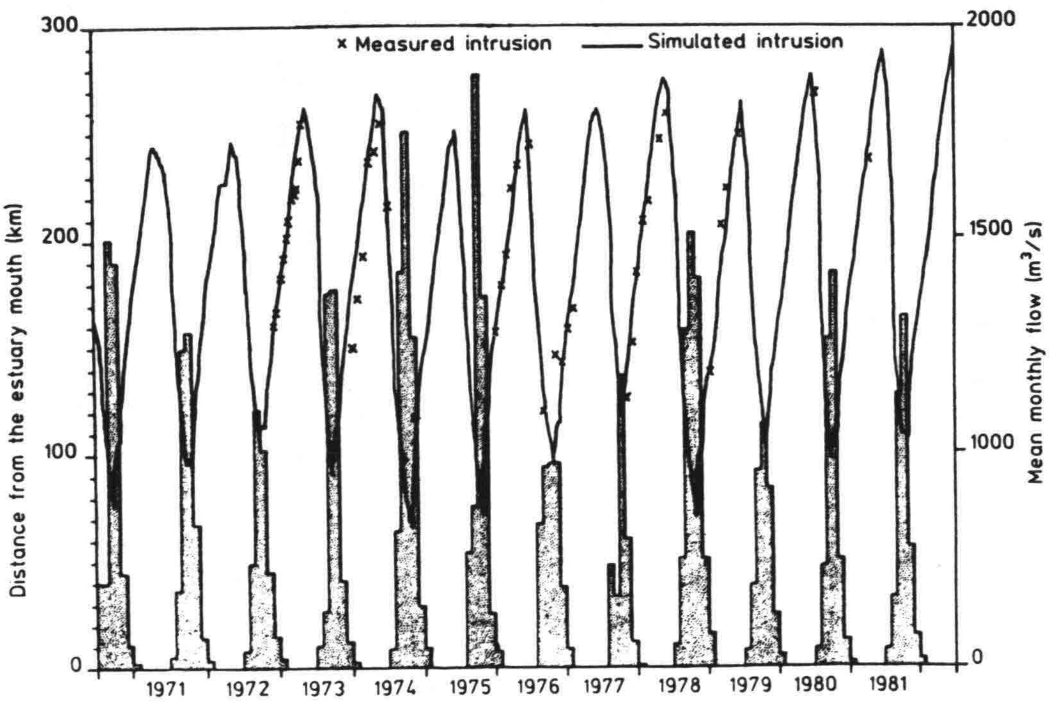

Fig. 5.4 Movement of calculated 1.0 kg/m^3 salinity front with time, measured intrusion, and mean discharge (Savenye, 1988)

Summarizing long term models can provide a reasonable simulation of the variation of salt concentration over the dry and wet seasons.
Again, models of this type cannot be reliably applied

- to estuaries where observational data are insufficient to determine D_t and/or the seaward boundary condition accurately, and
- to estuaries where some major change is proposed which might alter the value of D_t or the seaward boundary condition.

7. Calculation over long periods

Time averaged models and high or low water slack models were developed for calculations of the salinity intrusion over a long period, for instance a year. In principle, calculations over a long period can also be made by means of a real time model. Comparing the merits of the real time model for calculations over a long period with those of the other models, the following factors are of importance

- computational effort
- predictability of boundary conditions
- predictability of dispersion coefficients.

Real time models operate at time steps of a number of minutes. Time averaged models and high or low water slack models can be operated at a time step of a number of tidal cycles. Consequently, the real time model requires a larger computational effort (more computer time) than needed by the other models.

Depending on the problem to be studied, for the real time model formulating the boundary condition at $x = 0$ and predicting the dispersion coefficient could be less cumbersome than for the long term models. If so, these advantages of the real time model may justify its application over a long period, not withstanding the larger computational effort. On the basis of these arguments, Thatcher and Harleman (1974) applied the real time model for long term simulations of the salt intrusion into the Delaware estuary.

8 References

Bowden, K.F. The mixing processes in a tidal estuary, International Journal of Air and Water Pollution, 7, 1963, pp 295-310

Dyer, K.R. Salt balance in stratified estuaries, Estuarine and Coastal Marine Science, 2, 1974, pp. 273-281

Harleman, D.F.R. and Thatcher, M.L. Longitudinal dispersion and unsteady salinity intrusion in estuaries. La Houille Blanche, no. 1/2, 1974, pp. 25-33.

Ippen, A.T. and Harleman, D.R.F. One-dimensional analysis of salinity intrusion in estuaries. Technical Bulletin no. 5, Committee on Tidal Hydraulics, Corps of Engineers, Waterways Experiment Station, Vicksburg, June, 1961.

Ippen, A.T. (editor) Estuary and coastline hydrodynamics, McGraw-Hill, New York, 1966.

Nedeco. Siltation Bangkok port channel, Volume 2, Netherlands Engineering Consultants, The Hague, the Netherlands, 1965.

Prandle, D. Salinity intrusion in estuaries, Journal of Physical Oceanography, 11, 1981, pp. 1311-1324.

Sanmuganathan, K. and Abernethy, C.L. A mathematical model to predict long term salinity intrusion in estuaries, Proceedings Second World Congress, IWRA, New Delhi, December 1975, Vol. III, pp. 313-324.

Sanmuganathan, K. and Abernethy, C.L. Long term prediction of salinity intrusion in branched estuaries, Proceedings 18th Congress of IAHR, Cagliari, September 1979 (a), Vol. 3, pp. 279-286.

Sanmuganathan, K. and Abernathy, C.L. Discussion of Paper Bc1, authors' reply. Proceedings 18th Congress of IAHR, Cagliari, September 1979 (b), Vol. 6, pp. 242-244.

Savenye, H.H.G. A one-dimensional model for salinity intrusion in alluvial estuaries, Journal of Hydrology, 85, 1986, pp. 87-109.

Savenye, H.H.G. Influence of rain and evaporation on salt intrusion in estuaries, Journal of Hydraulic Engineering, American Society of Civil Engineers, 114, no. 12, 1988, pp. 1509-1524.

Savenye, H.H.G. Salt intrusion model for high-water slack, low-water slack, and mean tide on spread sheet, Journal of Hydrology, 107, 1989, pp. 9-18.

Uncles, R.J. and Radford, P.J. Seasonal and spring-neap tidal dependence of axial dispersion coefficients in the Severn - a wide, vertically mixed estuary, Journal of Fluid Mechanic, 98, 1980, pp. 703-726.

Chapter 6, Two- and threedimensional modelling, effect of stratification on turbulence

1. Introduction

In one-dimensional models, the estuary is considered to be sectionally homogeneous and only longitudinal effects are included. In the rather more realistic two-dimensional models, the estuary is either taken to have a lateral variation of the salt concentration and to be vertically homogeneous or to be laterally homogeneous with vertical variations of the salt concentration. The former model assumes that large scale advective mixing is dominant, the latter, the gravitational circulation in the vertical plane. By decomposition it can be determined which of these mechanisms is dominant. Only in three-dimensional models can both lateral and vertical effects be considered.

Two-dimensional laterally homogeneous and three-dimensional salt intrusion models, which give the vertical variation of the salt concentration, contain the turbulent shear stress and the turbulent transport of mass. Applying these models, the effect of stratification on these turbulence properties must be expressed in mathematical terms. This chapter deals with the latter effect. For the governing equations of the three-dimensional salt intrusion model reference is made to the literature on the subject (ASCE (1988)), those of the two-dimensional laterally homogeneous model are given below.

2. Reynolds equations and turbulent shear stress and turbulent transport of mass

Neglecting $\partial\ /\partial y$ and v, where v is the velocity in the lateral y direction, and omitting terms which are of second order for the flows considered in Chapters 3-5, the Reynolds equations read

continuity : $$\frac{\partial \bar{u}}{\partial x} + \frac{\partial \bar{w}}{\partial z} = 0 \tag{6.1}$$

x-momentum: : $$\frac{\partial \bar{u}}{\partial t} + \bar{u}\frac{\partial \bar{u}}{\partial x} + \bar{w}\frac{\partial \bar{u}}{\partial z} = -\frac{1}{\rho}\frac{\partial \bar{p}}{\partial x} + \frac{\partial \tau_{xz}}{\partial z} \tag{6.2}$$

z-momentum: : $$\frac{\partial \bar{w}}{\partial t} + \bar{u}\frac{\partial \bar{w}}{\partial x} + \bar{w}\frac{\partial \bar{w}}{\partial z} = -\frac{1}{\rho}\frac{\partial \bar{p}}{\partial z} - g \tag{6.3}$$

scalar transport: $$\frac{\partial \bar{c}}{\partial t} + \frac{\partial \overline{uc}}{\partial x} + \frac{\partial \overline{wc}}{\partial z} = -\frac{\partial F_z}{\partial z} \tag{6.4}$$

where u, w : longitudinal and vertical velocity component
x, z : longitudinal and vertical coordinate (z is positive when measured upward from bottom)
p : pressure
ρ : density
g : acceleration by gravity
τ_{xz} : turbulent shear stress acting in x-direction in horizontal plane perpendicular to z-direction
F_z : turbulent transport of mass in vertical direction
c : concentration

The parameters c, u, w, p en ρ, included in Eqs. 6.1 - 6.4, are time mean values obtained by filtering out turbulent components.

Turbulence is contained through the turbulent shear stress and the turbulent transport of mass. The dominant components of the turbulent shear stress and the turbulent transport are given by

$$\tau_{xz} = - \rho \, \overline{u'w'} \tag{6.5}$$

and

$$F_z = \overline{w'\rho'} \tag{6.6}$$

where $-$: symbol denoting time mean value
$'$: symbol denoting turbulent fluctuations.

Adopting the gradient-transport hypothesis, these turbulence properties are expressed as

$$\tau_{xz} = \rho \, \nu_t \frac{\partial \bar{u}}{\partial z} \tag{6.7}$$

and

$$F_z = - K_t \frac{\partial \bar{\rho}}{\partial z} \tag{6.8}$$

where ν_t : eddy viscosity

K_t : eddy diffusivity

For homogeneous open channel flow

$$\nu_t \approx K_t \approx 0.07\ h\ u_* \tag{6.9}$$

where h : water depth

u_* : shear velocity = $(\tau_b/\rho)^{1/2}$, where τ_b is bottom shear stress.

3. Limiting conditions at local level

3.1 Limiting conditions based on gradient Richardson number

We consider turbulence in local equilibrium. Under stably stratified conditions this means that the production of turbulent energy by the time mean flow (referred to as Prod.) is equal to the sum of the potential energy to be delivered in order to maintain vertical mixing (referred to as Pot.) and the dissipation of turbulent energy by viscous effects (referred to as Diss.), all per unit mass and unit time.

In formulae

$$(\text{Prod.}) = (\text{Pot.}) + (\text{Diss.})$$

or

$$- \overline{u'w'}\ \frac{\partial \bar{u}}{\partial z} = \frac{g}{\rho}\ \overline{w'\rho'} + \varepsilon \tag{6.10}$$

where ε: rate of dissipation of turbulent energy per unit mass of fluid.

Substituting Eqs. 6.7 and 6.8 into 6.10, it can be shown that

$$(\text{Diss.}) = (\text{Prod.}) \left[1 - \frac{(\text{Pot.})}{(\text{Prod.})}\right]$$

or (6.11)

$$\varepsilon = \nu_t \left(\frac{\partial u}{\partial z}\right)^2 \left[1 - \frac{R_i}{\sigma_t}\right]$$

with

$$Ri = -\frac{g}{\bar{\rho}}\frac{\frac{\partial\bar{\rho}}{\partial z}}{\left(\frac{\partial\bar{u}}{\partial z}\right)^2} \qquad \sigma_t = \frac{\nu_t}{K_t} \tag{6.12}$$

where Ri : gradient Richardson number

σ_t : turbulent Prandtle number.

The above derivation breaks down when (Prod.) = 0, i.e. when $\partial\bar{u}/\partial z = 0$ and therefore $Ri = \infty$. Hence, Ri becomes meaningless to characterize turbulence characteristics for $Ri = \infty$.

The dissipation rate, ε, is a positive quantity. Hence, turbulence can exist only when Ri/σ_t = (Pot.)/(Prod.) is smaller than one. This leads to an existence criterion for turbulence (see e.g. Monin, 1959).

$$Ri < Ri_{cr}$$

$$R_f = \frac{Ri}{\sigma_t} < 1 \tag{6.13}$$

where Ri_{cr} : critical value of gradient Richardson number,

R_f : mixing efficiency, i.e. (Pot.)/(Prod.)

In the literature on the subject the mixing efficiency is also referred to as the flux Richardson number.

In accordance with measurements collected by Abraham (1988), the maximum efficiency is in the order 0.15 - 0.20 (see Fig. 6.9).

3.2 Limiting conditions based on length scale of turbulence

We consider an element of stratified fluid, which initially at rest, having at all its levels the same density as the surrounding fluid (Fig. 6.1). This means that its density varies over its height and that the density, averaged over its shaded lower half, is larger than the density, averaged over its not-shaded upper half.

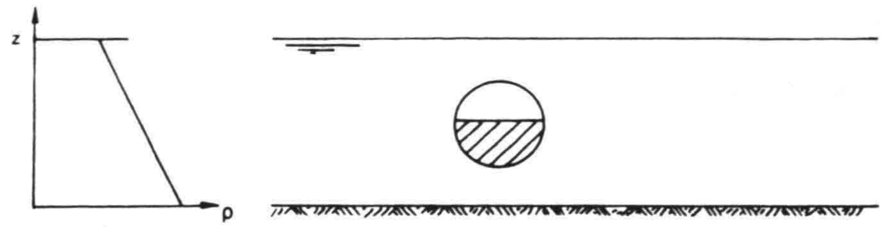

Fig. 6.1 Initial position of considered fluid element

We assume that in the fluid surrounding the element turbulent kinetic energy is produced and that enough of this kinetic energy is supplied to the element to make it turn around as an eddy. Fig. 6.2 shows consecutive stages of the overturning of the eddy

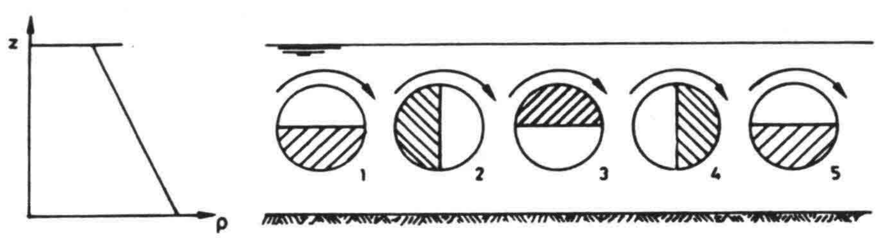

Fig. 6.2 Position of considered fluid element in consecutive stages of overturning; 1: initial position, 2: 1/4 around, 3: 1/2 around; 4: 3/4 around, 5: 1/1 around.

When half around the shaded part of the element with the largest density is above the not-shaded part with the smallest density. Thus, while the element turns around as an eddy, there is a conversion of kinetic energy to potential energy and vice versa. For the largest eddy, which can overturn, all its kinetic energy is converted into potential energy when it is upside down.

The difference in density between the shaded and not-shaded part of the eddy is proportional to $L|\partial\bar{\rho}/\partial z|$, where L is the size of the eddy, i.e. the length scale of the considered turbulence. Hence, the potential energy needed to make it turn around is proportional to $g|\partial\bar{\rho}/\partial z|L^2$. The kinetic energy supplied to the eddy is proportional to $\bar{\rho}U^2$, where U is the velocity scale of the considered turbulence. In formula

$$E_{kin} = C_1 \bar{\rho}U^2 \tag{6.14}$$

and

$$E_{pot} = C_2 g \; |\partial\bar{\rho}/\partial z| L^2 \tag{6.15}$$

where E_{kin}: kinetic energy available to cause overturning
E_{pot}: potential energy needed for overturning
C_i : dimensionless constant.

For the largest overturning eddy $E_{kin} = E_{pot}$. Hence

$$L_{max} = \left(\frac{C_1}{C_2}\right)^{½} \frac{U}{\left|\frac{1}{\bar{\rho}} g \frac{\partial\bar{\rho}}{\partial z}\right|^{½}} \tag{6.16}$$

The large scale turbulent motion is related to that at the small scale by the relationship (Tennekes and Lumley, 1972, Sections 3.1 and 3.2)

$$\varepsilon = \frac{U^3}{L} \tag{6.17}$$

Substituting Eq. 6.17 into Eq. 6.16 gives

$$L_{max} = \left(\frac{C_1}{C_2}\right)^{3/4} L_R = C_3 L_R \tag{6.18}$$

with

$$L_R = \left[\frac{\varepsilon}{\left|\frac{1}{\bar{\rho}} g \frac{\partial\bar{\rho}}{\partial z}\right|^{3/2}}\right]^{1/2} \tag{6.19}$$

where L_R: Ozmidov length scale of turbulence.

Eq. 6.18 defines the upper limit for the size of overturning turbulent motions (Ozmidov, 1965). Larger eddies cannot overturn. They perform a bobbing wave-like motion (Fig. 6.3)

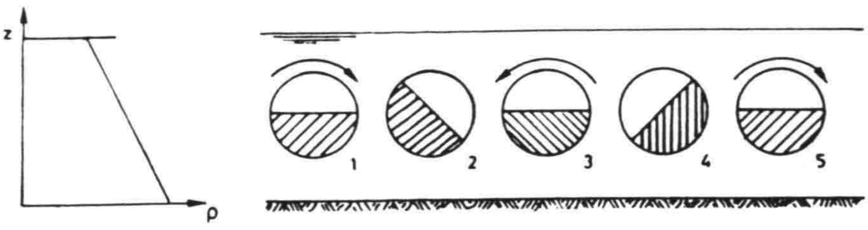

Fig. 6.3 Position of eddy in consecutive stages of bobbing wavelike motion; 1: initial condition, 2: rotation stops ($E_{kin} = E_{pot}$); 3: rotation in opposite sense, 4: rotation stops ($E_{kin} = E_{pot}$), 5: rotation in opposite sense, etc.

On the basis of experiments summarized by Abraham (1988, Section 4.1.1)

$$C_3 = (\frac{C_1}{C_2})^{3/4} = 1 \text{ to } 2 \qquad (6.20)$$

The smallest scales of turbulence are characterized by the Kolmogorov scale, L_k, i.e.

$$L_k = (\nu^3 \varepsilon^{-1})^{1/4} \qquad (6.21)$$

where ν: kinematic viscosity.

On the basis of the aforementioned experimental information collected by Abraham (1988) the smallest overturning eddies are of the order 10 L_k.

Fig. 6.4 summarizes the constraints imposed by the above length scales.

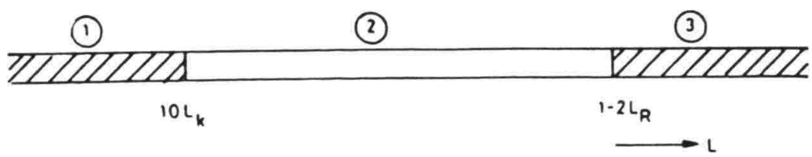

Fig. 6.4 Ranges of eddy sizes, local effects; 1: viscous damping, 2: overturning eddies, 3: buoyancy damping.

3.3 Connection between length scales and gradient Richardson number

Now the mixing length concept is adopted, which means that the velocity scale is supposed to be linearly proportional to the length scale and the vertical derivative of the horizontal velicity:

$$U \approx L \frac{\partial u}{\partial z} \tag{6.22}$$

Substituting Eq. 6.22 into Eq. 6.16 gives

$$\frac{L}{L_{max}} \approx \left(\frac{C_2}{C_1}\right)^{1/2} Ri^{1/2} \tag{6.23}$$

The bobbing wavelike motion occurs for $L \gtrsim L_{max}$, or in accordance with Eqs. 6.20 and 6.23 for

$$Ri \gtrsim 1 \text{ to } 2.5 \tag{6.24}$$

This finding is compatible with experimental observations by Kondo et al (1978), Komori et al (1983) and West et al (1986).

4. Combined effect of geometry and stratification on turbulence

4.1 Effect on length scales of turbulence

In homogeneous, unstratified flows the length scale of the large energy containing eddies is limited to a length L_n which is controlled by the external boundaries (e.g. bed and free surface). This length scale will be referred to as the length scale for neutral conditions, L_n.

In stably stratified flows, the upper limit permissible for the size of overturning eddies is either the Ozmidov length scale (Eq. 6.19) or the length scale for neutral conditions, depending on which is the smallest of these two length scales.

In formula, the above finding can be expressed as

$$L = L_n \quad \text{if} \quad L_R \gg L_n \qquad\qquad L = C_3 L_R \quad \text{if} \quad L_R \ll L_n \tag{6.25}$$

The implications of Eq. 6.25 are shown schematically in Figs. 6.5 and 6.6.

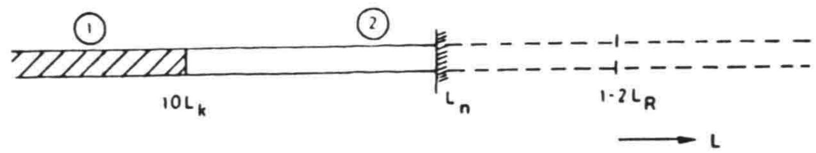

Fig. 6.5 Ranges of eddy sizes, combined effect of geometry and stratification ($L_n < 1\text{-}2\ L_R$); 1: viscous damping, 2: overturning eddies; eddies larger than L_n cannot exist because of geometric constraint.

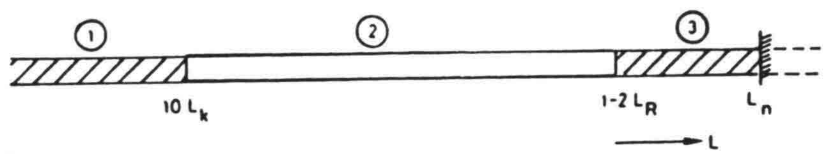

Fig. 6.6 Ranges of eddy sizes, combined effect of geometry and stratification ($L_n > 1\text{-}2\ L_R$); 1: viscous damping, 2: overturning eddies, 3: buoyancy damping; eddies larger than L_n cannot exist because of geometric constraint.

For intermediate values of L_R/L_n (Kranenburg, 1985)

$$\frac{L}{L_n} = f_1\left(\frac{L_R}{L_n}\right) \qquad \begin{array}{lll} L = L_n & \text{for} & L_R \rightarrow \infty \\ L = C_3 L_R & \text{for} & L_R \rightarrow 0 \end{array} \tag{6.26}$$

where f_1: functional relationship, defined by Eq. 6.26, represented in Fig. 6.7

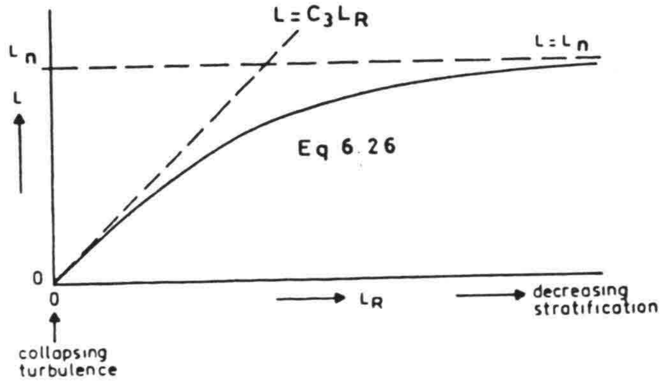

Fig. 6.7 Suggested relationship between length scales L and L_R, defined by Eq. 6.26 (after Kranenburg, 1985); $L > L_n$ excluded by geometric constraints; $L_n > L > C_3L_R$ (shaded area) excluded by stratification.

4.2 Damping functions

Applying the mixing length concept to stably stratified flows, Eq. 6.26 implies (Abraham, 1988, Section 5)

$$\nu_t = L_n^2 \left|\frac{\partial \bar{u}}{\partial z}\right| F_o(Ri) \qquad K_t = L_n^2 \left|\frac{\partial \bar{u}}{\partial z}\right| G_o(Ri) \tag{6.27}$$

The damping functions, $F_o(Ri)$ and $G_o(Ri)$, which decrease with increasing Ri, express the damping effect of a stable density stratification on ν_t and K_t. For homogeneous conditions there is no damping. Hence, F_o and G_o are equal to one for Ri = 0.

Eq. 6.27 applies to turbulence in local equilibrium, as introduced when deriving Eq. 6.11. Therefore, Eq. 6.27 is based on the assumption that locally there is a production of turbulent kinetic energy and that this turbulent kinetic energy is dissipated locally at the same rate it is produced. This assumption implies that transport of turbulent energy and history effects are neglected. Hence, Eq. 6.27 is not very suitable when these effects are important as is the case in unsteady flows such as occur in estuaries (ASCE, 1988 and Abraham, 1989).

The scale of turbulence is such that any eddy covers a considerably height range. Therefore it is by no means obvious that there should be a simple dependence of F_o and G_o on a strictly local parameter as the gradient Richardson number, Ri (Ellison and Turner, 1960).

Further, the effect of stratification on turbulence is different for flow conditions which are significantly influenced by boundaries and flows which are not (Gibson and Launder, 1978). Fig. 6.15 shows how the proximity of boundaries influences K_t.

5. Experimental data

5.1 Steady flow

Mizushina et al (1978), Ueda et al (1981) and Komori et al (1982 and 1983) describe different aspects of the same series of laboratory experiments. Together, they present detailed experimental information on the turbulence structure in stably stratified steady open channel flow, under conditions of local equilibrium.

Fig. 6.8 gives the correlation of σ_t with the local Ri-value, given by Mizushina et al (1978) for the area where the wall effect on the turbulent pressure field is weak. Fig. 6.9 gives the corresponding correlation between Rf and Ri. This figure gives a maximum value of the mixing efficiency of the order 0.1 to 0.2.

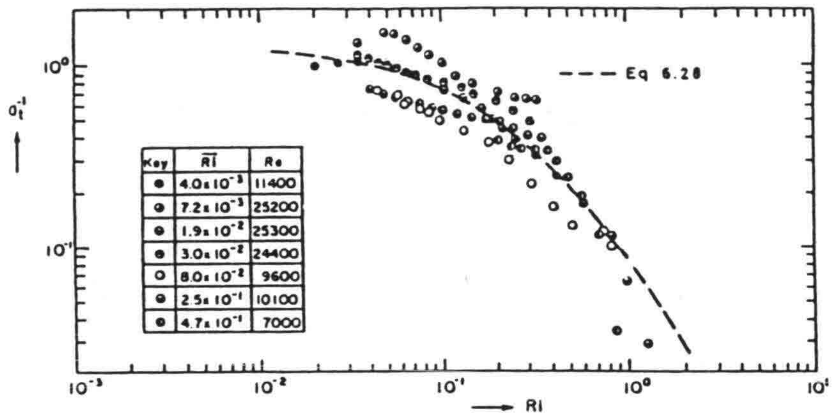

Fig. 6.8 σ_t^{-1} versus Ri; experiments of Mizushina et al (1978) compared with empirical relationship proposed by Bloss et al (1988) (Eq. 6.28).

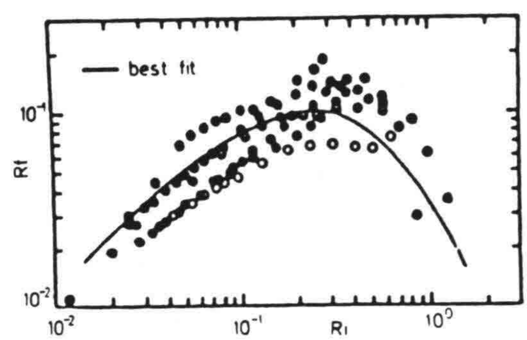

Fig. 6.9 Rf versus Ri, experiments of Mizushina et al (1978).

Figs. 6.10 and 6.11 give respectively $\nu_t \nu_{t.o}^{-1}$ and $K_t K_{t.o}^{-1}$ (where index 0 refers to neutral non-stratified conditions) as a function of the local Ri-value from the Mizushina experiments.

According to Bloss et al (1988) the above results of the Mizushina experiments may be described by the following empirical relationships, which are plotted in Figs. 6.8, 6.10 and 6.11

$$\nu_t \nu_{t.o}^{-1} = (1+3\ \mathrm{Ri})^{-1} \qquad K_t K_{t.o}^{-1} = (1+3\ \mathrm{Ri})^{-3} \tag{6.28}$$

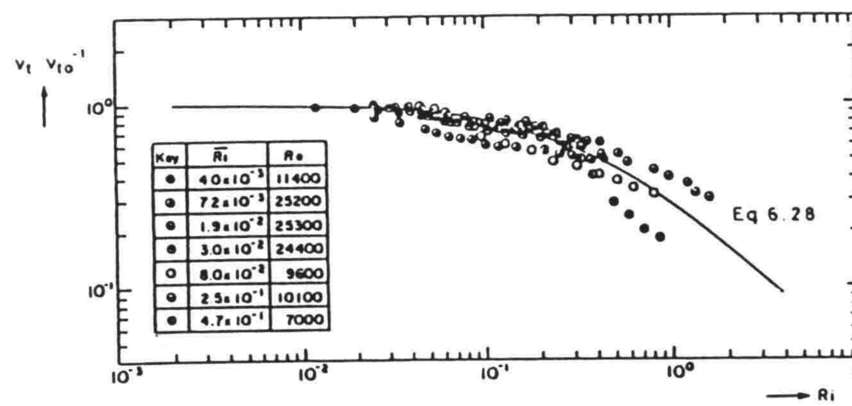

Fig. 6.10 $\nu_t \nu_{to}^{-1}$ **versus Ri; experiments of Mizushina et al (1978) compared with empirical relationship proposed by Bloss et al (1988) (Eq. 6.28)**

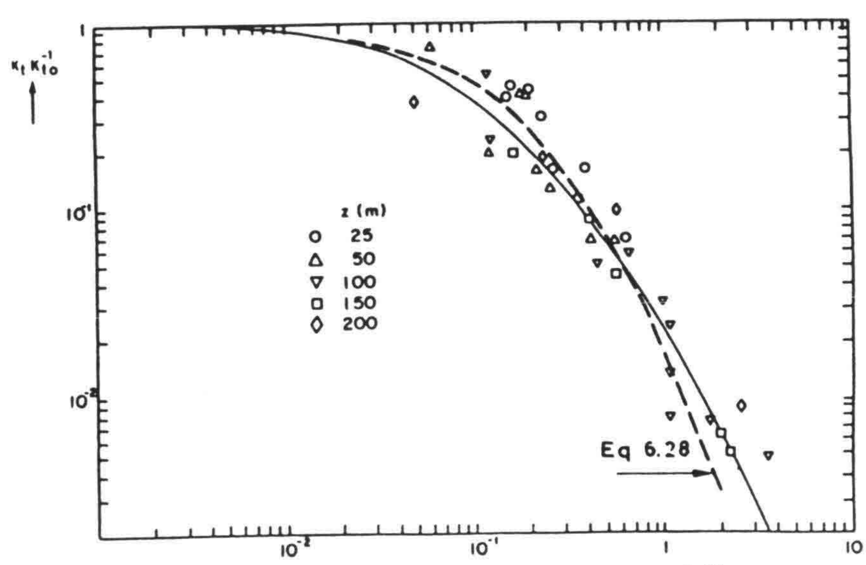

Fig. 6.11 $K_t K_{t.o}^{-1}$ versus Ri; experiments in atmospheric outer layer compared with Mizushina laboratory experiments (solid line) and empirical relationship proposed by Bloss et al (1988) (Eq. 6.28) (after Ueda et al, 1981).

A variety of relationships of the type of Eq. 6.28 can be found in the literature, each in agreement with a particular set of experimental data (Figs. 6.12, 6.13 and 6.14).

In line with the final observation of Section 4.2, Ueda et al (1981) found the effect of stratification on transport processes in the lower atmosphere to vary with the level of the atmosphere observed (Fig. 6.15).

Information on the effect of stratification on turbulence quantities, which is of interest for the development of turbulence models and to determine model-constants, can be derived from the Mizushina experiments (e.g. Komori et al, 1983) and from the experiments of Webster (1964) and Young (1975). Further it can be obtained from the experiments summarized by Abraham (1988, Section 4.1.1).

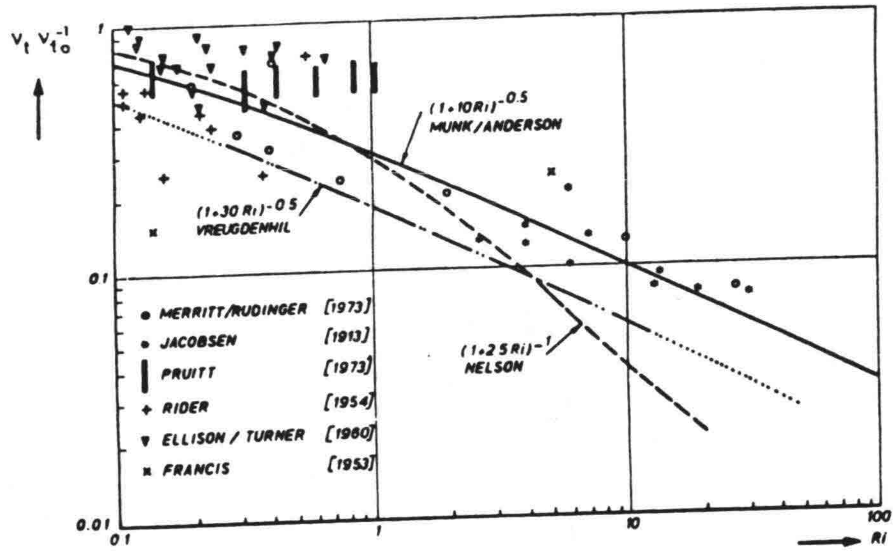

Fig. 6.12 The effect of stability as a function of Richardson number on the coefficient of eddy viscosity as compared to its value for neutral conditions, $\nu_{t.o}$

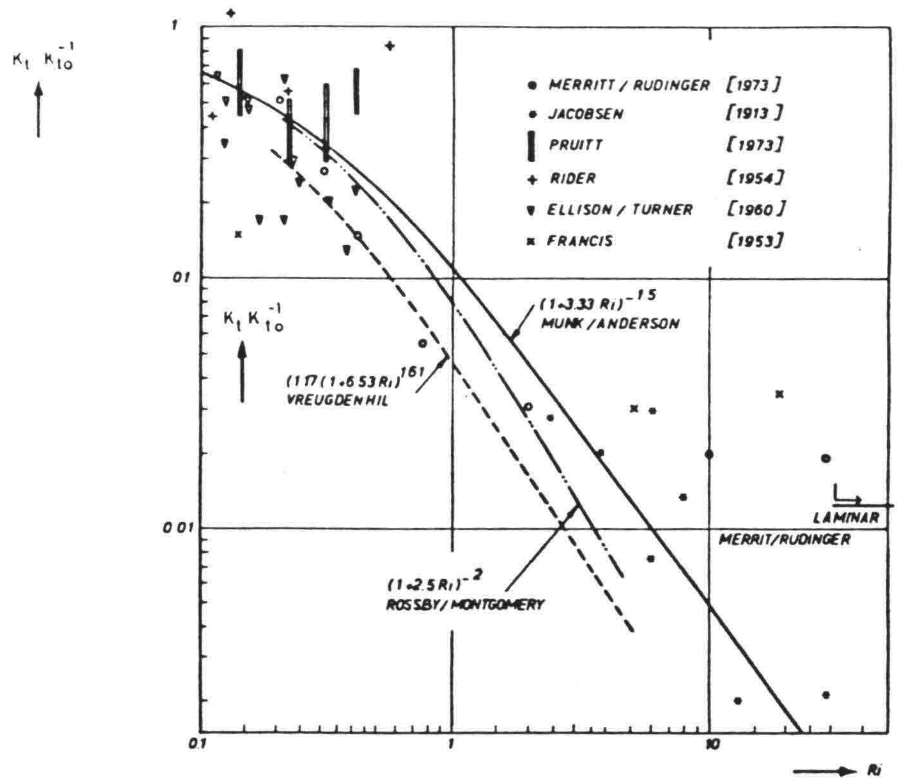

Fig. 6.13 The effect of stability as a function of Richardson number on the coefficient of eddy diffusivity as compared to its value for neutral conditions, $K_{t.o}$

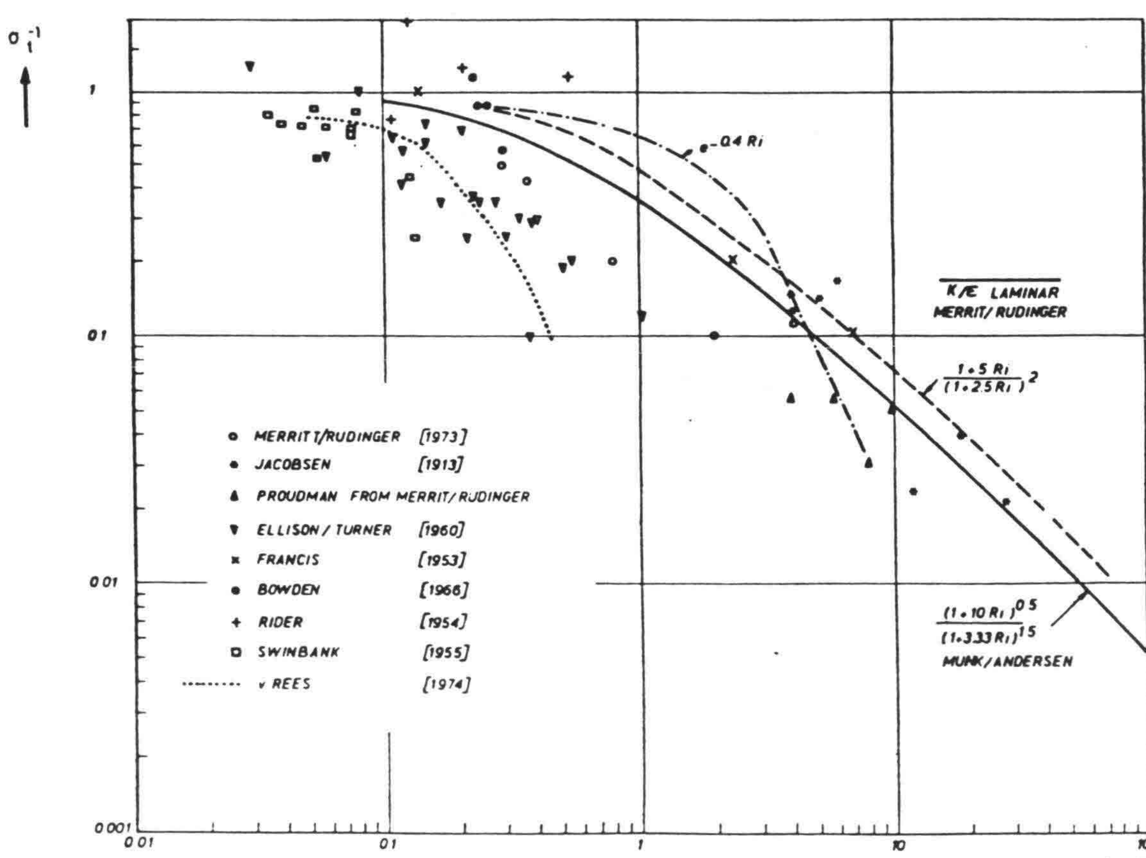

Fig. 6.14 The effect of stability as a function of Richardson number on the ratio of the eddy diffusivity to the eddy viscosity.

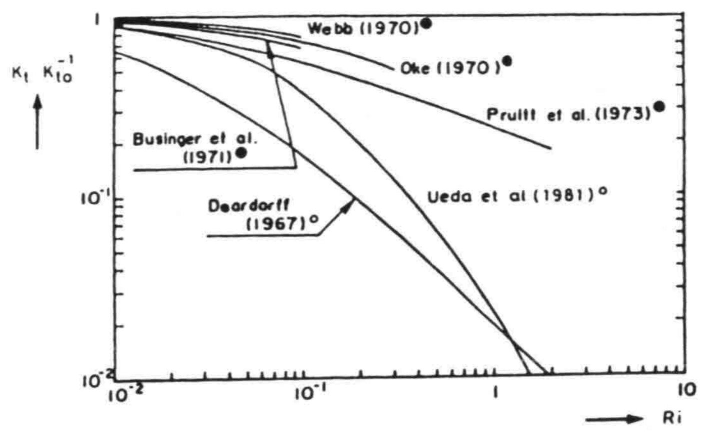

Fig. 6.15 Comparison of measurements in atmosphere (after Ueda et al, 1981); closed circles: measurements in surface layer, within a few meters adjacent to ground surface; open circles: measurements from 25 to 200 m from ground surface.

5.2 Tidal flow

For salinity intrusion into a partially mixed estuary Odd and Rodger (1978) present field data on damping functions as observed at different instances of time on the ebb tide. Similar data are presented by Knight et al (1980). From their measurements Odd and Rodger derive an empirical expression for $L\ L_n^{-1}$. This parameter is given as a function of the local Ri-value, when Ri increases continuously from the bed upwards. If not, they relate $L\ L_n^{-1}$ with the magnitude and relative depth of the local peak Ri-value.

Further field data on the effect of stratification on damping functions are based on tidally averaged parameter values (e.g. Kent and Pritchard, 1959, Bowden and Gilligan, 1971).

Measurements on turbulence quantities in tidal flow and the effect of stratification thereon are scarce. A summary is given by West et al (1986) and West and Shiono (1988), who further present the result of exploratory measurements on the subject which they made themselves.

6. Final remarks

The preceding text deals with the effect of stratification on turbulence, in particular the physical issues involved. It discusses the capabilities and limitations of the mixing length turbulence model. It does not discuss the advanced turbulence models, which have been developed over the past 20 years, to describe the effect of stratification on turbulence. For a comprehensive state of the art review on this subject, the reader is referred to Viollet (1988) and ASCE (1988). The latter review concludes that it is not certain yet whether the advanced turbulence models just now being developed contain the correct representation of turbulence physics (ASCE, 1988, p. 1059).

Three-dimensional mathematical modelling of salt intrusion is not common practice due to to complexity of the modelling and the large computer capacity needed. The three-dimensional mathematical modelling of the salt intrusion into the Hudson-Raritan Estuary by Oey et al (1985) is one of the most advanced modelling efforts, using an advanced turbulence model, made thusfar. As such it is discussed by ASCE (1988, pp. 1022-1031).

Computationally less complicated two-dimensional vertical salt intrusion models which contain the longitudinal and the vertical coordinates as independent space variables and which use mixing length turbulence models are given by Hamilton (1975), Blumberg (1977), Odd and Rodger (1978), Perrels and Karelse (1981), Smith and Takhar (1981) and Wang (1983) and further by Lehfeldt and Bloss (1988) and Bloss et al (1988) as discussed by Abraham (1989). The above models use a variety of damping functions, each in agreement with a particular set of experimental data (Figs. 6.12, 6.13 and 6.14).

The above observations imply that three-dimensional vertical salt intrusion models are still in the stage of development.

References

Abraham, G., 1988. Turbulence and mixing in stratified tidal flows. In: Dronkers, J. and Van Leussen, W. (eds.). Physical processes in estuaries. Springer, Berlin.

Abraham, G., 1990. Discussion of Bloss et al (1988), J.Hydr.Eng. ASCE, 115 accepted.

ASCE Task Committee on Turbulence Models in Hydraulic Computations, 1988. Turbulence modeling of surface water flow and transport: Part I, J.Hydraul.Eng. ASCE, 114 (9): 970-991. See also Parts II-V, 992-1073.

Bloss, S., Lehfeldt, R. and Patterson, J.C., 1988. Modeling turbulent transport in stratified estuary. J. Hydraul.Eng. ASCE, 114 (9), (1115-1133).

Blumberg, A.F., 1977. Numerical model of estuarine circulation. J. Hydraul.-Div. ASCE, 103 (3), 295-310.

Bowden, K.F. and Gilligan, R.M., 1971. Characteristic features of estuarine circulation as represented in the Mersey Estuary, Limnology and Oceanography 16, 490-502.

Ellison, T.H. and Turner, J.S., 1960. Mixing of dense fluid in a turbulent pipe flow, Part 2, Dependence of transfer coefficient on local stability. Journal of Fluid Mechanics, 8, 529-544.

Gibson, M.M. and Launder, B.E., 1978. Ground effects on pressure fluctuations in the atmospheric boundary layer. Journal of Fluid Mechanics, 86, 491-511.

Hamilton, P., 1975. A numerical model of the vertical circulation of tidal estuaries and its application to the Rotterdam Waterway. Geophys. J. R. Astron.Soc. 40, 1-21.

Kent, R.E. and Pritchard, D.W., 1959. A test of mixing length theories in a coastal plain estuary. Journal of Marine Research, 18, no. 1, 62-72.

Knight, D.W., Rodger, J.G., Shiono, K., Waters, C.B. and West, J.R., 1980. The measurement of vertical turbulent exchange in tidal flows. Proceedings 2nd International Symposium on Stratified Flows. Trondheim, 1, 362-366.

Komori, S., Ueda, H., Ogino, F. and Mizushina, T., 1982. Lateral and longitudinal turbulent diffusion of scalar quantities in thermally stratified flow in open channel. Heat Transfer 1982, Proceedings 7th International Heat Transfer Conference, München, 2, 431-436.

Komori, S., Ueda, H., Ogino, F. and Mizushina, T., 1983. Turbulence structure in stably stratified open-channel flow. Journal of Fluid Mechanics, 130, 13-26.

Kondo, J., Kanechika, O. and Yasuda, 1978. Heat and momentum transfers under strong stability in the atmospheric surface layer. Journal of the Atmospheric Sciences, 35, 1012-1021.

Kranenburg, C., 1985. A k-model for stably stratified nearly horizontal turbulent flows. Department of Civil Engineering, Delft University of Technology, Report No. 4-85.

Lehfeldt, R. and Bloss, S., 1988. Algebraic turbulence model for stratified tidal flows. In: Dronkers, J. and Van Leussen, E. (eds.) Physical processes in estuaries, Springer, Berlin.

Mizushina, T., Ogino, F., Ueda, H. and Komori, S., 1978. Buoyancy effect on diffusivities in thermally stratified flow in open channel. Heat Transfer, Proceedings 6th International Heat Transfer Conference, Toronto, 1, 91-98.

Monin, A.S., 1959. Turbulence in shear flow with stability, Journal of Geophysical Research, 64, no. 12, 2224-2225.

Odd, N.V.M. and Rodger, J.G., 1978. Vertical mixing in stratified tidal flows. Proceedings American Society of Civil Engineers, Journal of Hydraulics Division, 104, no. HY 3, 337-351.

Oey, L.Y., Mellor, G.L. and Hires, R.I., 1985. A three-dimensional simulation of the Hudson-Raritan Estuary, Part I: Description of the model and simulations; Part II: Comparison with observation; Part III: Salt flux analysis. J. Phys. Oceanogr. 15, 1676-1692, 1693-1710, 1711-1720.

Ozmidov, R.V., 1965. On the turbulent exchange in a stably stratified ocean. Izv., Atmospheric and Oceanic Physics Series, 1, no. 8, pp. 853-860.

Perrels, P.A.J., Karelse, M., 1981. A two-dimensional laterally averaged model for salt intrusion in estuaries. In: Fischer H.B. (ed.), Transport models for inland and coastal waters. Academic Press, New York.

Smith, T.J., Takhar, H.S., 1981. A mathematical model for partially mixed estuaries using the turbulent energy equation. Estuarine Coastal Shelf Sci. 13 (1), 27-45.

Tennekes, H. and Lumley, T.L., 1972. A first course in turbulence, M.I.T. Press, Cambridge.

Ueda, H., Mitsumoto, S. and Komori, S., 1981. Buoyancy effects on the turbulent transport processes in the lower atmosphere. Quarterly Journal Royal Meteorological Society, 107, 561-578.

Viollet, P.L., 1988. On the numerical modelling of stratified flows. In: Dronkers, J. and Van Leussen, W. (eds.). Physical processes in estuaries, Springer, Berlin.

Wang, D.P., 1983. Two-dimensional branching salt intrusion model. J. Waterway, Port, Coastal Eng. ASCE, 109, (1), 103-112.

Webster, C.A.G., 1964. An experimental study of turbulence in a density stratified shear flow. Journal of Fluid Mechanics, 19, 221-245.

West, J.R., Knight, D.W. and Shiono, K., 1986. Turbulence measurements in the Great Ouse Estuary, American Society of Civil Engineers, Journal of Hydraulic Engineering, 112, (3), 167-180.

West, J.R. and Shiono, K., 1988. The structure of turbulence in partly mixed estuaries. In: Dronkers, J. and van Leussen, W. (eds.). Physical processes in estuaries, Springer, Berlin.

Young, S.T.B., 1975. Turbulence measurements in a stably stratified turbulent shear flow. Queen Mary College, London, Report QMC-EP 6018 (quoted from Gibson and Launder (1978)).

References referred to in Figs. 6.12, 6.13 and 6.14.

Bowden, K.F. and Sharaf El Din, S.H., 1966. Circulation, salinity and river discharge in the Mersey Estuary, Geoph. J. Roy, Astr.Soc. 10, pp. 383-399.

Ellison, T.H. and Turner, J.S., 1960. Mixing of a dense fluid in a turbulent pipe flow. J. Fluid Mech., 8 (4), 514-544.

Francis, J.R.D. and Stommel, H., 1953. Observations of turbulent mixing processes in a tidal estuary. Tech.Rep. no. 53-22, Woods Hole Oceanogr.Inst.

Jacobsen, J.P., 1913. Beitrag zur Hydrographie der dänisachen Gewässer, Medd. Komm. Havundersog Kbh., 2, 94.

Merrit, G. and Rudinger, G., 1973. Thermal and momentum diffusivity measurements in a turbulent stratified flow. AIAA Journal, 11, 1465-1470.

Pruitt, W.O., 1973. Momentum and mass transfer in the surface boundary layer. Quart. J.R. Met. Soc., 99, pp. 370-386.

Rider, N.E., 1954. Eddy diffusion of momentum, water vapour and heat near the ground. Phil. Trans. Roy. Soc., London, A246, 481-501.

Swinbank, W.C., 1955. An experimental study of eddy transport in the lower atmosphere. Div. of Meteor. Physics, Comm. Wealth Scient. and Ind. Res. Org. Australia, paper no. 2.

Van Rees, A.J., 1975. Experimental results on exchange coefficients for non-homogeneous flow. Proceedings, 16th Congress. IAHR. Sao Paulo, 3, pp. 309-318.

Vreugdenhil, C.B., 1967. Turbulente viscositeit en diffusie-coëfficiënt bij variabele dichtheid, unpublished report, Delft Hydraulics, nota S 114.

Chapter 7, Field surveys and physical scale modeling

1. Introduction

Modelling estuaries, as characterized by the complex interaction of river discharge, tidal movement and density differences, is still a difficult operation.

In general, the following methods are available:
- field studies;
- mathematical (analytical and numerical) models;
- physical scale models.

For all methods information on accuracy, possibilities and limitations is required. Each method has to start with a definition and schematization of the problem area, and boundary conditions have to be defined.

Salinity intrusion in estuaries is the result of a complicated interaction between several mechanism. Both mathematical and scale models have to be validated by field data. However, each method is limited, so that in general only a combination of all methods will lead to reliable results.

Field data can be obtained only for the existing situation. Systematic changes in the variables (depth etc.) are not possible. Sufficiently complete sets of field data are essential for obtaining physical insight.

Mathematical models are based on the knowledge of the physical processes involved such as turbulent mixing, boundary resistance, etc. Their predictive ability depends on the degree of schematization of the physical processes.

Physical scale models are based on the fact that water is obeying the rules of hydraulics in nature as well as in the model, as long as this model is built according to the relevant scale rules. Consequently the problem with respect to this type of modelling is to know the scale rules and the possible scale effects.

2. Field Surveys

All studies on salt intrusion need information on the particular estuary. Field surveys therefor are essential. So, every study should start with

- an inventory of the data that are available and
- an inventory of the data that are needed as a minimum to perform the study.

Confrontation of these inventories will give the minimum amount of measurements that have to be performed.

The data that are needed for a study depend on the type of study and the accuracy one wishes to achieve. For instance distinction can be made between data needed for a first impression of the estuary (e.g. by applying one of the salt intrusion formulae) and data needed for the application of a salt intrusion model, where of course a further distinction is needed according to the type of model.

2.1 First impression, salt intrusion formulae

For a first impression information on the type of estuary is needed. For instance the estuary can be

- deltaic (Mekong)
- funnel shaped (Mersey, Western Scheldt)
- man made (Rotterdam Waterway, Solo river, Indonesia).

This information can be obtained from maps or aerial photography

Secondly information on the tide and the river discharge regime is needed. For instance the tide can be

- weak (Mediterranean)
- semidiurnal with or without a daily inequality (North Sea)
- diurnal (the Gulf)

and the river discharge can be determined by

- melting water from a mountain area (Rhine)
- rainfall (various tropical rivers)
- hydropower dams in the upstream regions (Nakdong, Korea).

The tidal information can be obtained from local tide tables or from the Admirality tide tables. The information on the river discharge regime should be measured.

If a first impression of the salt intrusion with the formulae of chapter 3 is to be obtained the parameters α and F_o should be known. This means that Q_f, P_t or $u_{1,0}$, the sea water salinity and the average depth h_o have to be measured, or calculated.

2.2 Models

For the application of models for salt intrusion studies data are needed for

- set up of the model
- calibration of the model, i.e. the varation of the roughness parameter for the watermovement and the dispersion coefficient for the salt distribution in such a way that the results of the model coincide satisfactorilly with waterlevels, velocities and salt concentrations measured in nature
- validation/verification, i.e. a comparison of the results of the model under circumstances (= boundary conditions) different from those of the calibration with measurements.

Moreover to run a mathematical model boundary conditions and initial conditions with respect to waterlevels and/or velocities and salinities along the estuary are needed. The extent of these conditions depends on the type of model:

2.2.1 1D-models

As boundary conditions the waterlevel and salinities at the seaward boundary are needed, along with the fresh water river discharge upstream. For real time models the seaward boundaries have to be known for at least one tidal cycle (13 hours meausurements with a semidiurnal tide), but if there is a strong daily inequality, or if one wishes to incorporate in the model the effect of spring tide and neap tide, then a much longer measuring period is needed (25 hours for the daily inequality and at least two weeks for the spring/neap tide influence).
For the river discharge of course stage-discharge curves can be used if available. However if the variation in time of the river discharge is one of the parameters involved in the study, one should take into account the traveltime of the discharge wave from the position upstream where it is measured (or calculated) to the upstream boundary of the model. For instance

for the Rhine river salt intrusion models the river discharge as measured at the Dutch/German border is taken, but shifted over two days, since it takes these two days for the discharge wave to arrive at the upstream boundaries of these models.
If the influence of seasonal variations of the riverdischarge on the salinity is to be modelled a long term measuring campaign is needed. (Hydraulics Research Division (1980), Nedeco (1965), Nedeco (1976))

To start the calculations with a mathematical model initial conditions are needed. The speed of convergence of the model is dependant on the accuracy of these conditions. Especially the distribution of salt in the estuary is important, since dispersion is a rather slow process. Therefor it is worthwile to put some effort in a reliable choise of this initial conditon, i.e. the salinity along the estuary as a function of the longitudinal coordinate. This means that the salinity has to be measured at several places either simultaneously, or with the moving boat method. In the latter case the measurements should be processed in order to account for the timeshift due to this method. (Nguyen Hac Vu and Chu Thai Hoanh (1983))

2.2.2 Two-layer models

Here the location of the interface is an important parameter. This means that measurements of the salinity should comprise the salinity distribution over the vertical in order to obtain this location. It is common practice to define the interface as the location where the vertical salinity gradient has its maximum value.

2.2.3 2DV- , 3D-models an hydraulic scale models

These models need information on the salinity and velocity distribution over the vertical an the total cross-section respectively. This means that setting up, calibrating and verifying such models needs quite a number of accurate and intensive measurements. Broad methods as the moving boat method will not do. Only carefully organised simultaneous measuring campaigns with a lot of moored measuring boats in various cross-sections along the estuary will give enough information. So, these measuring campaigns are rather costly and very dificult to organise, while also the interpretation of the results is very cumbersome and should be done with great care.

3. Physical scale modeling, problem areas

Physical scale models are commonly used to solve salinity intrusion problems in estuaries with a complex geometry where often, various conflicting interests are involved (Fischer and Dudley (1975), Breusers and Van Os (1981), Roelfzema and Van Os (1978)).

With reference to these problem areas the following aspects could be covered by a model:

- navigational aspects: reproduction of the flow field, both depth averaged and vertical flow distribution;
- salinity intrusion: reproduction of salinity distribution under the influence of tides and river discharges ; possibilities of reducing salinity intrusion;
- transport of pollutants and silt; possibilities of reducing siltation.

This requires the reproduction of the driving mechanism:

- tidal movement;
- river discharge;
- density difference between sea and river water;

with the resulting flow phenomena such as:

- tidal elevation and currents, displacing and mixing water masses;
- estuarine circulations induced by density differences;
- mixing by turbulence generated by bed shear and wall roughness (groynes, harbour entrances) and mixing due to exchange currents between harbours and estuary and the confluence of tidal branches;
- erosion, transport and deposition of sediments.

It will be clear that no model provides an exact reproduction of all relevant phenomena. A discussion of reproductive capabilities and possible scale effects will therefore be necessary in the design phase of a model.

The required accuracy of a model in the reproduction of natural phenomena will depend on the type of investigation:

- comparative tests, in which various alternatives are compared mutually or with the original situation; the required accuracy will be determined by the detectability of changes in practice. Moreover, this type of test requires a very easy and stable model control.

- absolute tests, in which velocity and salinity have to be predicted for a certain condition (tide, river discharge) at a certain location; here the accuracy of the model results will depend also on the "measurability" of the present situation in nature, because this determines the accuracy of the model calibration.
- fundamental research, giving information to improve the understanding of physical phenomena, which is necessary to develop both hydraulic (scale) models and mathematical models. The accuracy of the results must be sufficient to detect the effect of the various parameters during this type of research.

3.1 Selection of model area and model scales

3.1.1 Definition of model area

The choice of the model boundaries depends on the physical phenomena to be reproduced. The sea boundaries have to be chosen in such a way that the conditions at these boundaries are not affected by changes in the problem area and that the fresh water discharge of the river leaves the model in a correct way. The salinity distribution in the estuary should not be affected by the conditions at the boundaries (Van Rees et al (1972)).

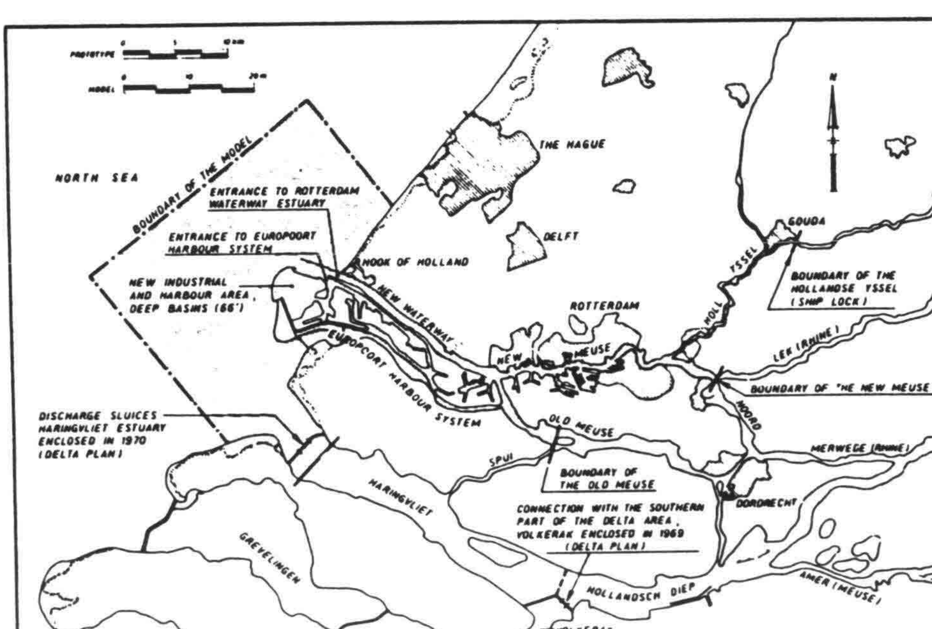

Fig. 7.1 Plan view of tidal model Rhine estuary

For instance in the case of the tidal model of the Rhine estuary (Fig. 7.1) flow conditions near the harbour mouth are governed by tidal and density currents. The tidal range is from 1.35 (neap tide) to 1.75 m (spring tide). The fresh water discharge through the Rotterdamse Waterweg ranges from 400 to 4000 m^3/s (average 1000 m^3/s). The salinity of the North Sea is about 33 ppt. The tidal flow pattern at sea is nearly parallel to the coast with high-water slack at sea at 3.5 hours after H.W. at Hook of Holland. In view of this tidal flow pattern it was decided to take a closed western model boundary parallel to the dominant flow
direction and to have two control boundaries (north and south) at some 10 to 15 km from the entrance, perpendicular to the main flow direction. The distance of the western boundary to the coast was roughly estimated from a potential flow computation on the influence of the proposed harbour extension. This estimate was verified later with two-dimensional flow calculations which showed that the influence of the closed western boundary was within the experimental accuracy limits.
The choice of the river boundaries often is a compromise between cost and accuracy. If only the salinity-affected part of the estuary is reproduced, tidal discharges and fresh water discharges have to be known at the river boundaries. This is a weak point because the scale model becomes dependent on a mathematical model to calculate these river boundaries. The other possibility, extension of the model up to the limits of tidal influence, is costly but makes the model self-supporting. In both cases, however, calibration is necessary to obtain accurate values for the discharges.

3.1.2 Selection of model scales

Selection of model scales, defined here as the ratio of quantities in nature and model, is finding a compromise between cost and accuracy. This holds also for mathematical models. Several aspects are of importance (see also Hermann (1975)):

- length and depth scales should be large to reduce model dimensions, discharges and use of salt. In the Rhine-model case tidal discharges up to 250,000 m^3/s have to be simulated which certainly presents a lower limit to the scales.
- depth scales should however be not so large that the flow in the model becomes laminar. This means that the Reynolds number in the model should be well above 1000.

- reproduction of tidal flow phenomena requires Froude scaling (velocity scale = length scale $^{1/2}$),
- reproduction of density-influenced flow and mixing requires at least reproduction of the internal Froude number which means, in combination with the previous requirement, a one-to-one scaling of densities,
- dimensions of instruments require a minimum water depth
- the distortion of a model (ratio of length to depth scale) has to be limited for several reasons (see Fig. 7.2):
  - slopes are exaggerated in a distorted model but should remain below a certain value to avoid flow separation,
  - the correct reproduction of vertical mixing becomes increasingly difficult with augmenting distortion,
  - distortion means an increase in roughness. The friction in the model has to be increased in the same ratio as the distortion. Bed roughness (cubes, strips) is often preferred in these models, which gives an upper limit to the model friction factor.

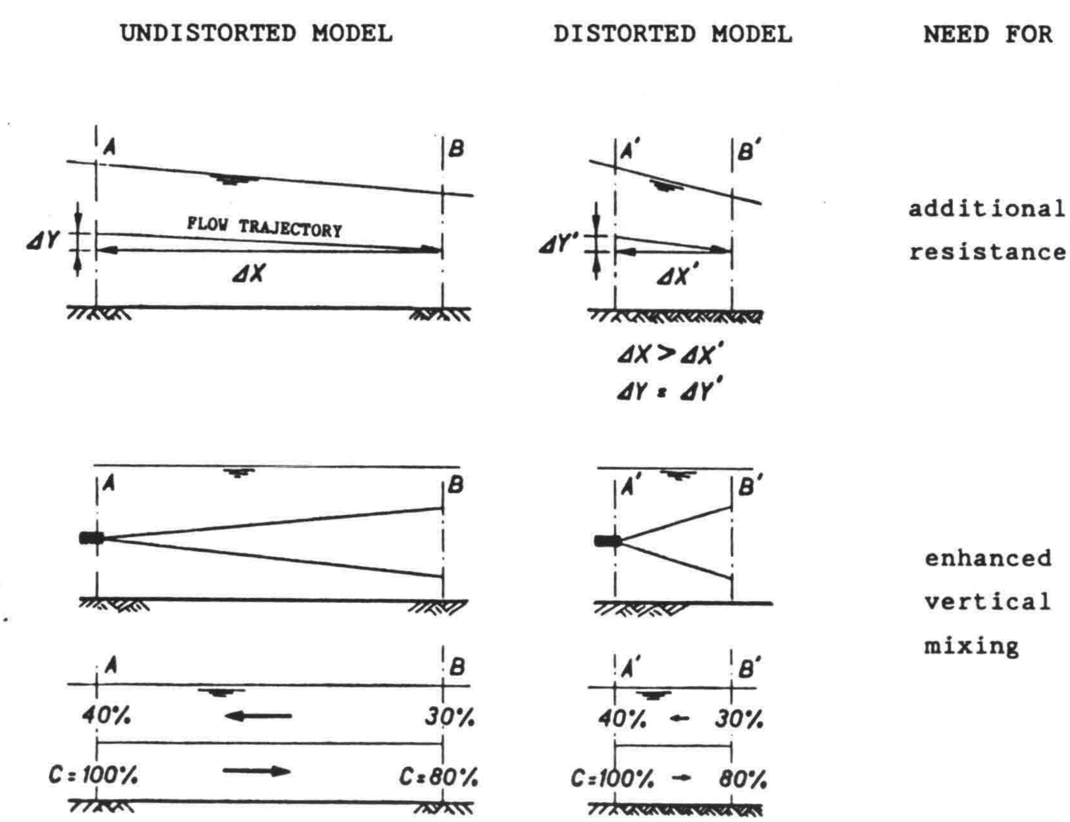

Fig. 7.2 Consequences of model distortion

Several other aspects should also be considered or reproduced:

- waves and navigation: the effects of waves and navigation on vertical mixing can be neglected in general, but with shallow stretches or heavy navigational traffic the influence should be accounted for;
- wind: wind can change the tide-averaged circulation (drift) in the Sea. If necessary, storm effects can be reproduced by changing the boundary conditions of a model,
- Coriolis acceleration: neglecting the effects of the wrong representation of the Coriolis acceleration in models causes deviations in water levels and flow direction in general. Simulation of these effects requires rotation of the model or the use of rotating cylinders, where the lift force (Magnus effect) can simulate the Coriolis acceleration effects (Schoemaker 1958).

3.2 Model boundaries

For the river boundary almost always a discharge control is chosen, since the river discharge is the parameter commonly known from measurements or stage-discharge curves.
For the sea boundaries the type of control to be chosen depends on the area of the sea to be reproduced in the model and the number of open sea boundaries. A review of existing tidal models shows that for long (relative to the length of the tidal wave) estuaries a water level control at the mouth of the estuary gives good results. However, for a relatively small sea a water level control on all sea boundaries gives an unstable and inaccurate control of velocities in the sea area (Fischer 1976). Therefore for the Rhine-estuary model a complete discharge control was chosen.

3.3 Roughness and mixing

The distortion of estuary models necessitates the adjustment of roughness and mixing. The roughness can be separated in wall and bed roughness. Wall roughness effects due to groynes, harbour entrances and other protrusions is reproduced correctly, because their shape is reproduced geometrically similar.

The distortion does not have a significant influence here because these protrusions are already sharp (in the sense that the flow will separate from the protrusion) in nature. The friction factor for the bed roughness has to be increased with the distortion factor, to obtain the correct water level shapes.

Means to provide the required model roughness are cubes, strips and vertical bars. The effective roughness of these elements can be measured separately so that _if_ the prototype roughness is known, the model roughness can be determined also. In general, a calibration of the roughness is necessary, however, because the prototype roughness is not known sufficiently accurate. The optimum model roughness is determined by comparing water levels and gradients in model and nature.

If all mixing in an estuary is thought to be caused by bed-shear generated turbulence it can be shown that the vertical mixing in a distorted model is too small. So the vertical mixing has to be increased. On the other hand, mixing due to wall-roughness generated turbulence (groynes, harbour inlets, confluence) is correctly reproduced in a distorted model. This was proven in the systematical salt intrusion research in the tidal salinity flume. It depends therefore on the relative importance of wall and bed roughness whether the mixing in the model is to scale (De Jong and Abraham). Tests in the Europoort model and in the tidal salinity flume have shown that the vertical mixing can be influenced by the choice of type of roughness elements, used for the additional roughness (Abraham et al. 1975). With the same total roughness, generated with different means (strips on the side walls, vertical bars and cubes or small plates on the bed) different values for the vertical mixing and the salinity intrusion were found. Wall strips produced the maximum mixing.

The conclusion is therefore that in reproducing the _roughness_, lack of knowledge of the prototype roughness is the weak point, but that calibration of the model will provide a sufficient solution. For the turbulent _mixing_, the model acts more or less as a "black box" and has to be calibrated also. The choice of the type of roughness element is here a calibration parameter. Additional mixing can be provided by air-bubble screens, giving almost no effect on the roughness.

3.4 Model calibration and verification

The most important feature of the river is the salinity intrusion, but of course tidal propagation and velocities have to be similar as well.

For calibrating the tidal propagation two parameters are of importance:

- the model roughness,
- the river boundary conditions

The longitudinal distributions of amplitude and phase of the M2 tidal component of the water levels can be used as parameters for calibration (Fig. 7.3). From sensitivity tests with the Rhine-estuary model it was found that the change in amplitude and phase over a certain section was almost linearly related to the amount of additional roughness. The use of these parameters therefore provides a good means to obtain the optimum roughness in the model.

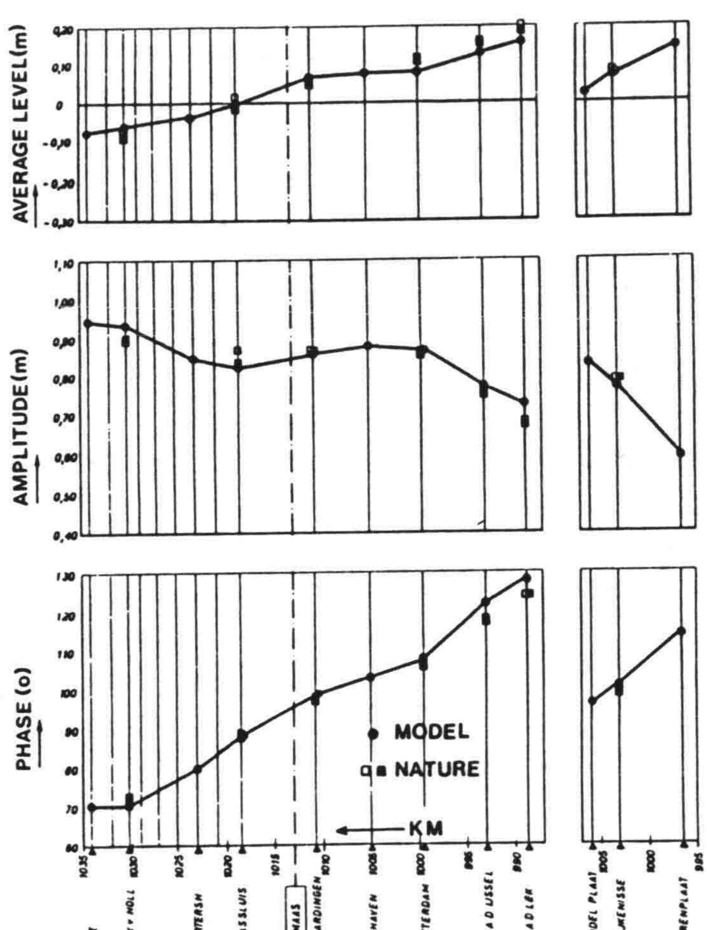

Fig. 7.3 Comparison of tidal components of water level in model and nature

The required capabilities of a model to simulate natural phenomena depends on the nature of the investigation (comparative or predictive, support of fundamental research).
The capability of the model depends on several factors:

- accuracy of boundary conditions,
- accuracy of the model boundary control,
- accuracy of instruments,
- drift of boundary control and instruments.

For the tests in which a comparison has to be made between two situations (for example deepening of part of the estuary) a high accuracy is required. These tests should preferably be carried out on the same day because incidental errors in model control and instrument calibration are avoided.

The salinity distribution and intrusion in the model can be influenced in several ways, assuming tidal propagation has already been adjusted:

- the <u>type of roughness</u>: from observations in the tidal flume and the Rhine-estuary model is has been concluded that for the same total friction factor, the vertical mixing and salinity intrusion depends on the roughness type,
- <u>additional mixing</u> can be obtained by the injection of air. Experimentally it has been found that quantities up to 20 $cm^3/m^2/s$ of air hardly affect the roughness but greatly enhance the vertical mixing and reduce the salinity intrusion,
- the <u>"history" effects</u> of the tidal movement: It cannot be assumed that the salinity intrusion during a certain tide is independent of the preceeding tides, for example a spring tide following a normal tide. In the model the tides have to be made cyclic. Comparisons, where the measurement period of 12.5 hours (one tide) is part of a cycle of 25 (one preceeding tide) or 75 hours (five preceeding tides) showed that for practical applications (normal tidal variations) "history" effects can be neglected; however, if the effect of a storm surge is to be studied, boundary conditions should be given as long term time series.

For the optimum condition with respect to the reproduction of tidal propagation, the velocity and density distribution should be compared for model and prototype without any further adjustment of the model for a number of prototype measurements under different conditions with respect to tide (spring/neap) and river discharge.

Some results for the measuring station at km 1015 of the Rhine-estuary model are presented in Fig. 7.4.

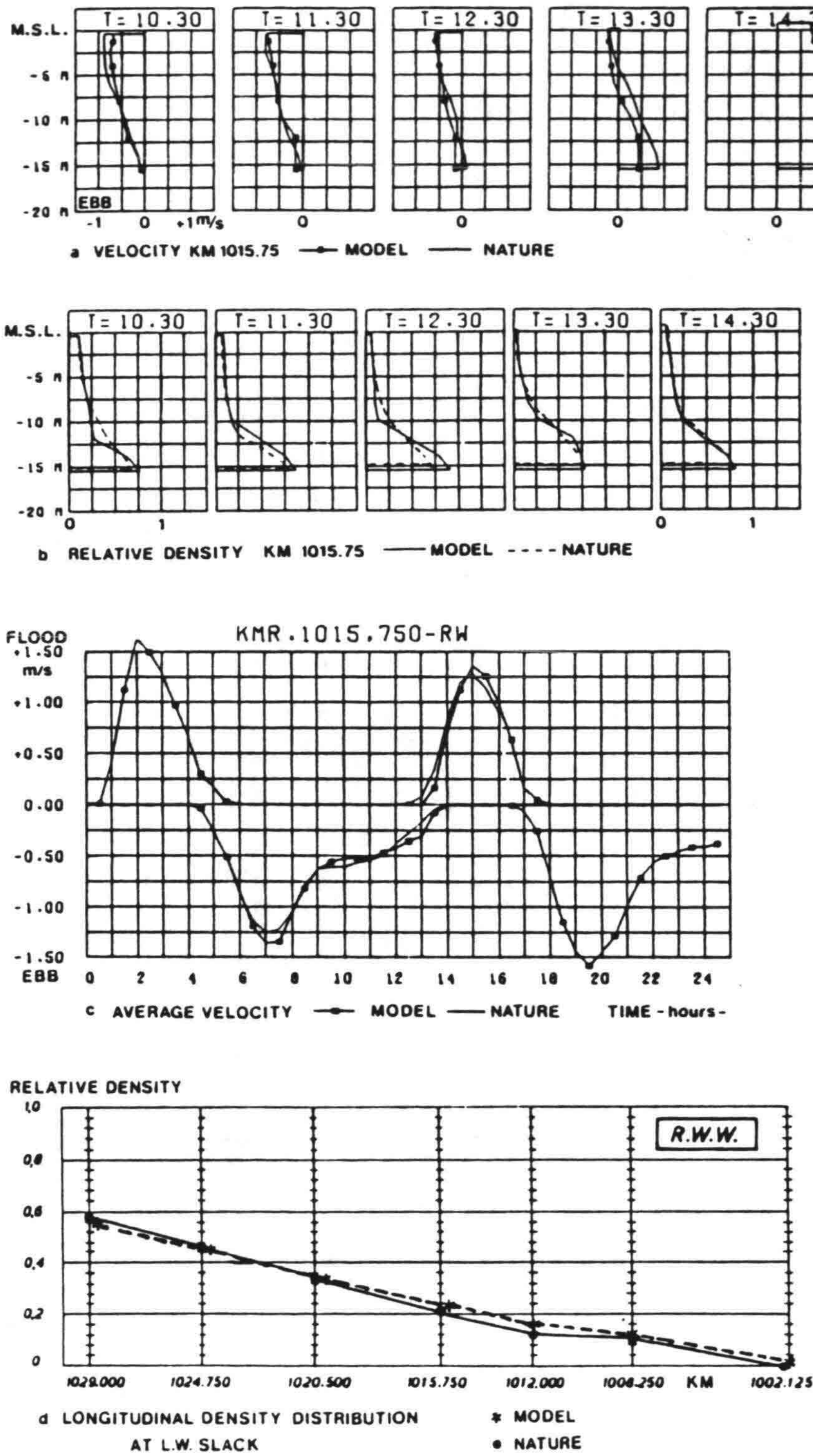

Fig. 7.4 Verification of density and velocity distribution tidal model of the Rhine estuary

Fig. 7.4a shows a comparison of some velocity profiles, Fig. 7.4b the distribution of the relative density (difference between the local density and the river water density divided by the difference in density between sea and river water). Fig. 7.4c shows the velocity averaged over the vertical. These velocities are averaged for each flow direction (ebb vs. flood); thus the density currents round slack tide become visible. Fig. 7.4d shows the depth averaged salinity distribution at Low Water Slack.

4. Final remarks

Salt intrusion and water quality modeling of a complex estuary makes high demands upon the capabilities of modeling techniques. Increased environmental problems and the impact of large infrastructural works have stressed these requirements. In those cases only a complimentary approach with hydraulic and mathematical modeling supported by extensive field surveys in the actual estuary is feasible. With respect to modeling of the estuary phenomena the following final remarks should be made:

- Although the scaling of all phenomena in a hydraulic scale model is not yet completely understood, which gives the model a partial black-box character, it proves to be an expensive but powerful tool for the study of estuaries.

- The hydraulic model should be calibrated very carefully with special emphasis on the influence of possible scale effects due to distortion and Reynolds number influences (De Jong and Abraham).

- The model should be provided with good boundary conditions.

- The purpose of the model research and the required accuracy have a large impact on the cost of the research.

References

Abraham, G., Karelse, M., Lases, W.B.P.M., 1975. Data requirements for one-dimensional mathematical modelling of salinity intrusion in estuaries, Proc. 16th IAHR Congress Sao Paulo, Vol. 3, pp. 275-283.

Breusers, H.N.C. and van Os, A.G., 1981. Physical modelling of the Rotterdamse Waterweg estuary, Publication no. 249, Delft Hydraulics Laboratory, 1981.

Fischer, H.B. and Dudley, E. (1975). Salinity intrusion mechanisms in San Francisco Bay, California, Proceedings IAHR Congress, Sao Paulo, August 1975, Vol. 1, pp. 124-133.

Fischer, H.B., 1976. Mixing and dispersion in estuaries, Annual Review of Fluid Mechanics, Vol. 18, pp. 107-133.

Jong, P. de and Abraham, G. (1990). Physical Modeling of Salinity Intrusion into Rotterdam Waterway Estuary, DELFT HYDRAULICS, May 1990.

Hermann Jr., F.A., 1975. Overview of physical estuary practice, Modelling Techniques, ASCE New York, Vol. 2, 1975, pp. 1270-1290.

Hydraulics Research Division, 1980. A study of the salt intrusion in the Lower-Corantijn, Ministry of Public Works and Traffic, Hydraulics Research Division, Paramaribo, Suriname, May 1980.

Nedeco, 1965. Siltation Bangkok Port Channel, Netherlands Engineering Consultants, The Hague, July 1965.

Nedeco, 1976. Nagdong River Basin Delta Study, Watermanagement, waterrequirements for Salinity Repulsion, technical report 1 - part 4, December 1976.

Nguyen Hac Vu and Chu Thai Hoanh, 1983. Discharge measurements by the moving boat method in the Mekong river and its estuaries, Technical note, Mekong Secretariat, Bangkok.

Van Rees, A.J., van der Kuur, P., Stroband, H.J. 1972. Experiences with tidal salinity model Europoort, Proc. 13th Int. Conf. on Coastal Engineering Vancouver, Vol. 3, 1972, pp. 2355-2378.

Roelfzema, A., Van Os, A.G., 1978. Effect of harbours on salt intrusion in estuaries, Publication no. 204, Delft Hydraulics Laboratory, 1978.

Schoemaker, H.J., 1958. Influence of earth rotation in hydraulic tests, De Ingenieur, Vol. 70, 1958, p. A608.

main office
Rotterdamseweg 185
p.o. box 177
2600 MH Delft
The Netherlands
telephone (31) 15 - 56 93 53
telefax (31) 15 - 61 96 74
telex 38176 hydel-nl

location ' De Voorst '
Voorsterweg 28, Marknesse
p.o. box 152
8300 AD Emmeloord
The Netherlands
telephone (31) 5274 - 29 22
telefax (31) 5274 - 35 73
telex 42290 hylvo-nl